MULTIPLEXED COMPREHENSIVE DESIGN AND CHARACTERIZATION OF AN ELECTROCHEMICAL INTERFACE ACCESSING NON-INVASIVE BODILY FLUIDS TOWARDS QUALITY-OF-LIFE MONITORING

by

Ashlesha Bhide

APPROVED BY SUPERVISORY COMMITTEE:

Shalini Prasad, Chair

Sriram Muthukumar

Stuart Cogan

Soudeh Ardestani Khoubrouy

To my daughter Anushka,

To my husband Kapil,

To my grandparents.

MULTIPLEXED COMPREHENSIVE DESIGN AND CHARACTERIZATION OF AN ELECTROCHEMICAL INTERFACE ACCESSING NON-INVASIVE BODILY FLUIDS TOWARDS QUALITY-OF-LIFE MONITORING

by

ASHLESHA BHIDE, BE, MSc

DISSERTATION

Presented to the Faculty of

The University of Texas at Dallas

in Partial Fulfillment

of the Requirements

for the Degree of

DOCTOR OF PHILOSOPHY IN

BIOMEDICAL ENGINEERING

THE UNIVERSITY OF TEXAS AT DALLAS

December 2021

ACKNOWLEDGMENTS

I wish to express my deep gratitude to my advisor Dr. Shalini Prasad for her guidance and unwavering support throughout this journey. She has inspired me to strive hard to achieve my goals, multitask, and take failures in my stride. I am grateful to her for being patient, kind, and encouraging throughout my Ph.D. and journey towards motherhood. I hope to have stood up to her expectations. I wish to sincerely thank my co-advisor Dr. Sriram Muthukumar for being a great mentor and for teaching me a structured thinking approach towards problem solving. I have always learned something new in my conversations with him and gained a new perspective towards science.

I am thankful to my committee members Dr. Stuart Cogan and Dr. Soudeh Khoubrouy for their thoughtful insights, valuable suggestions, and feedback on my research efforts. I would like to thank the BMNL family for all their support and guidance. I wish to acknowledge Ambalika Tanak, Badrinath Jagannath, Sayali Upasham, Devang Sankhala, Dr. Kai-Chun Lin, Rujuta Munje for their incredible support and insightful feedback that led me to proceed in the right direction in my research. I will cherish all the conversations we have had through these years. I would like to thank my undergraduate students Amreek Saini, Ankita Rugi, Sarah Cheeran for supporting me in this journey. I credit my success to you. I hope to have been a good mentor. I would like to thank Andrew Rhodes and Adriana Coronado for their academic and administrative support. I would like to acknowledge Gordon Pollak and Zane Borg for their assistance at the UTD cleanroom facility.

I cannot begin to express my gratitude to my family for all their love, support, and encouragement through this journey. To my daughter Anushka, you inspire me to strive for excellence and I hope to set a good example for you. I am thankful to my husband Kapil for his patience and for being

there for me every day. You are the reason that has helped me deal with my downs on days when I felt like giving up. To my parents -Keshav and Anjali Bhide and brother Ameya Bhide, your faith and sacrifices are the reason I am here. You have given me the courage to pursue my dreams fearlessly. To my parents-in-law- Subhash and Charusheela Patil, your optimism and confidence has kept me encouraged through this journey. I hope to have made you proud. I thank all my friends who have helped me stay positive and for always listening to my rants.

November 2021

MULTIPLEXED COMPREHENSIVE DESIGN AND CHARACTERIZATION OF AN ELECTROCHEMICAL INTERFACE ACCESSING NON-INVASIVE BODILY FLUIDS TOWARDS QUALITY-OF-LIFE MONITORING

Ashlesha Bhide, PhD
The University of Texas at Dallas, 2021

Supervising Professor: Dr. Shalini Prasad

The research presented in this thesis outlines the design and development of novel biosensing platforms for monitoring biomarkers by the non-invasive sampling of body fluids with emphasis on self-health and disease management. The purpose of this work is to demonstrate the efficacy of two combinatorial biosensors – Continuous awareness through sweat platform (CLASP) and Exhaled breath condensate scanning using rapid electro analytics (EBC-SURE) for the detection of metabolic and inflammatory biomarkers towards integration onto low-power internet of things (IoT) platforms for wearable and point-of-care diagnostic applications. First, this work demonstrated the technical utility of a lancet-free, label-free platform for the combinatorial, and continuous monitoring of alcohol and glucose in perspired human sweat produced without external sweat induction strategies. The motivation of this study was to develop a sweat-based wearable platform for alcohol and glucose management to monitor glucose levels on moderate consumption of alcohol of diabetic social drinkers. A nanotextured sensor stack was embedded into a flexible nanoporous substrate to achieve sensitive and specific affinity-based biomarker detection within

physiologically relevant ranges in ultralow volumes of sweat. Non-faradaic EIS is employed as the signal transduction mechanism for biomarker detection to give an insight into the binding events occurring at the sensor interface. Additionally, the CLASP platform was benchmarked against commercially available hand-held devices to establish a one-to-one performance correlation. Furthermore, this platform was employed to demonstrate the epidermal functionality and sensor performance of CLASP for the on-body detection of sweat lactate to monitor restricted oxygen supply in sedentary populations. The successful implementation of CLASP in detecting metabolic biomarkers for health monitoring led to the transition of assessing the performance metrics of this platform for the detection of inflammatory biomarkers such as cortisol and TNF-α for chronic disease monitoring. The important highlight of this work was to establish the long-term temporal stability of the CLASP in detecting a simulated rise and fall in cortisol levels over a 6-hour sleep cycle. The last effort was focused on developing a point-of-care aid platform- EBC-SURE for the trace detection of inflammatory biomarkers in exhaled breath condensate for monitoring respiratory disorders. Exhaled breath condensate is considered a promising source of inflammatory biomarkers that can determine the pathophysiological processes underlying lung inflammation in a simple and non-invasive manner. EBC-SURE displayed a stable performance after rigorous testing enabling its integration onto diagnostic platforms for rapid quantification of biomarkers related to a healthy and acute inflammatory disease condition.

TABLE OF CONTENTS

LIST OF FIGURES

LIST OF TABLES

CHAPTER 1

INTRODUCTION

1.1 Biomarkers: Advantages and Challenges

Biological markers are measurable characteristic indicators critical to understanding the physiological state of the body. According to the National Institute of Health Biomarkers Definitions Working Group, a biomarker is defined as "a characteristic that is objectively measured and evaluated as an indicator of normal biological processes, pathogenic processes, or pharmacologic responses to a therapeutic intervention." Biomarkers serve as early warning indicators of exposures and disorders by providing a cellular level image of the fundamental processes occurring from the early to terminal stages of the disease[1]. The pursuit of developing advanced technologies has led to identifying molecular cues or 'biomarkers' that have the potential to revolutionize healthcare[2]. Biomarkers are widely accepted standards in scientific and clinical research and have been repeatedly evaluated to validate the relevant outcomes in clinical investigations and drug development. The success metrics of biomarkers depend on the experimental conditions and their validity with various other scientific techniques. Biomarkers can be considered as substitute clinical endpoints that encompass a small subset of well-characterized biomarkers that provide robust scientific evidence of accurately predicting a clinical result[3]. Biomarkers are divided into two categories – disease biomarkers and drug-related biomarkers. The disease biomarkers group includes risk, diagnostic, prognostic, and monitoring biomarkers and the drug-related biomarkers include predictive, response, and safety biomarkers. In the research and clinical fields, biomarkers find their applications in diagnosing/predicting diseases; health monitoring for disease detection; determination of treatment efficacy; prediction of effective and

adverse drug effects in specific treatment groups[1]. With the revolution in mobile health care, digital biomarkers have been accepted in medicine to monitor patient health and rapidly diagnose underlying diseases. Digital biomarkers are quantifiable physiological indicators collected by digital modalities integrated on portable, wearable platforms for use in personalized setting[4]. Biomarkers add significant value to personalized medicine by its non-invasive or minimally invasive testing features further allowing for rapid, economical, point-of-care diagnostic evaluation. However, the successful utility of biomarkers for a particular application is limited by weak experimental design, tedious statistical analysis, lack of background study, poor reproducibility, and the inability to translate bench study into clinical study. Biomarker investigations suffer from dilutions, variations in gender, variations at a particular time of the day, and limitations in achieving the statistical power criteria for carrying out the study[5].

1.2 Technology for continuous biomarker monitoring

Wearable technology has emerged as an innovative solution to continuous health monitoring and is the answer to numerous unmet clinical needs. The novel, emerging field of wearable biosensing has revolutionized the way healthcare is delivered by allowing continuous monitoring of health and disease biomarkers in a wide demographic to better evaluate their body status in emergency and hazardous situations. Continuous monitoring systems serve as primary intervention platforms by collecting the user's clinical statistics that can further assist in self-health monitoring, disease diagnosis, disease progression, and track therapy[6]. These can assist caregivers to track progressions in disease and assure continued recovery in remote settings and prompt immediate intervention thereby reducing the monetary burden of $200 billion on the U.S. health care system. Continuous biochemical sensors (biosensor) enable real-time receptor-biomarker interaction and

report quantifiable signals that are proportional to the biomarker concentration. The field of biosensing first came into existence with the invention of the glucose biosensor by Clark and Lyon in 1962[7]. Over a period, with the advances in technology, biosensors have become skin-integrable and implantable to give a detailed account of the body's vital state and underlying disease state. For continuous monitoring, the biosensors are required to be sensitive, specific, repeatable, reproducible, combinatorial, and skin compatible[8]. However, current clinical techniques suffer from reproducibility under varying conditions and the inability to report symptoms in real-time. Wearable technology is still in the stage of infancy, and some of the major technical gaps that need to be addressed are low sample volumes, low biomarker concentrations, mechanical resilience, biocompatibility, sensor stability, and fouling[9]. Non-invasive wearables are integrated into smart clothing and daily-use accessories for chronic disease monitoring, critical health vitals management, contractions monitoring, nausea management, and inflammation monitoring through body fluid-based metabolite analysis in morbid and mobility constrained populations encompassing old-aged people, infants, and pregnant mothers (see Figure 1.1). Wearable sensors are increasingly being developed in temporary patch or tattoo forms to detect and track core body temperature, blood pressure, electrical heart and muscle activity, hydration levels and a host of other biomarkers in hostile military settings for soldier wellness monitoring. In resource-challenged settings where access to electricity is limited, harvesting energy from natural resources, vibration, and human motion is the future energy source for powering future wearable devices. Many research efforts have been focused on the development of efficient battery-free systems such as nanogenerators, biofuel cells, and photovoltaic cells for self-powering health and disease monitoring devices in defense and pandemic environments. The current

advances in wearable research will help migrate lab prototypes into futuristic commercial devices for seamless health monitoring in physically demanding tasks and in day-to day-lives.

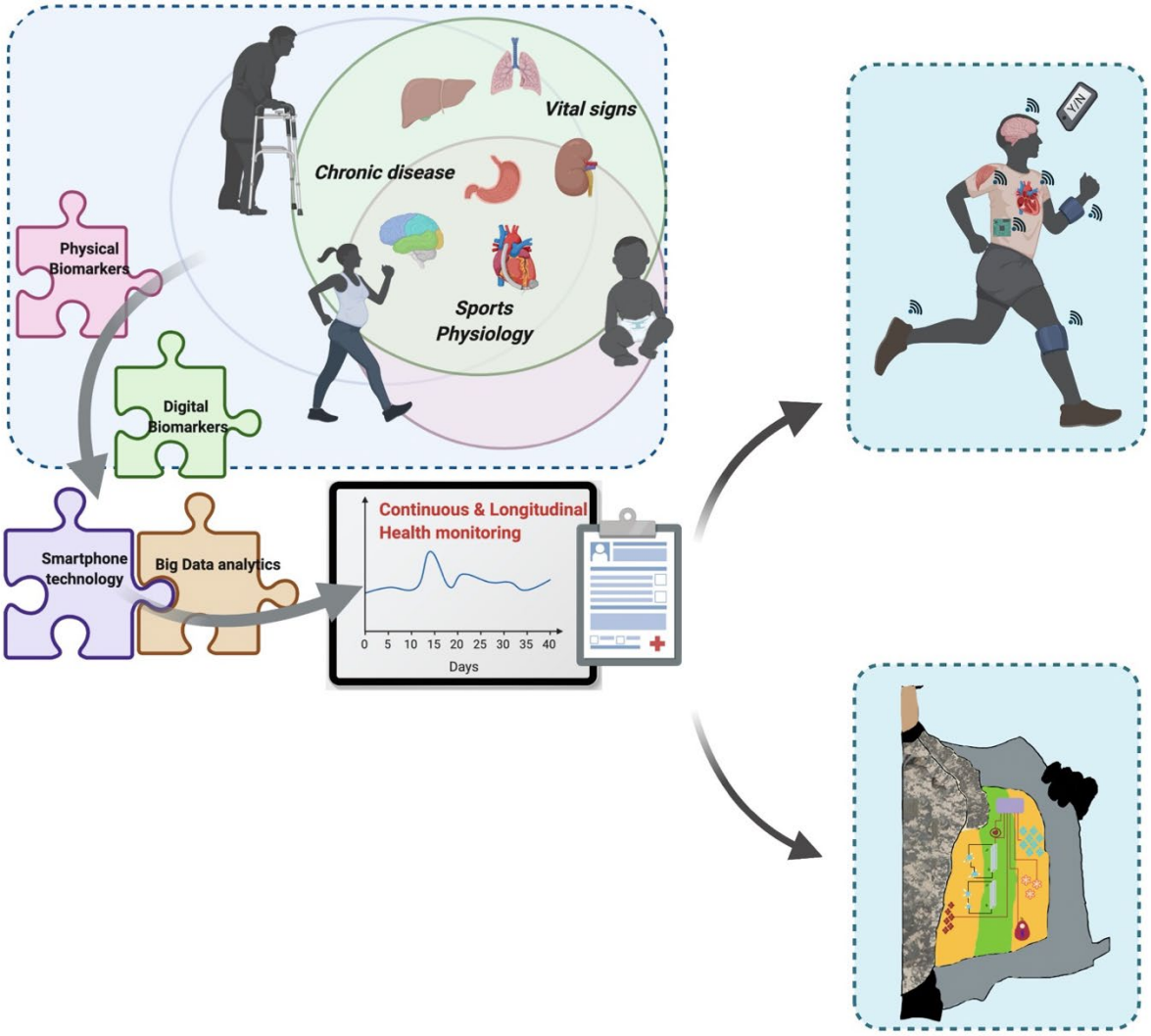

Figure 1.1. Overview of emergent biosensors that have been explored for continuous monitoring of diseases and health status created by authors using BioRender.com.

1.3 Need for combinatorial biomarker detection

Technologies centered around wellness management and early detection of underlying disease conditions necessitate the need for biosensors to perform simultaneous, combinatorial analysis of biomarkers. From the perspective of clinical relevance in disease diagnostics, detection of several targets on a single platform is indispensable for the accurate determination of specific diseases. Several instances require urgent treatment decisions to be made at the site of testing wherein evidence provided by a single biomarker is inadequate for determining the disease diagnosis and further plan of treatment. Hence, it is reliable to screen multiple analytes combinatorially for biomarker quantification. Customarily, combinatorial detection is accomplished by assigning separate spaces or detection sites for biomarker detection through the use of wells, different channel networks, electrode arrays, and labels such as enzymes, redox molecules, dyes, and beads to achieve an extended dynamic range of sensing. In addition, clinical applications require combinatorial diagnostic platforms to operate on low sample volumes with easy access to non-invasive body fluids; be user-friendly; require minimal user intervention; have rapid response time; have an extended shelf-life; give out accurate results adhering to clinical and laboratory standards institute (CLSI); be low-cost and portable; suitable to use with disposable test strips; perform continuous monitoring; and be amenable with smart phone technology in resource-limited settings. Some drawbacks of combinatorial biomarker detection are complicated device fabrication, assay development, signal analysis, readout complexity with the use of multiple labels for several analytes, and cross-reactivity between spatially separated detection sites through diffusion[2].

1.4 Existing commercial technology

Tremendous efforts have gone into extracting clinical information from digital biomarkers for self-health management such as heart rate, blood pressure, temperature, respiratory rate, motor function, sleep patterns, nervous functions, cognition, etc. for the development of wearable devices[10]. Existing commercial biosensing technology for disease biomarker detection has been brought into reality by lab-on-chip systems employing microfluidics to facilitate rapid, low-volume, user-friendly, miniaturized detection of multiple targets. Although the current state-of-art lab technology is in the developmental stage due to rigorous requirements and complexity, substantial progress has been made in the personalized healthcare and lifestyle monitoring arena by reducing features to minimize complexity and use disposable cartridges for easy fluid handling towards integration of exiting technology on a miniaturized platform. Point of care diagnostic devices employ paper, array, and bead-based systems to perform multi-analyte detection. Lateral flow assay-based detection is by far best-established owing to their nanomaterial-based recognition sites for signal amplification and quantification of multiple analytes using optical and electrochemical signal transduction techniques[11]. Electrochemical sensing and colorimetric approaches are preferred for combinatorial detection of biomarkers to enhance the sensitivity of detection and enable label-free, wash-free, reagent-free monitoring of biomarkers. The commercial success of hand-held analyzers for continuous detection of electrolytes and metabolites have made electrochemical biosensors popular in wearable and diagnostic platforms due to their performance metrics, portability, cost-effectiveness, low analyte volume requirements, ease of design, and convenient interfacing with low power electronics[12]. In the past decade, microfluidic principles have been applied to paper-based lateral flow assay systems to manipulate liquids and accurately

control fluid transport to provide higher degree of multiplexing and detection sensitivity. Integration of microfluidics on flexible materials has opened up new prospects for continuous monitoring of multiple target molecules by real-time sampling of body fluids for accurate biomarker quantification. Other detection technologies include array and bead-based systems. Array-based systems consist of individually functionalized microdot or electrode arrays for high throughput biomarker screening. Bead-based systems are favored primarily due to highly specific responses to biomarkers as these systems detect individual biomarkers by distinguishing beads based on size, shape, color, redox labels, enzyme, or separation into different sections of channels.

1.5 Non-invasive biofluids for biosensing

Current medical diagnosis techniques rely heavily on highly standardized blood sampling techniques that are intrusive and obstructs the extraction of temporal dynamics of biomarkers required for continuous monitoring. Frequent blood sampling poses a risk of infection, especially in elderly, neonatal, and immunocompromised populations. In addition, blood sample handling requires trained individuals and further processing to isolate plasma or serum. In order to enable non-invasive and pain-free continuous monitoring of biomarkers, alternative counterparts of blood such as human sweat, tears, saliva, urine, and interstitial fluids are being researched to provide information on health and disease status. With the advent of wearable technology eccrine sweat has emerged as a promising source of biomarkers. Human sweat consists mainly of water (~99%), electrolytes, metabolites, hormones, proteins, nucleic acids, and micronutrients that have shown a strong correlation with blood-based biomarkers[13], [14]. The biomarkers in sweat partition from the blood through the cell membranes by paracellular pathways, active channels, and vesicles which can help draw important conclusions about sweat-blood biomarker correlations. Ions such

as sodium, chloride, potassium, calcium are found to be in higher ranges (mM) in sweat than in blood. These ions play a pivotal role in maintaining the body's hydration status and predict muscular activity. Biomarkers such as lactate and urea partition from blood or are produced locally by the sweat glands are found in mM ranges which are relevant in monitoring the body's endurance during intense physical activity. Larger biomolecules such as glucose, neuropeptides, and hormones are found in nM and pM ranges which carry information on the body's glycemic indices, stress levels, and clinical depression. Other analytes such as drugs, heavy metals, and alcohol are found in human sweat when the body releases its toxins naturally[15]. Cytokines are found in human sweat in pg concentrations during infections and are released from the intravascular membrane and diffuse into the eccrine sweat glands through the dermal interstitium[16]. Unlike other body fluids that can be collected directly, sweat has to be induced to produce sufficient volumes for biomarker analysis. Sweat induction relies on many factors such as exercise intensity, stress, temperature, humidity, hormonal imbalance, diet, and sweat inducing chemical compounds[17]. Iontophoresis is a localized sweat-inducing method used in diagnostic applications where movement is constricted. Herein, a sweat-inducing chemical such as pilocarpine is delivered transcutaneously by the application of a low-intensity electric current (~3.0mA) for a short duration (~5 mins) to collect sweat volumes in the range 15μL-0. 5mL.In this era of wearable technology, sweat-based wearable sensors can provide an avenue for non-invasive, non-destructive biomarker continuous monitoring with less sample degradation, efficient sampling, and robust biomarker detection. However, further attention is required to address some of the key challenges of the deployment of these sweat-based wearables in practical scenarios such as improving the availability of sweat biomarkers, sustained production of adequate sweat volumes

and maintaining the sample integrity under varying environmental conditions[15][17]. Some of the technological challenges that have to be resolved for the commercial development of sweat wearables are the development of efficient power supply methods, advanced signal processing, system integration methods, and reduction of delays in information relay to healthcare providers.

Recent research in the development of diagnostic platforms for self-monitoring of disease symptoms has opened opportunities for exhaled breath condensate (EBC) as a non-invasive matrix of disease markers. Given that the global population is impacted by an ongoing COVID-19 pandemic and increased need for self-sample collection and analysis, EBC serves as a tool that can yield clinical information regarding respiratory infection and evaluate further course of treatment[18]. Current techniques to assess airway inflammation such as bronchoscopy and bronchoalveolar lavage are not recommended in clinical settings due to their invasiveness, tedious procedures, and user discomfort. Although blood and serum diagnostic tests are considered a standard, they may not necessarily reflect localized airway inflammation. EBC's dominant component is condensed vapor (~99%), hydrogen peroxide, reactive oxygen species, reactive nitrogen species, isoprostanes, cytokines, leukotrienes, prostanoids, proteins, enzymes, hormones, and micro-RNA's[19]. EBC is derived from airway lining fluid when turbulence from the exhaled air creates nebulized droplets and is subsequently condensed on contact with a cold condenser surface (-20-80°C). EBC is collected during tidal breathing at a defined temperature using a nose-clip with saliva traps to prevent salivary contamination and a one-way valve to avoid inhalation or condensation of ambient air through the condenser. EBC sampling can be done in healthy individuals in a sitting position, mechanically ventilated patients through an in-line connection with the expiratory circuit of the ventilator, and in children through face masks. A collection time

of 3-60mins can yield 1-2mL of EBC. EBC biomarker profiling is generally done using mass spectroscopy, multiplexed array systems, and NMR techniques[20]. Limited research has been done in the area of metabolic and inflammatory biomarkers in EBC. The advantages of using EBC lies in its non-invasiveness, pain-free analytics, availability of large volumes, the ability to continuously monitor disease status, and provision of rapid and low-cost diagnostic solutions. However, the standardization of normal biomarker reference points has to be determined which would require screening of large EBC sample set representing the global demographic. Some of the challenges faced in EBC based-biosensor development are – (1) sensor stability, (2) experimental accuracy effected by humidity and temperature, and (3) need of correlation with a laboratory gold standard[21].

1.6 Prior Publication

This chapter has been adapted from two prior publications:

1. Ashlesha Bhide, Antra Ganguly, and Tejasvi Parupudi contributed equally. Ashlesha Bhide, Antra Ganguly, and Tejasvi Parupudi cowrote the manuscript, Mohanraj Ramasamy contributed to the schematics, Sriram Muthukumar and Shalini Prasad conceived the framework for this mini review and reviewed the manuscript. This article was published in ACS omega in 2021. This article has been reproduced by permission from American Chemical Society and the link to this article is: https://doi.org/10.1021/acsomega.0c06209
2. Some parts of this chapter have been published as a part of a book chapter in Reference module in Biomedical Sciences. This chapter has been reproduced by permission from Elsevier publishing company and link to this chapter is: https://doi.org/10.1016/b978-0-12-822548-6.00044-3.

CHAPTER 2

SIMULTANEOUS LANCET-FREE MONITORING OF ALCOHOL AND GLUCOSE FROM LOW-VOLUMES OF PERSPIRED HUMAN SWEAT

2.1 Abstract

A lancet-free, label-free biosensor for simultaneous detection of sweat glucose and alcohol was demonstrated using zinc oxide thin films integrated into a nanoporous flexible electrode system. Sensing was achieved from perspired human sweat at low volumes (1–3μL), comparable to ambient conditions without external stimulation. Zinc oxide (ZnO) thin film electrodes were surface functionalized with alcohol oxidase enzyme and with glucose oxidase enzyme towards developing an affinity biosensor specific to the physiologically relevant range of alcohol comprising of 0-2 drinks (0 mg/dL to 50mg/dL) and physiologically relevant range of glucose ranging from hypo to hyper-glycaemia (50mg/dL to130mg/dL) in perspired human sweat. Sensing was achieved by measuring impedance changes associated with alcohol and glucose binding onto the sensor interface using electrochemical impedance spectroscopy with a dynamic range from 0.01mg/dL to 200mg/dL and a limit of detection of 0.01mg/dL for alcohol in human sweat. Sensor calibration in synthetic sweat containing interferents (25mg/dL to 200mg/dL) and comparison using regression and Bland-Altman analysis of sweat sensor performance was done with reference standards. Combinatorial detection of glucose and ethanol in perspired human sweat and comparison of sweat sensor performance with reference blood glucose monitoring system that we expect would be relevant for pre-diabetics and diabetics for monitoring their glucose levels and alcohol consumption.

2.2 Introduction

Alcohol consumption is prevalent in the United States, with an estimated 109 million Americans who drink alcohol. The effect of alcohol on the causation or prevention of diabetes has been studied. It appears that there may be a U-shaped relationship between alcohol and type 2 diabetes such that there is a higher risk of developing diabetes with both low and high intake levels and a lower risk with moderate intake[22]. Moderate alcohol consumption was defined as ~ 5–30 g/day. This corresponds to about 0.5–2.5 drinks per day[23][24]. Alcohol consumption in people with type 2 diabetes can result in hypoglycemia because of decreased gluconeogenesis, decreased glycogenolysis, and possibly reactive hypoglycemia in response to carbohydrate intake. However, most data are retrospective or observational, and hence there is an immediate and significant need to determine the long-term effects of alcohol consumption on glycemic control, self-management behaviors, and the complications of diabetes. In this research, we demonstrate the first technological proof of feasibility in using human sweat-based biosensors towards combinatorial monitoring of alcohol and glucose content in perspired human sweat towards the larger goal of designing diagnostics wearables that can quantify and dynamically report both alcohol and glucose content from users. The use of wearable biosensing in health care in the form of diagnostics wearables is still in a stage of infancy, but market research from TrustMarque points toward 81% of respondents wanting more use of connected devices in the area of chronic disease management[25].Wearable biosensing technologies that detect biomarkers from human sweat have evolved from this need for non-invasive monitoring of social lifestyle choices coupled with a view of chronic disease management. Human sweat is one such biomarker rich fluid containing valuable medical information that can be the key driver for developing sweat based point-of-care

health management devices[26]. Sweat is a preferred candidate for bodily fluid-based analysis amongst others such as serum, saliva, and urine due to the ease of gland stimulation, sample gathering, and analysis. Biosensors that monitor human sweat biomarkers are required to have a wide dynamic range of response, robust sensitivity, and specificity in the physiologically relevant range. Non-invasive sweat monitoring is one of the most researched areas in recent times[27]. Alcohol biosensing has gained attention in clinical and forensic analysis of bodily fluids, and food and beverage industries [see supplementary table S1 of [28]]. Alcohol abuse and addiction are leading causes of violence, driving under influence causing fatal vehicle crashes and poses a severe threat to the lives of other drivers. Blood alcohol content (BAC) is an accurate indicator of ingested alcohol in the human circulatory system but requires tedious procedures (e.g., gas chromatography) and trained personnel to analyze samples[29]. Breathalyzers are currently being used to indirectly estimate BAC through the measurement of breath alcohol content (BrAC). The standard breath alcohol to blood alcohol ratio is 2100:1 is based on Henry's law which estimates breath alcohol present in the exhaled volume of air from the blood alcohol present in the bloodstream[30]. Breath alcohol is susceptible to other alcohol components present in the environment and hence generates false positives. About 1% of alcohol metabolized by the liver leaves the body through sweat through diffusion from the skin and secretion from eccrine gland[31]. Previous studies have established a correlation between transdermal alcohol content and blood alcohol content[32]. Alcohol consumption modifies glucose homeostasis exerting contradictory effects on blood glucose levels contingent on nutrition states. Diabetes Mellitus requires frequent monitoring of glucose levels with glucose being present in the range 0.1mg/dL to 50mg/dL in human sweat[33]. Alcohol consumption in a fasting state induces hypoglycemia

affecting the process of gluconeogenesis; the response to alcohol intake in a fed state is the development of hyperglycemic condition inhibiting the effects of insulin[29]. Turner *et al.* studied the effects of alcohol consumption on glucose levels the next morning in Type I diabetes individuals. Moderate consumption of alcohol (~ 2 standard drinks) accompanied by the intake of food increased chances of developing delayed, acute hypoglycemia after breakfast the following morning[34]. The premise of this research is to demonstrate a lifestyle monitor based on sweat alcohol detection designed on a flexible platform towards building a wearable, point-of-care diagnostic for (1) Glucose management to monitor blood glucose levels after consumption of alcohol (2) addressing the rising need for controlling alcohol induced fatalities and damages.

2.3 Results and Discussions

The organization of this section organized is as follows (1) Structural characterization and functionalization of the developed sensor for alcohol sensing; (2) Evaluation of sensor performance in synthetic sweat buffers through AC and DC step based techniques; (3) Evaluation of sensor performance and calibration in human sweat through AC based technique; (4) Sensor calibration in synthetic sweat containing interferents and comparison of sweat sensor performance with BACtrack® S80 Pro breathalyzer; (5) Combinatorial detection of glucose and ethanol in human sweat and comparison of the sweat sensor performance with Accu-Chek® Nano SmartView blood glucose monitoring system.

2.3.1 Structural characterization and functionalization of the developed sensor for alcohol sensing

Human eccrine glands secret sweat at the rate 5-10nL/min/gland typically which necessitates the use of low volumes for sensor functioning when it comes in contact with the skin[35]. We use flexible, nanoporous polyamide membranes as the substrate material to fabricate the zinc oxide sensor stack. Analysis volumes as low as 1-3µL are maintained through this study of biosensing in sweat buffers. Nanopores of the flexible substrate allow absorption of sweat molecules which are carried across to the sensor surface when sweat is introduced into the membrane. Affinity biosensing is primarily achieved through the capture probes bound to the active sensing region which interact with the biomolecules of interest as shown in Figure 2.1A. Figure 2.1B shows the wicking of the 1-3µL volume of the sweat on the active sensing region on both faces of the sensor and sensor flexing when subjected to bending. The intercalated nanopore structures of the polyamide substrate act as a biomolecule sieve allowing only desirable biomolecules to travel to the sensor surface. Figure 2.1C shows the scanning electron microscope (SEM) image of ZnO sputtered on polyamide substrate with energy dispersive X-ray analysis (EDAX) spectrum represented in the inset. The peak at 1KeV corresponds to the Zn L-shell of ZnO indicating the deposition of the film within the nanopores. Nanoconfinement of biomolecules based on size offers an enhanced signal-to-noise ratio (SNR) which is feasible for detecting small analytes because human sweat consists of ions and lipids that would otherwise contribute to the noise factor[36]–[39]. The binding events occurring within the nanopores in the vicinity of the electrode are reported in terms of impedance changes contributed by electrical double layer modulations and electron charge transfer.

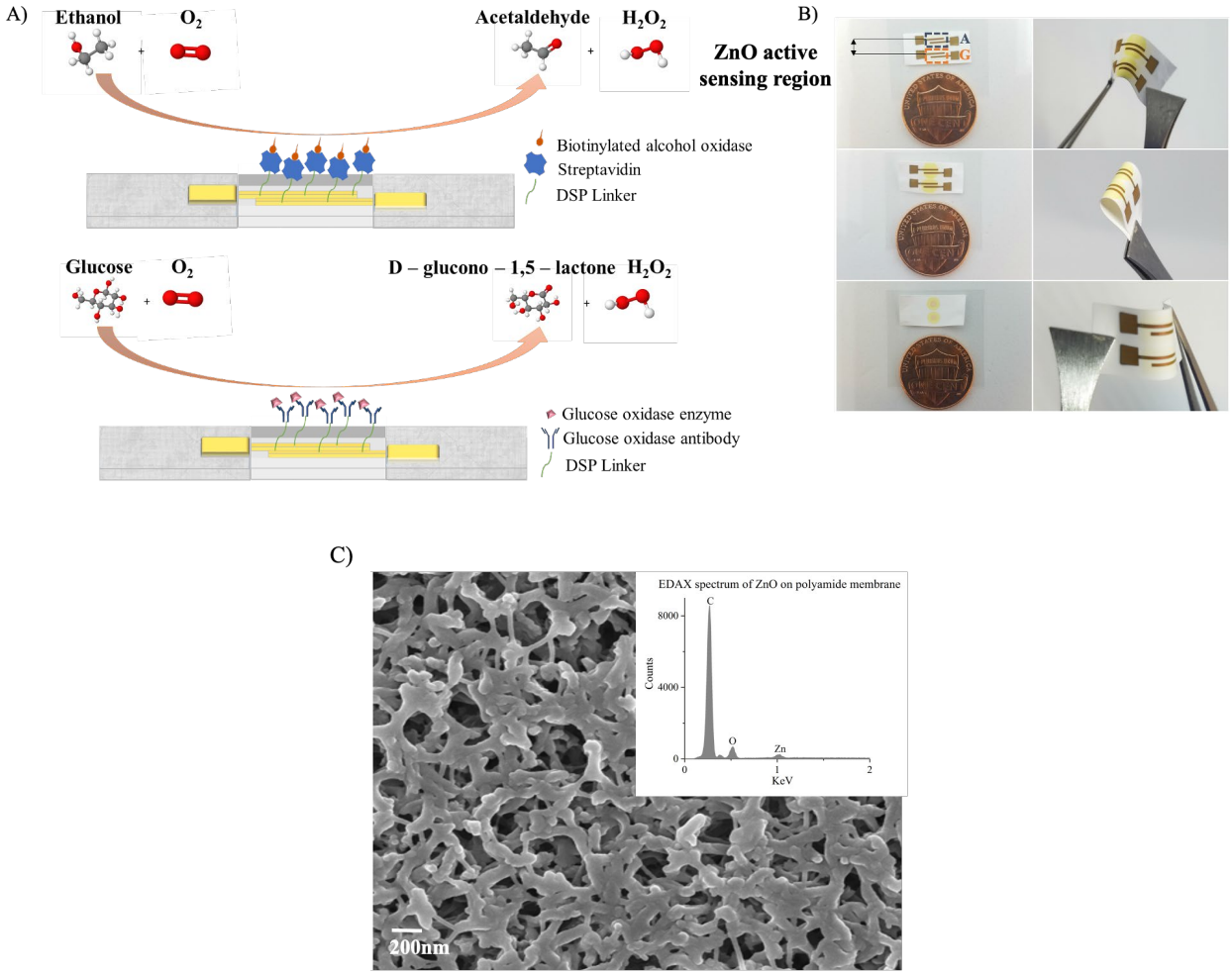

Figure 2.1.(A) Schematic of the immunoassay for the combinatorial detection of alcohol and glucose (B) Sweat sensor array showing fluid confinement in the active sensing region, sensor flexibility, and size comparison with one cent (C) SEM of polyamide membrane sputtered with ZnO. Inset shows the EDAX spectra of the sputtered membrane surface.

2.3.2 Evaluation of sensor performance in synthetic sweat buffers through AC and DC step-based techniques

An AC based signal transduction technique electrochemical impedance spectroscopy is used to record the sensor response over a range of frequencies from 1MHz to 1Hz with a small AC excitation signal. This technique enables us to understand the charge modulation arising at the electrode-electrolyte interface as an outcome of biomolecular binding events and catalytic oxidation of alcohol by the enzyme occurring at the electrode surface. The interaction of a buffer with a semiconducting electrode surface modulates the capacitive reactance which is primarily driven through charge accumulation within the electrical double layer (EDL). These dynamic changes occurring within the EDL at the electrode-electrolyte interface are derived from the imaginary impedance (Z_{imag}) component characterized by EIS. Charge modulation in the EDL is affected by its Debye length (λ_D) which is also a measure of the thickness of the double layer. The thickness of the Debye length is influenced by the ionic concentration of the buffer and hence dictates the charge screening effects at the electrode-electrolyte interface[40], [41].

The responses of the sensor to varying ethanol concentrations in 0.1xPBS and synthetic sweat (SS) buffers of pH 4 to 8 captured in terms of percentage changes in imaginary impedance (Z_{imag}) at 50Hz and 500Hz are shown in Figures 2.2A and 2.2B respectively for N= 3 replicates. The percentage change in Z_{imag} is calculated as the variation in the impedance of the ethanol concentration response with respect to impedance of baseline measurement using the expression (100*(baseline Z_{imag} - spiked ethanol concentration Z_{imag})/baseline Z_{imag}). A signal to noise (SNR) of 3 is chosen to compute the specific signal threshold (SST)[42]. SST is estimated by the expression (3*(standard deviation baseline /average baseline)). Control studies are performed by

spiking 0.1xPBS with ethanol concentrations ranging from 0.01mg/dL to 200mg/dL that corresponds to the alcohol content present in perspired human sweat after consumption of 0 to 5 standard drinks. In this study, we chose to use 0.1x PBS buffer (pH ~ 7.4) which has a λ_D of ~2.5nm which is approximately equivalent to the size of biomolecules. Hence, the effect of charge screening on biosensing is minimized and a dose-dependent impedance response was observed. The percentage change in Z_{imag} for 0.01mg/dL ethanol concentration in 0.1xPBS at 50Hz and 500Hz is ~ 8.5%. At 200mg/dL ethanol concentration, the percent changes in Z_{imag} observed at 50Hz and 500Hz are ~30-35% respectively. The percentage impedance changes in Z_{imag} are distinguishable from its SST for the lowest ethanol concentration of 0.01mg/dL which is identified as the limit of detection (LOD)[20] . The dynamic range of ethanol in 0.1xPBS is 0.01mg/dL to 200mg/dL. Smaller percentage changes in Z_{imag} are observed in 0.1xPBS owing to the lower electrical conductivity of the buffer contributing to smaller charge accumulation changes[43]. The percentage changes in Z_{imag} across the frequency range 50Hz-500Hz increase as the pH of synthetic sweat buffer varies from pH 4 to pH 8. At 0.01mg/dL ethanol concentration, the percentage changes in Z_{imag} for SS of pH 4 in the range 50Hz-500Hz are ~11-13%. The percentage changes in Z_{imag} at 200mg/dL ethanol concentration for SS of pH 4 in the range 50Hz to 500Hz is ~40-45%. For SS of pH 6, the percentage changes in Z_{imag} for 0.01mg/dL and 200mg/dL ethanol concentrations are observed to be ~24- 26% and ~60% respectively across the 50-500Hz frequency range. In SS of pH 8, the percentage changes in Z_{imag} for 0.01mg/dL ethanol concentration lie between ~25-30% for 50-500Hz range while for 200mg/dL ethanol concentration the percentage change is found to be ~63% in the frequency range 50Hz-500Hz. The LOD is found to be 0.01mg/dL while the linear dynamic range (LDR) is preserved in the range 0.01mg/dL to

200mg/dL for synthetic sweat buffers of pH range 4 to 8. Heinonen *et al.* have demonstrated the stability of nanotextured ZnO films in acidic and basic conditions over an 8-week period[44]. We observed a higher response to ethanol dose concentration in synthetic sweat buffers of pH 6 and pH 8 than pH 4. The pH values of buffer solution favorable for a stable enzyme activity lie in the range 6.0-8.0[45], [46]. Lower percentage changes in Z_{imag} at lower pH's can also be attributed to the H^+ ions from the surrounding buffer that interfere with the charge modulation in the EDL at the electrode-electrolyte interface[24]. The ZnO sensors used in this work can be operated over a frequency window of 50Hz to 500Hz as the percentage change in Z_{imag} is preserved for buffers over varying pH ranges allowing for the sensors to be interfaced with portable electronics and tuned as per their frequency operation range.

Chronoamperometry (CA) technique allows for the measurement of non-faradaic capacitive current generated at the electrode-electrolyte interface by applying a step DC potential. The chronoamperometric response curves, as shown in Figure 2.2C for N= 2 replicates, represent the dose dependent changes in double layer capacitance through the charging currents in SS of pH 6. The current spike seen within ~1s of the response is a result of non-faradaic charging of the electrical double layer following which there is an exponential decay in the current that is termed steady state current. The steady state current represents a linear change between 2.8-4.8µA with increasing ethanol concentrations in the range 0.01mg/dL to 200mg/dL and is represented as a calibration curve as shown in Figure 2.2D. The sensitivity calculated from the calibration curve is 0.2±0.02µA/mM with the R^2 of 0.986 which is comparable to the sensitivity reported by Kim *et al.* which demonstrates a wearable tattoo sensor based on the amperometric detection of alcohol in sweat using alcohol oxidase enzyme by using printed Prussian blue electrode[47].

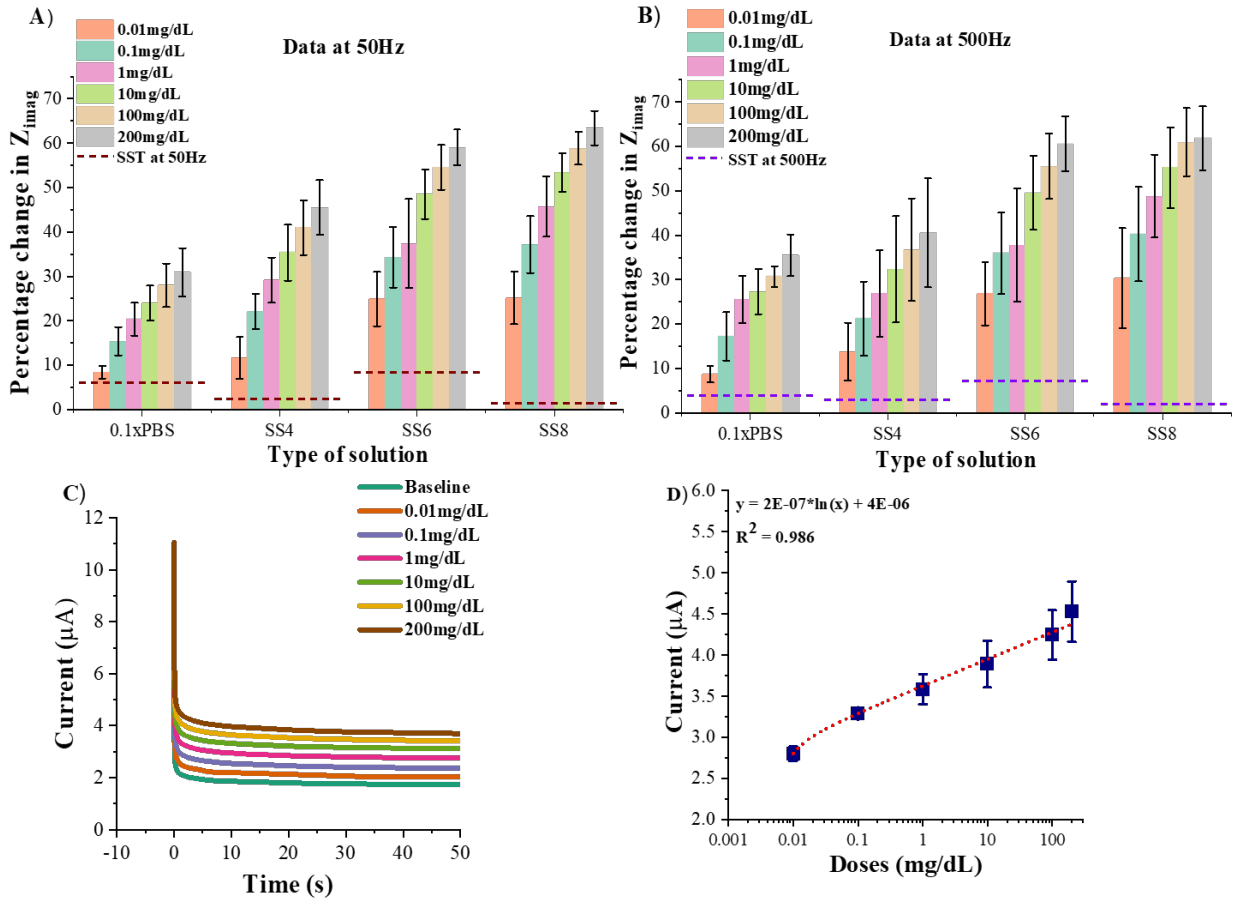

Figure 2.2.(A) Calibration dose response of ethanol in 0.1xPBS and synthetic sweat buffers of pH 4 to 8 as a function of percentage change in imaginary impedance (Zimag) at 50Hz (B) Calibration dose response of ethanol in 0.1xPBS and synthetic sweat buffers of varying pH as a function of percentage change in imaginary impedance (Zimag) at 500Hz (C) Chronoamperograms for ethanol concentrations in the range 0.01mg/dL to 200mg/dL spiked in SS of pH 6 (D) Calibration curve plotted for ethanol concentrations from 0.01mg/dL to 200mg/dL spiked in SS of pH 6 in terms of steady state current.

2.3.3 Evaluation of sensor performance and calibration in human sweat through AC based technique

The response of the sensor in human (pH ~5.98) sweat spiked with ethanol concentrations over the frequency window 50Hz to 500Hz is shown in Figure 2.3A for N= 6 replicates. The percentage change in Zimag is analyzed over the frequency range from 1Hz to 1MHz. The outcome of this analysis is that highest SNR is obtained over the frequency window 50Hz to 500Hz with highest percentage change in Zimag being observed at 50Hz and the calibration trend being preserved across the frequency window. The sensor is sensitive within the chosen frequency window to capture the contributions from non-faradaic charge modulation. The same frequency window was used for evaluating the performance of the sensor in SS of pH 6. At 0.01mg/dL, the percentage change in Zimag between 50Hz to 500Hz is ~5-9%. The percentage change in Zimag at 200mg/dL ethanol within 50Hz to 500Hz is ~30-34%. The SST for ethanol detection in human sweat is calculated to be ~5-7%. The LOD of ethanol in human sweat is measured to be 0.01mg/dL. Higher standard deviation and lower percentage changes in Zimag are observed in human sweat relative to SS of pH 6 because of contributions from interferents present in human sweat. The Nyquist plot for ethanol detection in human sweat ranging from 0.01mg/dL to 200mg/dL over frequencies 1Hz-1MHz is shown in Figure 2.3B. The Nyquist plots can be divided into three regions. In the first region, real impedance (Zreal) component varies from 3.7KΩ to 8.7KΩ and Zimag varies from 500Ω to 1.35KΩ. This region corresponds to 1MHz–10KHz region on the Bode magnitude plots as shown in Figure 2.3C. There is a shift in the semicircle towards left side on the x-axis of the plot with increasing ethanol concentration. This shift can be attributed to the change in the solution resistance as more ethanol molecules are catalytically oxidized in the presence of AOx forming

reaction products. In the second region, corresponding to the mid frequency range 10Hz to 1KHz in the Bode magnitude plot, Z_{real} varies 5.6-13.2KΩ and Z_{imag} varies from 1.5-5KΩ. This represents the capacitive and charge transfer properties of the semiconducting oxide film deposited on the nanoporous membrane. In the low frequency region between 1KHz–10Hz, Z_{real} varies between 14-34KΩ while Z_{imag} varies between 4.1-15.4KΩ. These changes reflect the binding events occurring within the EDL across the interface contributing to the variations in the capacitive reactance. The equivalent circuit, as shown in Figure 2.3D, is represented by a Randles circuit models a charged electrode surface in contact with an ionic buffer consisting of biomolecules of interest forms an EDL at the interface. The charge accumulation within the EDL is measured by the double layer capacitance (C_{dl}); the solution resistance (R_s) is a measure of the resistance of the bulk solution extending beyond the EDL; the electron transfer between the enzyme biomolecule complex and the electrode is represented by the charge transfer resistance (R_{ct}). The first semicircle in the frequency range 1MHz-10KHz is a characteristic of the electrode material properties and is indicated as a parallel combination of resistor (R_{ZnO}) and a capacitor (C_{ZnO}). The second semicircle in the low frequency captures the changes within the EDL and is represented by a parallel combination of R_{ct} and C_{dl}. Using ZView® circuit fitting analysis tool, the experimental impedance spectrum for ethanol dose concentrations in the range 0.01mg/dL to 200mg/dL is fitted to the equivalent circuit shown in Figure 2.3D and tabulated in Table 2.1. The double layer capacitance shows a dose dependent response validating a higher charge accumulation in the EDL with increasing dose concentrations as a result of more target ethanol molecules being catalytically oxidized.

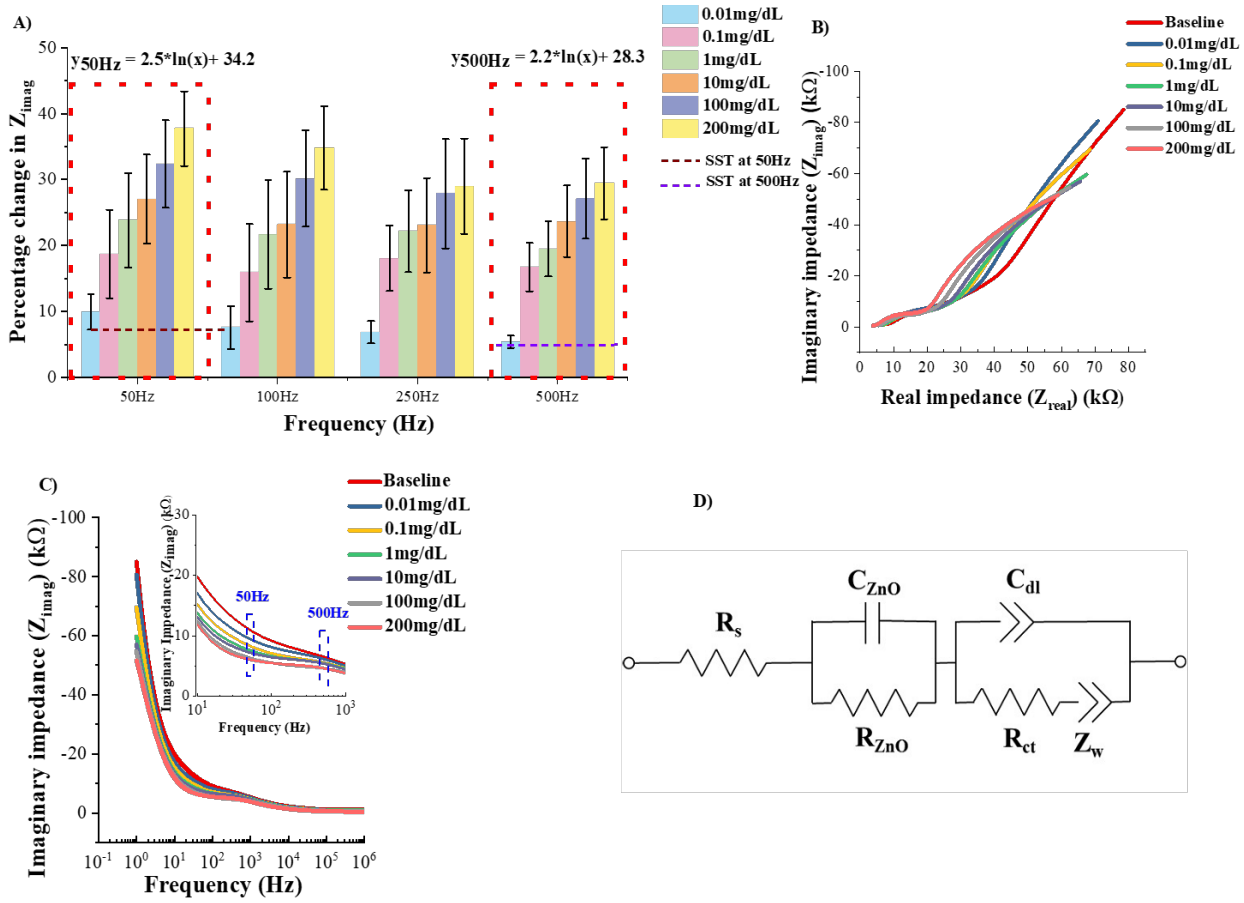

Figure 2.3.(A) Calibration dose response of ethanol in human sweat as a function of percentage change in imaginary impedance (Zimag) (B) Nyquist plots for ethanol concentrations 0.01mg/dL to 200mg/dL spiked in human sweat (pH ~5.98) (C) Bode magnitude plots for ethanol concentrations 0.01mg/dL to 200mg/dL spiked in human sweat (pH ~5.98). Inset shows the bode magnitude plots over the frequency range 10Hz to 1KHz (D) Equivalent circuit representation of the ethanol detection sweat sensor system.

Table 2.1. Extracted circuit fit parameters obtained by fitting the impedance response to the equivalent circuit.

Ethanol concentrations (mg/dL)	**Extracted circuit fit parameters**				
	R_s(KΩ)	**R_{ZnO}(MΩ)**	**C_{ZnO}(μF)**	**R_{ct}(KΩ)**	**C_{dl}(nF)**
Baseline	7.3	0.28	3.44	29.3	550
0.01	6.3	0.26	2.94	22.8	520
0.1	6.5	0.13	4.25	19.1	504
1	6.1	0.08	3.93	19.4	490
10	5.3	0.072	3.54	16.8	445
100	5.1	0.066	3.84	13.9	438
200	3.9	0.064	3.53	14.6	423

2.3.4 Sensor calibration in synthetic sweat containing interferents and comparison of sweat sensor performance and BACtrack® S80 Pro

An interference study was carried out in SS of pH 6 (N= 3 replicates) to validate the selectivity of ethanol in the presence of interferents such as glucose, lactate, uric acid, ascorbic acid, and creatine. The calibration dose response for ethanol ranging from 25mg/dL to 200mg/dL present in the interferent spiked SS of pH 6 at 50Hz and 500Hz is shown in Figure 2.4A. For 25mg/dL ethanol concentration, the percentage change in Z_{imag} at 50Hz and 500Hz is ~25-32% whereas the percentage change in Z_{imag} for 200mg/dL ethanol concentration across 50Hz to 500Hz is ~45-55%. The LOD of ethanol in SS of pH 6 with interferents is 25mg/dL. We observe an increasing percentage change in Z_{imag} with increasing ethanol dose concentrations as a results of increasing

charge accumulation within the EDL. Here, the SST is established by the impedance response obtained in the absence of target ethanol molecules. The interferents study suggests the ability of the enzyme biomolecule complex to selectively react to ethanol molecules by neglecting the presence of interferents.

The performance of our sensor system in the presence of interferents is compared to a commercially available breathalyzer BACtrack® S80 Pro. Blood alcohol content (BAC) measured by BACtrack® is used to estimate sweat alcohol content (SAC) by the equation BAC (g/L) = 0.71*SAC (g/L)[32]. The responses of our sweat sensor and BACtrack® to sweat alcohol measured in the presence of interferents are correlated to the actual ethanol concentrations presented to both the systems through (i) Regression analysis to quantify the goodness of a fit between the ethanol concentrations measured by developed sweat sensor and BACtrack® in comparison to the actual ethanol spiked interferent-based sweat samples presented to them (ii) Bland-Altman analysis to quantify the agreement between the two measurement techniques. Regression analyses was carried out on N= 4 ethanol spiked synthetic sweat samples of pH 6 in the range 25mg/dL to 200mg/dL with interferents as shown in Figure 2.4B. In section 2, we have demonstrated alcohol sensing in synthetic buffers over the frequency window 50Hz to 500Hz. We chose to present the outcomes of the statistical analyses at 50Hz in this section. The results of the analyses at 500Hz are displayed in supplementary in Figs. S1and S2[28]. R^2 value of 0.99 is obtained for sweat sensor correlation at 50Hz with the actual ethanol concentrations spiked in interferent based SS of pH 6. A significantly linear relationship can be drawn between the alcohol measured by the sweat sensor and the actual alcohol concentration dosed on it. We obtain an R^2 of 0.97 for the correlation analysis done between BACtrack® and the actual dose concentrations presented to it. Although a

linear fit is obtained between the actual and measured alcohol doses, a one-to-one agreement of the measurements is not seen between them. The linear fits obtained for both the sweat alcohol measurement techniques exhibit a linearly increasing offset with increasing ethanol dose concentrations. The offset observed in measuring the sweat alcohol content using BACtrack® is mainly because breathalyzers are designed to estimate BAC from a breath sample. We have simulated a breath like environment by nebulizing ethanol samples spiked in synthetic sweat of pH 6 with interferents [48][see Methods section]. The differences in analysis volumes utilized on both sensing platforms is another source of this offset. Figure 2.4C displays the Bland-Altman plots for sweat sensor compared to BACtrack® highlighting the bias and variations associated with the sensor and BACtrack®[49]. The normalized difference between sensor and BACtrack® is computed to address the variability in the differences of both measurement techniques. A mean bias value of 82.86% indicates that on an average the sensor estimates the ethanol concentrations accurately. All measurements except one lie within ±1.96SD of the mean bias and are spread equally on either side of the bias. We find six measurements lying within the ±95% CI [74.4–91.3%] with minimum of one measurement per ethanol concentration to be in these limits.

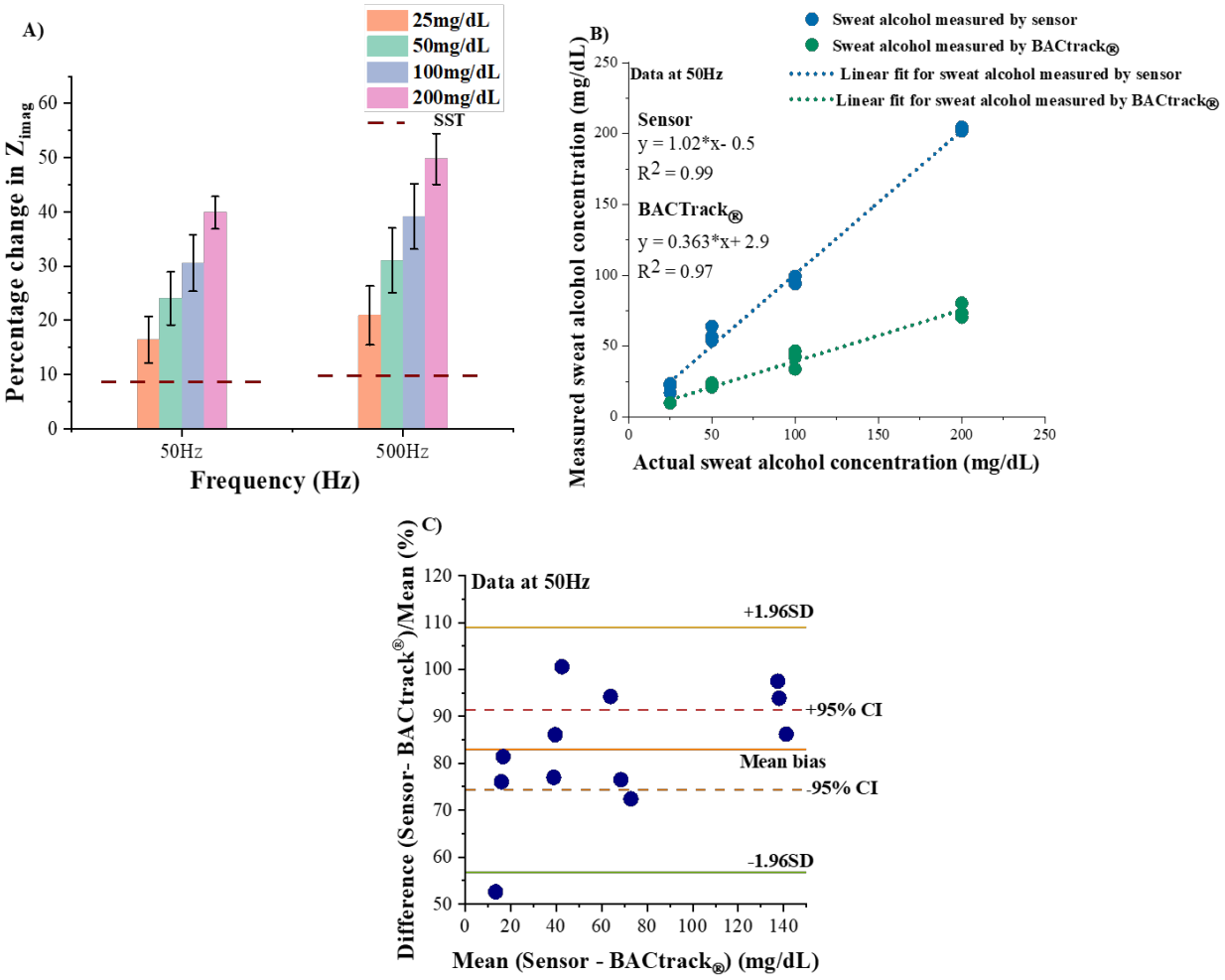

Figure 2.4.(A) Calibration dose response of ethanol spiked in SS of pH 6 with interferents as a function of percentage change in imaginary impedance (Zimag) (B) Regression plot for sweat ethanol measured by the sweat sensor at 50Hz and BACtrack® in comparison to the actual ethanol concentrations spiked in interferent based SS of pH 6 (C) Bland-Altman plot for the developed sweat sensor at 50Hz compared to BACtrack®.

2.3.5 Combinatorial detection of ethanol and glucose in human sweat and comparison of the sensor performance and Accu-Chek® Nano SmartView blood glucose monitoring system

In this section, we present the results of our study on glucose and alcohol level modulations when combined in human sweat and detected on the developed glucose and alcohol sensing systems. Previously, correlations between blood glucose and sweat glucose levels have been established which are utilized in this study[50]–[52]. A dose combination index table, shown in Table 2, consists of glucose and ethanol concentrations used to make the concoctions for this study. The impedance response to the dose combinations is presented as an imaginary impedance ratio (IIR) calculated relative to the baseline Z_{imag}. A specific analysis frequency of 100Hz for the combinatorial detection is chosen from previous work which reported glucose detection in human sweat using the same sensor platform[51]. The LOD and dynamic range for glucose detection in human sweat was reported to be 0.1mg/dL and 0.01mg/dL to 200mg/dL respectively. The sensitivity of glucose molecules to the assay was recorded as percentage changes in real and imaginary impedances which were attributed to the electron charge related to the biomolecule complex and ZnO sensor surface. The combinatorial effects of detecting a glucose level in the presence of alcohol as an interferent in human sweat on a glucose sensor is depicted as a box plot in Figure 2.5A for N= 3 samples. The average IIR varies from 0.11 to 0.21 with increasing glucose levels from 20mg/dL to 100mg/dL in the absence of alcohol with a tighter spread in the IIR's for increasing glucose levels. The average IIR for increasing glucose levels in the presence of alcohol (~ 2 standard drinks) as an interferent varies from 0.18-0.33[see supplementary table S2 of [28]]. The changes in IIR (δIIR) between the glucose levels in the absence and presence of alcohol lie in

the range 0.06-0.1. The shift and spread in IIR's for glucose levels in the presence of alcohol is a manifestation of background noise from human sweat, cross talk between the target molecules, and variations in the molarities of the target concentrations while combining them into a concoction. For this study, we chose to represent the IIR at 100Hz to draw a comparison between the combinatorial detection of glucose and alcohol on a glucose sensor in relation to an alcohol sensor. A box plot representation for the combinatorial detection of alcohol (0-2 drinks) in the presence of glucose at 100Hz for N= 3 samples as shown in Figure 2.5B. The average IIR range recorded by the sensor for a concoction consisting of only the interferent glucose in the absence of the target ethanol is 0.12-0.15; the IIR range recorded by the sensor for a concoction containing both the interferent and the target ethanol concentration (~2 standard drinks) is 0.21-0.13[See Table S2]. The modulation in the IIR in the presence of target molecules represented by the greater δIIR changes in the range 0.07-0.18 indicate the robustness of the alcohol assay in the presence of non-specific molecules. Higher impedance ratios observed in the presence of alcohol (~2 standard drinks) show a clear distinction in the frequency responses of the alcohol sensor in the absence and presence of alcohol.

Performances of the developed sweat glucose sensor and the commercially available Accu-Chek® Nano SmartView blood glucose monitoring system are gauged with relative to the actual glucose concentrations presented to both systems[53]. The correlation of the two measurement techniques with respect to actual glucose concentrations dosed is quantified by (i) R^2 value and (ii) Bland-Altman analysis. Figure 2.5C represents the correlation analysis performed on sweat sensor and Accu-Chek® using glucose samples (N= 3) without alcohol. Human sweat and blood samples are spiked with varying glucose and alcohol concentrations on the developed and the

commercial sensor respectively as per the dose combinations shown in Table 2.2. An R^2 of 0.97 for sweat and blood glucose samples without ethanol measured by both the systems relative to the actual sweat glucose concentrations dosed on sensor was determined. At 100mg/dL glucose concentration both the systems overlap. At 50 mg/dL glucose concentration, repeat measurements lie in proximity to each other with small deviations observed for the sweat sensor and Accu-Chek® respectively. For a low glucose concentration of 20mg/dL, only one blood glucose measure of the triplicate was recorded by the blood glucometer while the sensor recorded sweat glucose levels accurately with a ±1mg/dL deviation. Similar correlation analysis is performed on sweat sensor and Accu-Chek® to record their responses to glucose concentrations (N= 3) in the presence of alcohol and is represented in Figure 2.5D. R^2 values of 0.91 and 0.82 are observed for the sweat sensor and Accu-Chek® correlation respectively. The skew in the correlation can be attributed to the ethanol molecules that hamper the glucose measurements. The glucose sensor system developed is efficient in neglecting the effects of interferent ethanol molecules. According to ISO15197 standards, it is acceptable for commercial glucometers to show a ±15mg/dL deviation in measuring glucose concentration < 75mg/dL while for glucose concentrations ≥100mg/dL, the acceptable deviation is only about ±5mg/dL[54]. The differences between the developed sweat glucose sensor and Accu-Chek® Nano SmartView glucose monitoring system can be better inspected from the Bland-Altman plots as shown in Figure 2.5E. The mean bias for both the measurement techniques is -10 mg/dL or -0.39% indicating that differences between them are subtle and not significant. For sweat and blood glucose measurement performed in the absence of alcohol, 70% of the measurements lie within ±95% CI. At 100mg/dL glucose concentrations, the mean differences (circled by blue in Figure 5E) between developed sensor and Accu-Chek® meet

the ISO standards of measurement accuracy at glucose concentrations beyond 75mg/dL. Mean differences at 50 mg/dL glucose concentration vary by 25% from the mean bias owing to drift at low concentrations. Two measurements at 20mg/dL glucose concentration lying out of the limits of agreement due to the blood glucometer not being able to detect very low concentration and are recorded as zero. The alterations in the performances of the sensor and Accu-Chek® in the presence of ethanol (~2 drinks) is evident in the Bland-Altman plot. Triplicate measurements done at 20mg/dL glucose concentration exhibit a high degree of variability contributed by the interferent, sensor drift, and inability to obtain readings from the glucometer.

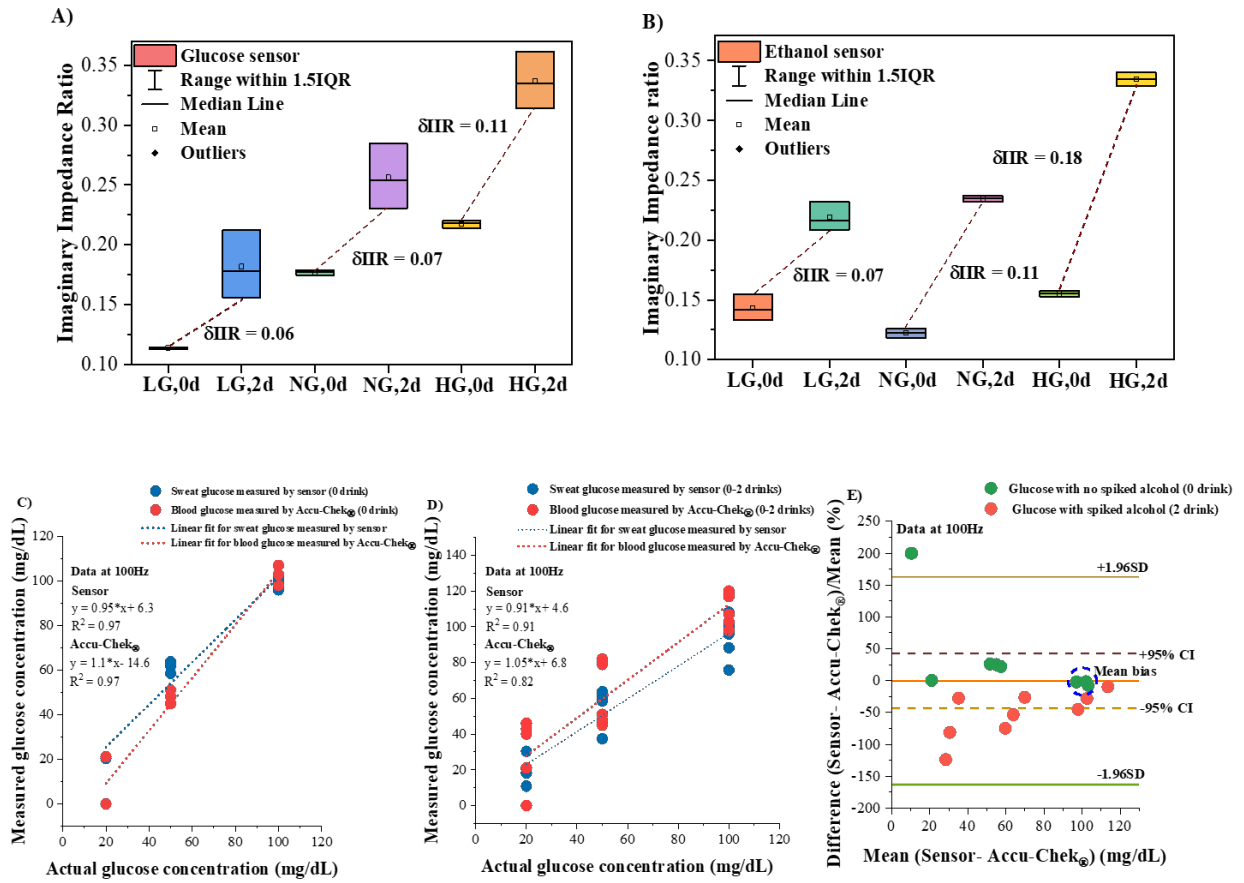

Figure 2.5.(A) Box plots for combinatorial detection of glucose levels in the presence of alcohol (0- 2 standard drinks) as an interferent in human sweat on a glucose sensor at 100Hz (B) Box plots

for combinatorial detection of alcohol (0-2 standard drinks) in the presence of glucose as an interferent in human sweat on an alcohol sensor at 100Hz (C) Regression plot for human sweat glucose measured by the sweat sensor at 100Hz and blood glucose measured by Accu-Chek® Nano SmartView glucose monitoring system in comparison to the actual glucose concentrations presented to them without alcohol (0 drink) (D) Regression plot for human sweat glucose measured by the sweat sensor at 100Hz and blood glucose measured by Accu-Chek® Nano SmartView glucose monitoring system in comparison to the actual glucose concentrations presented to them with and without alcohol (0-2 drinks) (E) Bland-Altman analysis for sweat sensor at 100Hz and Accu-Chek® for human sweat samples with varying glucose levels in the absence (0 drink) and presence of alcohol (2 drinks) at 100Hz.

Table 2.2. Dose combination index.

Dose combination index			
Dose combinations	**Labels**	**Glucose concentration (mg/dL)**	**Ethanol concentration (mg/dL)**
Low glucose level, zero drink	**LG,0d**	20	0
Low glucose level, two drinks	**LG,2d**	20	50
Normal glucose level, zero drink	**NG,0d**	50	0
Normal glucose level, two drinks	**NG,2d**	50	50
High glucose level, zero drink	**HG,0d**	100	0
High glucose level, two drinks	**HG,2d**	100	50

2.4 Conclusions

Wearable biosensing has provided a non-invasive platform to monitor metabolites in bodily fluids such as human sweat to track fluctuations in glucose levels on the consumption of alcohol as a part of social drinking in diabetic individuals that makes it imminent to address the need of developing a patch sensor that can accurately and non-invasively measure alcohol and glucose. The transdermal alcohol content is correlated in magnitude to blood alcohol content but lags in response time with respect to blood alcohol content which is governed by the parameters that control ethanol transport through the skin[55]. Desirable characteristics of wearable biosensors that make them commercially viable are enhanced sensitivity, capability to detect low target biomolecules in low analysis volumes within clinically relevant ranges, low power consumption, and cost-effectiveness. The novelty proposed in this research is an electrochemical biosensor fabricated on a flexible, nanoporous substrate to combinatorial detect glucose levels reliably in the absence and presence of alcohol in human sweat. Such a device is of help for pre-diabetic and diabetic individuals to monitor their glucose levels and limiting their intake of alcohol for healthier lifestyle choices. The findings of this study are that we could distinguish the effects of alcohol (~2 standard drinks) on low, normal, and high glucose levels prior to and post consumption of alcohol in low analysis volumes of 1-3μL. Standard agreement analyses as per Clinical and Laboratory standards institute (CLSI) such as regression and Bland-Altman analyses are used to compare the performance of the developed sensor in comparison to a commercially available Accu-Chek® blood glucometer. Electrical impedance spectroscopy is used to capture the impedance changes occurring at the interface of the sensor surface and the buffer containing the target biomolecules of interest. Biomolecule detection is affected by the ionic strength, pH, and conductivity of the

buffer. We demonstrated the performance of the sensor on detection of alcohol in changing pH levels of synthetic sweat and in the presence of other metabolites as interferents to show the selectivity of ethanol molecules to the immunoassay. The responses of the sweat sensor and a commercially available breathalyzer BACtrack® to synthetic sweat solution containing interferents are correlated to the actual alcohol concentrations made available to both the systems through regression and Bland-Altman analysis. Alcohol detection in human sweat is demonstrated over a linear dynamic range of 0.01mg/dL to 200mg/dL which is equivalent to 0-5 standard drinks with a lower detection limit of 0.01mg/dL. The detection of ethanol molecules in terms of changes in the capacitive reactance component of the impedance measurement can be attributed to the higher charge accumulation occurring within the EDL across the ZnO-sweat buffer interface and electron charge transfer occurring between the enzyme biomolecule complex and the ZnO surface. Nanoconfinement of target biomolecules within the pores of substrate reduces noise from other molecules present in the sweat matrix leading to a higher SNR and distinguishable impedance signal from background noise[36],[55].

2.5 Methods

2.5.1 Reagents and materials

Polyamide substrates with a pore size of 0.2µm were obtained from GE Healthcare Life Sciences (Piscataway, NJ, USA). The linker molecule dithiobis-succinimidyl propionate (DSP) and its solvent dimethyl sulfoxide (DMSO) were purchased from Thermo Fisher Scientific Inc. (Waltham, MA, USA). Salt-free streptavidin from Streptomyces avidiini, alcohol oxidase enzyme from Pichia pastoris, glucose oxidase from Asperigillus niger, D-(+)- glucose, absolute ethyl alcohol (≥

99.5%), and sodium bicarbonate (≥ 99.7%) were procured from Sigma- Aldrich (St. Louis, MO, USA). Sodium L-Lactate, Creatinine, L-Ascorbic acid, and Uric acid were obtained from Sigma-Aldrich (St. Louis, MO, USA). Biotin (Long arm) NHS was purchased from Vector laboratories (Burlingame, CA, USA). The antibody for glucose oxidase was obtained from Abcam (Cambridge, MA, USA). The antibody for glucose oxidase enzyme was diluted in 1X phosphate buffered saline (PBS, Thermo Fisher Inc., Waltham, MA, USA). Streptavidin was lyophilized in 1X PBS and biotin was dissolved in DMSO. Synthetic sweat was prepared as per the recipe described in Table 2.2 of M.T. Mathew *et al*[56]. The pH range was varied by varying the concentrations of the constituents. Single donor human sweat of pH ~6 was purchased from Lee Biosolutions Inc. (Maryland Heights, MO, USA). No preservatives were added to this product, and it was stored at below -20°C. Anticoagulated venous or arterial blood sample drawn from a patient was obtained from Carter BloodCare (Plano, TX, USA). Experiments were performed within two days of obtaining the blood samples. All ethanol dilutions are made in synthetic and human sweat. All glucose dilutions were made in human sweat. 0.1X PBS was made by diluting PBS in deionized water (conductivity 18.5 MΩ.cm). BACtrack® S80 Pro was purchased from Amazon.com, Inc. (Seattle, WA, USA). MQ5600 Nebulizer machine system was purchased from Mountainside Medical Equipment (Marcy, NY, USA). Accu-Chek® Nano SmartView blood glucose monitoring system and the test strips were purchased on the counter from CVS pharmacy (Plano, TX, USA).

2.5.2 Sensor fabrication

Fig 2.1B shows the sensor stack deposited on nanoporous polyamide substrate. The sensor stack consists of gold electrodes and a ZnO active sensing region. Gold electrodes are deposited using a shadow mask in a Temescal e-beam evaporator tool (Ferro Tec, Livermore, CA, USA). ZnO thin

films are sputtered using AJA Orion RF magnetron with a 99.999% ZnO target (Kurt J. Lesker) at room temperature. The thickness of the film is measured to be ~100nm using a Veeco Dektak 8 profilometer.

2.5.3 Structural characterization

The deposition of the ZnO thin film on the flexible nanoporous substrate is investigated and characterized through SEM images captured using SUPRA SEM (Zeiss, Oberkochen, Germany).
Sensor calibration for alcohol detection in synthetic and human sweat

The immunoassay protocol followed for the detection of alcohol in synthetic and human sweat is illustrated in Figure 1A. 10mmol of DSP linker is diluted in DMSO and functionalized on the sensor surface by dispensing 1-3µL volume for 3 hours. A PBS wash is carried out prior to incubation of streptavidin for 1 hour on the sensor surface [See Figure S3]. Another PBS wash is given post immobilization of streptavidin following which biotinylated alcohol oxidase enzyme is immobilized on the sensor surface by incubating for 15 minutes [See Figure S4]. Alcohol oxidase enzyme is biotinylated as per the recipe formulated by Du *et al* [57]. Synthetic sweat of desired pH is dosed on the sensor prior to introducing the doses and is considered as the baseline or the zero-dose step. Dilutions of ethanol made in synthetic sweat in the increasing range from 0.01mg/dL to 200mg/dL are dispensed on the sensor and incubated for 10 minutes. EIS measurements record the current flow taken using a potentiostat (Gamry Instruments, Warminster, PA, USA) after an AC excitation signal with a frequency sweep of 1Hz to 1MHz is applied. All measurements are carried out in dark and under ambient temperature conditions. Similar protocols are followed for detection of alcohol in human sweat and 0.1X PBS buffer solutions. CA measurements are performed using the same potentiostat after applying a constant step voltage of

200mV for 60 seconds. CA measurements are done for the same ethanol doses in synthetic sweat buffer of pH 6 to match the pH of human sweat (~6).

2.5.4 Sensor performance for alcohol detection in synthetic sweat with interferents and comparison with BACtrack® S80 Pro

Synthetic sweat of pH 6 is spiked with metabolites present in sweat by making additions of 5.6µM glucose, 3.7mM lactate, 8.8µM creatinine, 10µM ascorbic acid, and 4.2µM uric acid[58]. All ethanol dilutions are made in interferent spiked SS of pH 6 in the range from 25mg/dL to 200mg/dL and dispensed on the sensor. 6mL analysis volume of the same ethanol concentrations in the interferent spiked SS of pH 6 is used to nebulize the solution to mimic breath. The nebulized solution is passed into the mouthpiece of BACtrack® through a simple adapter system that connects the nebulizer output line to the mouthpiece of BACtrack® which further outputs BAC (%) readings corresponding to the concentration of ethanol solution used. The BAC (%) readings are converted into SAC (mg/dL) as per the equation mentioned in section 4.

2.5.5 Combinatorial detection of glucose and ethanol in human sweat and comparison of sensor performance with Accu-Chek® Nano SmartView blood glucose monitoring system for samples in the absence and presence of alcohol

Combinatorial detection of glucose and alcohol is done by preparing a concoction of glucose and ethanol in human sweat. Glucose is spiked in concentrations of 20mg/dL, 50mg/dL, and 100mg/dL in human sweat. Ethanol is spiked simultaneously in concentration of 50mg/dL in human sweat. Immunoassay protocol for glucose detection is followed as per the protocol outlined in Munje *et al*[51]. The glucose oxidase and alcohol oxidase enzyme biomolecule complexes are used on two

different sensors deposited on the same substrate as shown in Figure 1B. Combined concentrations of glucose and ethanol in the order as mentioned in Table 2 are dispensed in 1-3µL volume on the glucose and alcohol sensors individually in the regions depicted by G and A symbols in Fig 1B. EIS measurements post dose incubations are obtained in a similar manner with similar parameters as mentioned above. Test samples for blood glucose measurement using the Accu-Chek® blood glucose meter was prepared by spiking blood with glucose and ethanol concentrations are mentioned in Table 2. N=3 readings are obtained for every dose combination. No animal or human subjects testing was performed during data collection for this manuscript.

2.5.6 Statistical Analyses

All the data is analyzed using OriginPro software. Data is presented as mean± standard error of mean (SEM) throughout this manuscript. SEM is calculated for the number of replicates or repeats used for experimentation and are mentioned in the results section. Error bars are plotted in terms of SEM.

2.6 Acknowledgements

Funding for this research was supported by the National Institute on Alcohol Abuse and Alcoholism of the National Institutes of Health (R43AA026114). We acknowledge the contributions of Ms. Ankita Rugi, Ms. Pooja Hegde from Biomedical Microdevices and Nanotechnology Laboratory at University of Texas at Dallas for assisting in performing the experiments. We thank Mr. Jonathan Craven and Ms. Ambalika Tanak for helping with SEM and EDAX measurements. We thank Mr. Richard Willis for programming the data analysis software.

2.7 Prior publication

Ashlesha Bhide and Amreek Saini performed experiments and compiled the data from all the studies. Ashlesha Bhide fabricated the sensors and analyzed the data. Amreek Saini carried out the interferent study and BACtrack® related experiments. Sriram Muthukumar and Shalini Prasad conceived the design of the sensor stack and guided the experimental design. Ashlesha Bhide, Sriram Muthukumar, and Shalini Prasad interpreted the data and co-wrote the manuscript. This article was published in Scientific reports in 2018. This article has been reproduced by permission from Nature publishing group and the link to this article is: https://doi.org/10.1038/s41598-018-24543-4

CHAPTER 3

CLASP (CONTINUOUS LIFESTYLE AWARENESS THROUGH SWEAT PLATFORM): A NOVEL SENSOR FOR SIMULTANEOUS DETECTION OF ALCOHOL AND GLUCOSE FROM PASSIVE PERSPIRED SWEAT

3.1 Abstract

Wearable-IoT based low-cost platforms can enable dynamic lifestyle monitoring through enabling promising and exciting opportunities for wellness and chronic- disease management in personalized environments. Diabetic and pre- diabetic populations can modulate their alcohol intake by tracking their glycemic content continuously to prevent health risks through these platforms. We demonstrate the first technological proof of a combinatorial biosensor for continuous, dynamic monitoring of alcohol and glucose in ultra- low volumes (1-5µL) of passive perspired sweat towards developing a wearable-IoT based platform. Non-invasive biosensing in sweat is achieved by a unique gold-ZnO thin film electrode stack fabricated on a flexible substrate suitable for wearable applications. The active ZnO sensing region is immobilized with enzyme complexes specific for the detection of alcohol and glucose through non-faradaic EIS and CA. Biomolecular interactions occurring at the electrode-sweat interface are represented by the impedance and capacitive current changes in response to charge modulations arising in the double layer. We also report the detection of alcohol concentrations of 0.01mg/dL to 100 mg/dL and glucose concentrations of 0.01mg/dL to 50 mg/dL present in synthetic sweat and perspired human sweat. The limit of detection obtained for alcohol and glucose was found to be 0.1mg/dL in perspired human sweat. Cross-reactivity studies revealed that glucose and alcohol did not show any signal response to cross-reactive molecules. Furthermore, the stable temporal response of the

combinatorial biosensor on continuous exposure to passive perspired human sweat spiked with alcohol and glucose over a 120-minute duration was demonstrated.

3.2 Introduction

IoT platforms have emerged as a class of rapidly evolving embedded technologies that interconnects everyday objects in the environment with sensors using the internet to create application- specific solutions for remote, real-time monitoring[59], [60]. IoT has primarily made its way into the biosensing applications market through continuous self-tracking of health indicators and preventive medicine to provide immediate care without the need for hospitalization[61]. The rise in health risks and the steep increase in medical costs associated with treatments has led to the transformation of the current health care system into a highly industrialized ecosystem through the emergence of wearable personal devices. In addition to wellness management, wearable biosensing technology offers low-cost diagnostic solutions for chronic and fatal disease management in remote locations. Statistics suggest that the current market of wearable devices has benefited 80% of the consumers who have adopted wearable IoT enabled devices[62]. By 2021, healthcare devices will dominate the IoT space and are expected to grow into $45.4 billion market by then[63]. Wearable sensors provide users with the opportunity of seamless monitoring of the body's vital parameters and disease symptoms in a time-controlled manner. Biosensors can be integrated into a wearable platform by enclosing miniaturized sensors and electronics into smart portable form-factors with a capability to store data obtained in continuum and to periodically provide feedback to physicians for clinical diagnosis. Although in their nascent stages, wearable health tattoos and patches to monitor vital parameters such as ECG signals, respiration rate, oxygen saturation, and body temperature have forayed into the

market[64], [65]. With wellness devices gaining traction, one of the daunting challenges being faced in healthcare is the need for continuous, dynamic non-invasive monitoring of biochemical markers to understand chronic health conditions. Hence, integration of wearable diagnosis devices on an IoT platform proves promising for enabling continuous, point-of-care chronic disease detection improving early-stage detections and providing the user with warnings to seek medical care.

Existing wearables devices monitor digital biomarkers to track heart rate and physical activity, however, there is no information obtained on human health status which can be understood by probing biochemical markers. Biochemical markers play an acute role in determining the medical state of a person by quantifying relative changes in their molecular expressions[10]. Recent advances have been made towards understanding easily accessible human biofluids (sweat, saliva, urine) to non-invasively monitor biomarkers that reflect the physiological state of the body. Perspired human sweat is recognized to be a highly attractive source of valuable information for this type of monitoring due to its ease of access, presence of biomarkers, stimulation, collection, and analysis[66]. Literature studies show clinical correlations between sweat analyte and blood analyte levels which confirm that there is value in investigating sweat of wellness and disease management[49]. Some of the challenges faced in sweat-based sensing are (1) Very low sweat secretion rates of 1-5nL/min/mm^2 by the eccrine glands [35] (2) Large pH changes which affect ionic concentrations of sweat and (3) Changing the composition of sweat due to environmental factors[67]. Portable bioelectronic devices capable of detecting electrolytes, glucose, and lactate in small-volumes of sweat using amperometric techniques have been demonstrated previously[26], [68], [69]. Alcohol and glucose are two biochemical markers that

have a significant impact on the human lifestyle. Alcohol consumption by diabetics and pre-diabetics can alter blood sugar levels to either hyperglycemic or hypoglycemic stages depending on their nourishment state[23]. In the 18-50 age group of the U.S., an estimated population of 3 million are diagnosed with diabetes and 27. 4 million are prediabetic[70]. Almost 37% of the total U.S. population consumes alcohol at moderate levels[71]. A curvilinear relationship exists between alcohol consumption and incidence of type 2 diabetes posing serious risks to a large demographic within this age group[72]. Hence, there is an imminent need to monitor the effects of alcohol consumption on blood glucose levels for health and lifestyle management. Passive sweat based dynamic monitoring of these two biochemical markers offers a paradigm-shifting opportunity towards wholistic on body monitoring.

In this work, we have effectively demonstrated for the first time a wholistic approach towards biosensing alcohol and glucose combinatorially in a continuous, dynamic manner in ultra-low volumes (1-5μL) of passive perspired human sweat. Real–time monitoring of analytes gives a better understanding of the enzyme-analyte reaction mechanisms on continuous exposure to sweat which is required for the characterization of a wearable sweat-based biosensor. We also report the robust and stable performance of the combinatorial biosensor in perspired human sweat (pH ~5.98) and synthetic sweat buffers of varying pH ranges 4-8. We observed that pH changes in sweat microenvironment does not influence the performance of the developed biosensor enabling the continuous operation of the sensor without degradation in sensor response. AC- based EIS and DC-based CA techniques are the two detection modalities used to report the impedance and current changes in response to the target concentrations presented to biosensing system. EIS and CA provide an insight into the biomolecular interactions occurring at the electrode-buffer

interface through which information regarding the target analyte concentrations can be extracted[73], [74]. Additionally, the selectivity and the specificity of the combinatorial biosensor towards target analytes have been validated to demonstrate the feasibility of detection in human sweat buffer. Dynamic responses to varying levels of the biomolecules were demonstrated for a period of 120-minutes.

3.3 Results and discussion

3.3.1 Modulation of hybrid electrode-solution interface to evaluate the sweat-based combinatorial biosensor's performance through EIS and CA techniques

The combinatorial biosensor, as shown in Figure 3.1A, that was designed for the detection of alcohol and glucose employs a novel hybrid electrode with gold as the measurement electrode and a thin film of ZnO as the active sensing region on a flexible nanoporous substrate. The active sensing region of the biosensor is surface functionalized with specific enzyme biomolecule complexes for alcohol and glucose detection as shown in Figure 3.1B Biocompatibility and the ability to tailor the physical and chemical properties ZnO make it a suitable sensing element for enhanced biosensing performance[75], [76]. The response of the functionalized biosensor to the biomolecules of interest is captured through EIS and CA techniques. The sensor performance of the combinatorial biosensor towards detecting alcohol and glucose is characterized through the evaluation of a few key sensor metrics – dynamic range within the relevant concentration range, limit of detection, and signal to noise threshold[77].

The response of the combinatorial biosensor to the varying dose concentrations of the target biomolecule can be understood through non-faradaic electrochemical impedance spectroscopy.

Non-faradaic EIS is a label-free, AC based spectroscopic technique wherein a low amplitude sinusoidal excitation voltage over a wide frequency range is applied to the biosensing system and the corresponding frequency signatures of the combinatorial biosensor in terms of impedance are recorded[78]. Typically, in biological systems non-faradaic EIS allows one to understand the surface and bulk phenomenon that occurs in a biosensing system when a biological buffer solution interacts with a charged electrode surface[79]. We are interested in understanding the surface phenomenon that takes place at the hybrid electrode-solution interface which contributes to the impedance response of the combinatorial biosensor. The interaction of the buffer solution with the charged hybrid electrode results in the formation of an electrical double layer which comprises of a stern layer and a diffuse layer[41]. The stern layer is a thin, compact region consisting of ions with a charge opposite to that of the electrode held together by electrostatic forces of attraction. The diffuse layer consists of charges under the influence of residual electrostatic forces of attraction from the electrode surface and thermal motion. The EDL of the hybrid electrode-solution interface is modeled as a Randles circuit which is an equivalent circuit comprising of a solution resistance (R_s) in series with a parallel combination of a charge-transfer resistance (R_{ct}) and a double layer capacitance (C_{dl}) [See Figure S17 of [80]]. Capacitive effects are more predominantly observed in non-faradaic EIS in the frequency regime < 1KHz. In enzyme systems, charge transfer process occurs due to the electron-transfer between the enzyme complex and the electrode surface but its effects are more pronounced in lower frequencies[78], [79]. Non-faradaic CA is a DC based quantitative technique that captures currents from the non- faradaic processes occurring in the double layer as a function of time. In response to an applied DC pulse, the recorded current consists of a non-faradic current arising from the charging of the double layer, and a

capacitive decay current caused by the relaxation of the double layer ($I_{cap}\alpha$ $e^{-t/Rct*Cdl}$) reaching a steady state[73].

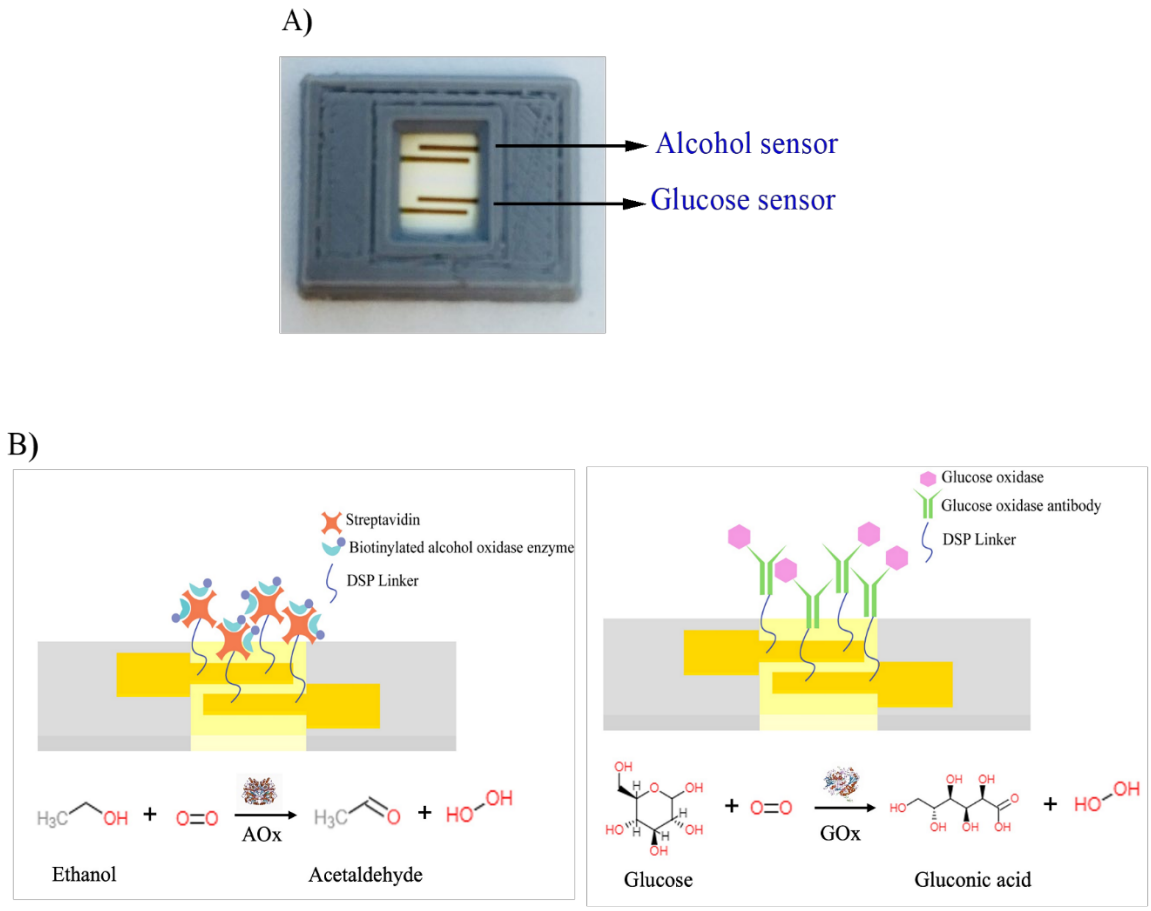

Figure 3.1.A) Picture of the combinatorial biosensor (B) Schematic of the functionalized immunoassays for the combinatorial detection of alcohol and glucose in synthetic sweat and perspired human sweat. C) Scenarios illustrating the relationship between evening alcohol consumption and next morning glucose levels in pre-diabetic and diabetic populations subject to their nourishment state, continued on pg 47,

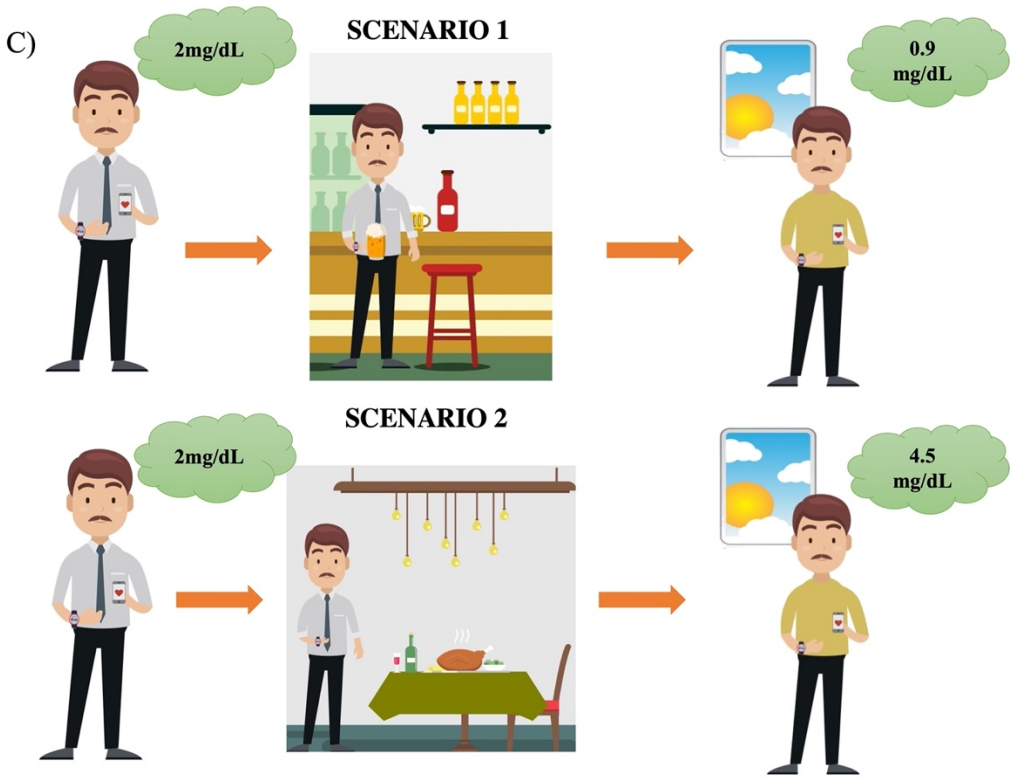

3.3.2 AC and DC based performance evaluation and sensor calibration of the alcohol biosensor in synthetic sweat of varying pH's

The calibration of the biosensor's response to alcohol concentrations in synthetic sweat buffers of pH 4, 6, and 8 for N= 3 replicates are represented as calibration dose response (CDR) curves in Figure 3.2A, 3.2B, and 3.2C. The CDR curves are plotted as percentage change in impedance of the dose concentrations with respect to baseline at which no alcohol molecules were present in the sweat buffers. The impedance variations across a frequency range of 1Hz to 1MHz were analyzed. A high signal to noise ratio (SNR) was observed within the 10Hz to 1KHz range at which the percentage change in impedance with respect to baseline was maximum. However, we choose 100Hz as our calibration frequency to compare the responses of the two biomolecules of interest

and for the ease of integration with portable electronics towards developing a point-of-care diagnostic device. As shown in Figures 3.2A, 3.2B, and 3.2C the percentage change in impedance response from 0.01mg/dL to 100 mg/dL was observed to be ~20% in synthetic sweat buffers of pH 4 and 6 and ~30% in synthetic sweat buffer of pH 8. A standard deviation of ~3-8% is observed in the impedance response across N= 3 replicates which lies in the acceptable range of deviation according to CLSI standards. The SST for alcohol biosensing in synthetic sweat buffers lies below the percentage impedance response of the lowest alcohol concentration being detected. It is observed that the LOD for the combinatorial biosensor in detecting alcohol in synthetic sweat buffers of varying pH's is 0.01mg/dL. The reliable range of alcohol concentrations that the biosensor can detect is described as the dynamic range which is 0.01mg/dL to 100 mg/dL.

Although the LOD and the dynamic range of alcohol detection are retained across the synthetic sweat buffers of varying pH, higher impedance response is observed in synthetic sweat of pH 8 than in pH's 4 and 6. The H_2O_2 produced by the catalytic oxidation of alcohol on interaction with the enzyme undergoes the reaction: $H_2O_2 \rightarrow 2H^+ + O_2 + 2e^-$. The excess H^+ ions present in synthetic sweat buffer at low pH's affect the linearity of the impedance response by interfering with charge transfer process. The pH of the buffer solution affects (1) the charge behavior of ZnO thus significantly affecting the interface and bulk properties when a buffer solution interacts with ZnO[81] (2) Stability of the enzymatic activity[68]. Alcohol oxidase and glucose oxidase enzymes are stable within our chosen pH range of operation. Change in impedance produced by the biosensor in response to the increasing target biomolecule concentrations is facilitated by a combination of two processes: (1) charge modulation occurring within the double layer as a function of change in permittivity (2) charge transfer occurring between the enzyme biomolecule

complex when the target biomolecules are catalytically oxidized by their specific enzyme complexes to produce reaction products and H_2O_2.

Chronoamperometric responses of the combinatorial biosensor in detecting alcohol was recorded by applying a step dc potential and measuring the resultant current vs. time. DC potential of ~0.6V was applied to the system corresponding to the catalytic oxidation of alcohol and generation of H_2O_2 by AOx enzyme as previously reported[47]. The measured current reflects the non-faradaic charge transfer between the enzyme complex and the capacitive current for the double layer. The calibration curves for N= 3 replicates shown in Figs. 3.2D, 3.2E, and 3.2F are plotted for the average change in steady state current from the baseline obtained for varying alcohol concentrations. We observe that the current response decreases with increasing pH which corroborates with the increasing impedance observed with increasing pH in the EIS studies. We attribute this behavior to the excess H^+ ions participating in the charge-transfer between the enzyme biomolecule complex and the ZnO electrode.

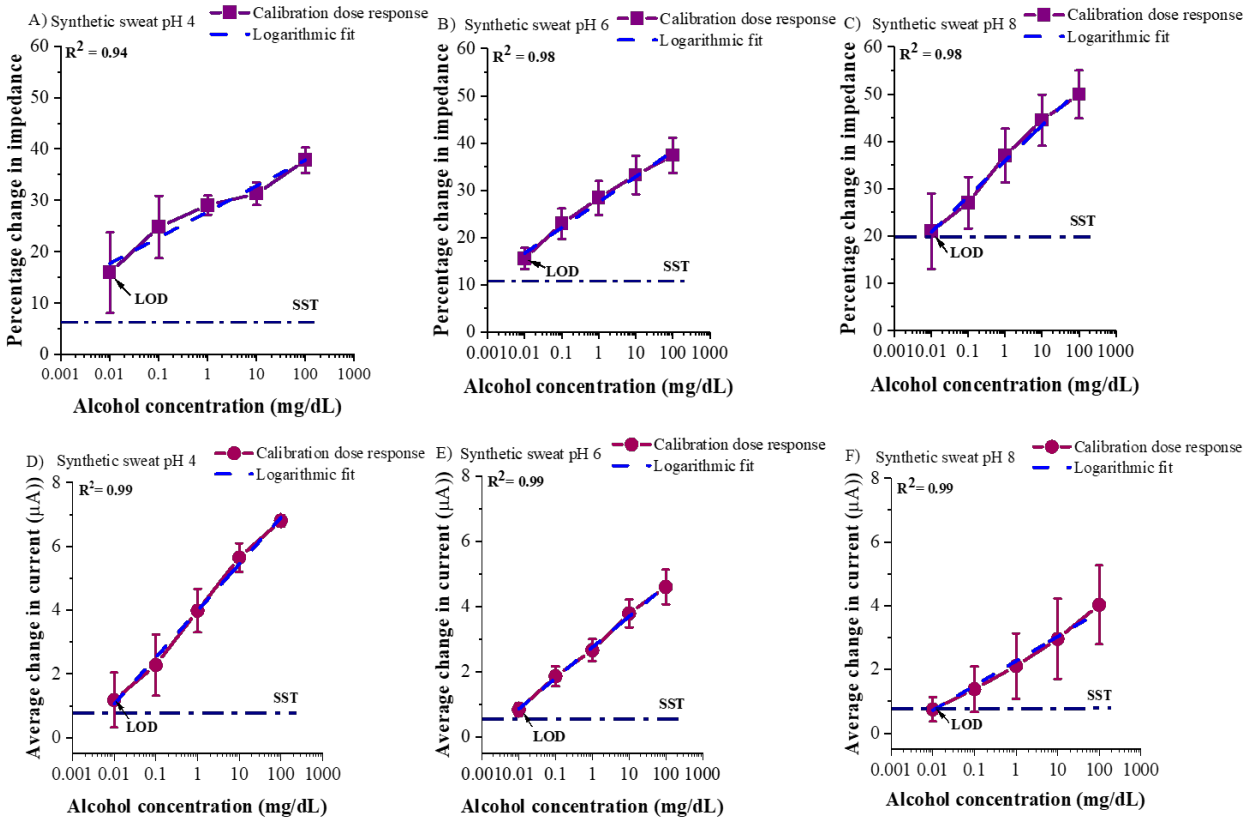

Figure 3.2. Calibration dose response of alcohol as a function of percentage change in impedance at 100Hz in (A) synthetic sweat buffer of pH 4 (B) synthetic sweat buffer of pH 6 (C) synthetic sweat buffer of pH 8. Calibration dose response chronoamperograms for alcohol as a function of average change in current from the baseline in (D) synthetic sweat buffer of pH 4 (E) synthetic sweat buffer of pH 6 (F) synthetic sweat buffer of pH 8

3.3.3 AC and DC based performance evaluation and sensor calibration of the glucose biosensor in synthetic sweat of varying pH's

The calibration of the combinatorial biosensor's response to glucose in sweat buffers of pH's 4, 6, and 8 for N= 3 replicates are shown in Figures 3.3A, 3.3B, and 3.3C. An increasing percentage

change in impedance is observed with increasing logarithmic glucose concentrations from 0.01mg/dL to 50 mg/dL spiked in synthetic sweat buffers of pH 4, 6, and 8. At pH 4, the percentage impedance change from the baseline was observed to be between 10-40% from the lowest to the highest glucose concentration with a standard deviation of 3-7%. The percentage changes in impedance in synthetic sweat of pH 6 for the increasing glucose concentrations varied from 16-50% with a standard deviation of 0.03-5%. Higher percentage changes in impedance of 22-58% with a standard deviation of 5-11% were observed in synthetic sweat of pH 8 in comparison to pH's 4 and 6. A larger deviation is observed for glucose dose concentrations 1mg/dL to 100 mg/dL detected in synthetic sweat pH's 4 and 8 in comparison to pH 6. At pH 6, lesser contribution from the buffer lowers the overall deviation of the impedance response. The LOD in synthetic sweat buffers of pH's 4, 6, and 8 was found to be 0.01mg/dL.

The chronoamperometric responses of the combinatorial biosensor in detecting glucose concentrations in synthetic sweat buffers of pH 4, 6, and 8 for N= 3 replicates are shown in Figures 3.3D, 3.3E, and 3.3F respectively. The GOx enzyme catalyzes the oxidation of glucose by producing H_2O_2 at ~0.7V as reported in literature[51]. For synthetic sweat pH 4, the average change in current produced by the increasing glucose concentrations from the baseline varies from 2.4 (±0.4)-8.4 (±1.2) µA. The current changes observed for glucose concentrations from 0.01-500mg/dL in synthetic sweat of pH 6 is 1.9 (±0.8)-5.5 (±1) µA whereas in synthetic sweat of pH 8, the current changes in the range of 1.7(±0.4)-5.4 (±0.9) µA were observed for the lowest to the highest dose concentration. The LOD computed across synthetic buffers for CA based glucose detection is 0.01mg/dL.

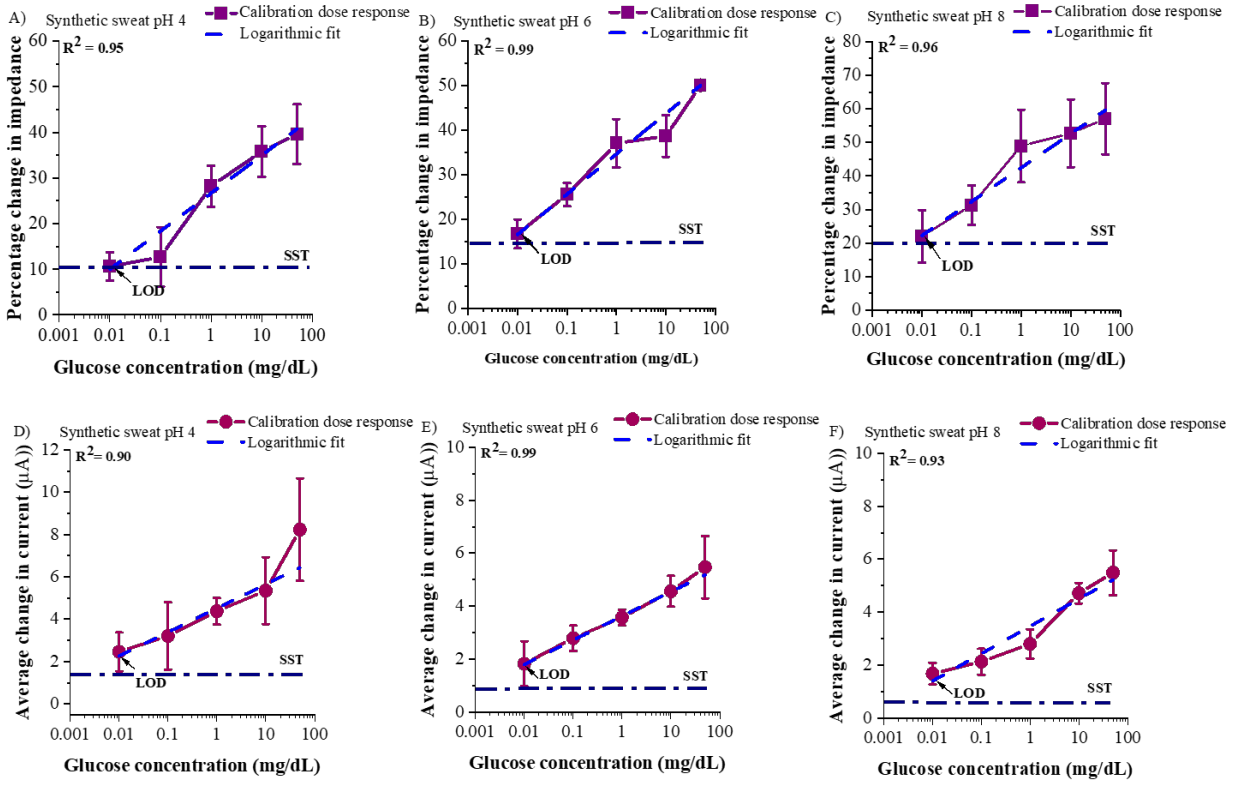

Figure 3.3.Calibration dose response of glucose as a function of percentage change in impedance at 100Hz in (A) synthetic sweat buffer of pH 4 (B) synthetic sweat buffer of pH 6 (C) synthetic sweat buffer of pH 8. Calibration dose response chronoamperograms for glucose as a function of average change in current from the baseline in (D) synthetic sweat buffer of pH 4 (E) synthetic sweat buffer of pH 6 (F) synthetic sweat buffer of pH 8

3.3.4 AC and DC based performance evaluation and sensor calibration of the alcohol biosensor in perspired human sweat

The calibration dose response curves obtained for alcohol biosensing in human sweat buffer (pH ~5.98) using EIS and CA are shown in Figures 3.4A and 3.4C. The percentage change in impedance for logarithmic alcohol concentrations between 0.01mg/dL to 100 mg/dL varies from

12-35%. The standard deviation across N= 3 replicates lies between 4-8%. The LOD of the combinatorial biosensor for alcohol detection in human sweat is found to be 0.1mg/dL with a dynamic range is 0.1mg/dL to 100 mg/dL. Sweat alcohol content equivalent to blood alcohol levels on consumption of <1- 3 drinks estimated by the correlation: Blood alcohol content (g/L) = 0.71* Sweat alcohol content (g/L), R^2 = 0.912[32]. The sweat alcohol content for <1-3 drinks detected by the biosensor marked by the color bands in Figure 4A lies well within the relevant range of alcohol found in human sweat. In comparison to the biosensor performance in synthetic sweat of pH 6, the LOD and the standard deviation is higher in human sweat as it as complex biomatrix consisting of interferents that contribute to the noise factor. The average current change from the baseline from the lowest to the highest alcohol concentration in the CDR is the 0.4(±0.17)- 2 (±0.8) μA. A correlation coefficient of R^2= 0.98 is calculated for the CDRs obtained using EIS and CA. The LODs measured using EIS and CA differed owing to the biochemical events occurring at the electrode-solution interface being recognized disparately by both these techniques.

CA captures the temporal response of the biosensor as an average function of current change derived from the double layer relaxation, concentration, mobility of ions in the solution, and the time dependent electric field experienced by the ions[74]. However, EIS is a powerful sensitive technique that allows characterization of biosensor system by detecting a time-based impedance response across a frequency spectrum. The impedance response is a summation of the individual responses obtained from the bulk solution resistance, charge transfer resistance, and the double capacitance. Due to the sensitivity of EIS in capturing the biomolecular events at the EDL interface as individual events rather than an average function, the LOD for alcohol detection in human sweat

is one logarithmic concentration higher than the LOD detected by the chronoamperometric technique.

3.3.5 AC and DC based performance evaluation and sensor calibration of the glucose biosensor in perspired human sweat

The EIS based performance of the combinatorial biosensor in detecting glucose in perspired human sweat represented by the calibration dose response curves are shown in Figure 3.4B for N= 3 replicates. The percentage change in impedance varies from 14-35% with a deviation of 4-13% for logarithmic glucose dose concentrations ranging from 0.01mg/dL to 50mg/dL. A correlation coefficient of $R^2 = 0.95$ was obtained after performing regression analysis. The LOD is found to be 0.1mg/dL and the dynamic range of glucose detection is 0.01mg/dL to 50mg/dL. The sweat glucose concentrations corresponding to hypoglycemic, normal, and hyperglycemic levels are marked by color bands in Figure 3.4B. A correlation factor of 0.017 ($R^2 = 0.83$) is used to compute the equivalent sweat glucose concentrations from the blood glucose concentration[49]. The noise threshold is found to be higher in comparison to synthetic sweat buffers due to the human sweat interferents and background noise form the higher antibody concentrations utilized in the detection. The larger deviations obtained at the elevated glucose concentrations could be induced by the steric hindrances from the size of glucose molecules and crosstalk from the sweat interferents [See section 3.6]. Despite of the larger deviations obtained on the 10mg/dL and 50mg/dL concentrations, the deviations are within 15% which meet the CLSI standards[82].

The chronoamperometric calibration dose response curve for glucose detection in human sweat as shown in Figure 3.4D. The average change in current for the glucose range 0.01mg/dL to 50mg/dL varies from 2.3(±0.7)-4.8(±0.6) μA. The current changes obtained from the non-specific

biomolecules present in human sweat cannot be decoupled from the behavior obtained from the specific biomolecules hence affecting the linearity and the lower detection limit of the CDR. The LOD obtained is 0.01mg/dL. A correlation coefficient $R^2 = 0.82$ is obtained from the regression analysis. Although the LOD obtained from CA is one logarithmic concentration lower than the LOD obtained by EIS, EIS has merits of being able to capture subtle EDL effects which are averaged in CA.

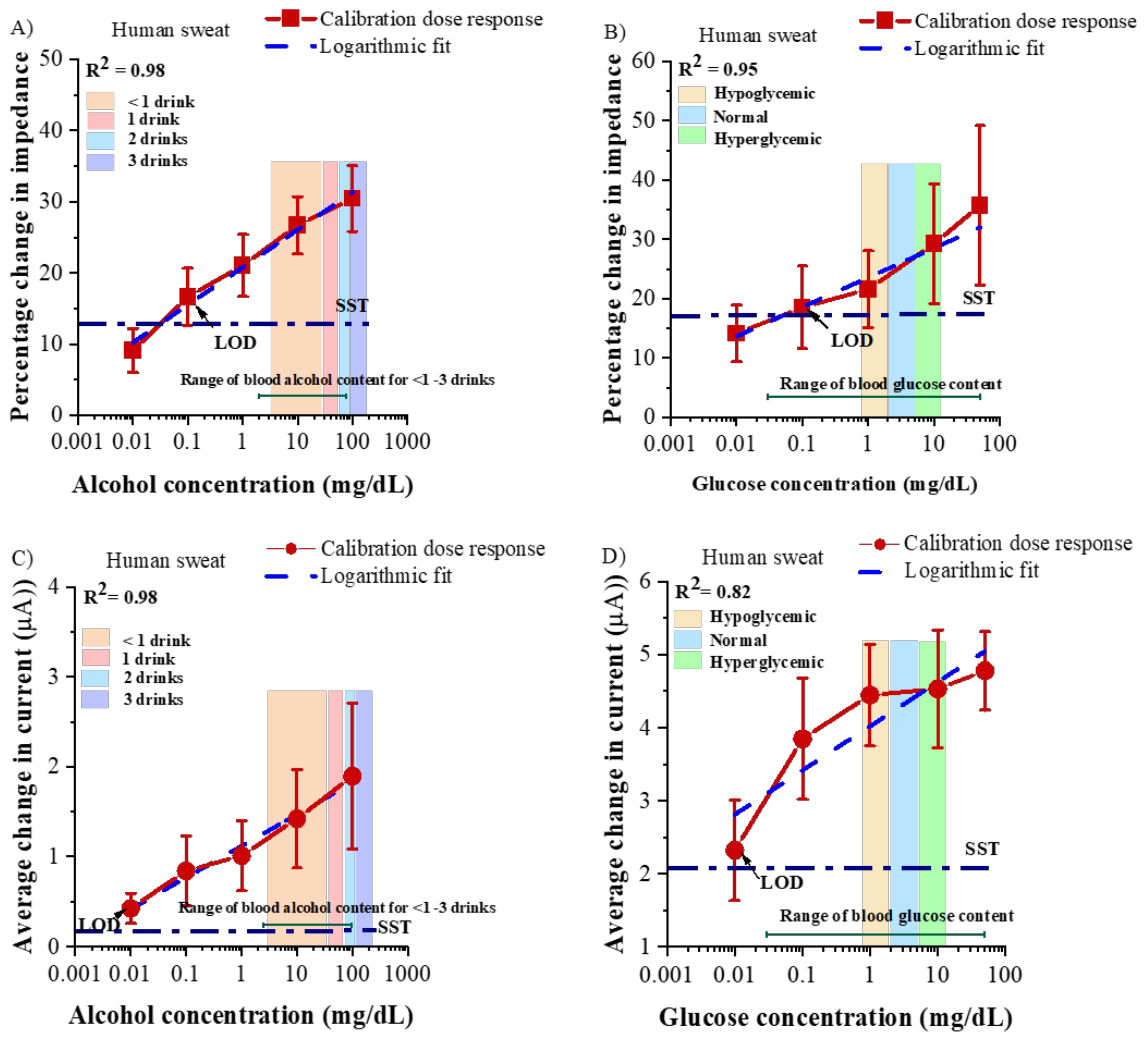

Figure 3.4.A) Calibration dose response of alcohol as a function of percentage change in impedance at 100Hz in perspired human sweat (B) Calibration dose response of glucose as a function of percentage change in impedance at 100Hz in human sweat (C) Calibration dose response chronoamperograms for alcohol as a function of average change in current from the baseline in perspired human sweat (D) Calibration dose response chronoamperograms for glucose as a function of average change in current from the baseline in human sweat

3.3.6 Performance of the biosensors in the presence of cross-reactive biomolecules in synthetic sweat

The reliability of the combinatorial sensor in detecting specific target biomolecules of interest and no other similar molecules can been investigated from cross-reactivity analysis. The label-free combinatorial biosensor relies on the functionalized enzyme-biomolecule complex to selectively oxidize specific biomolecules and to have minimal non-specific interactions. To assess the specificity of the alcohol and glucose immunoassays developed on the combinatorial biosensor, cross- reactivity studies were performed in synthetic sweat pH 6 with alcohol and glucose as described in Section 2.5. The cross-reactive response of glucose on the alcohol sensor is shown in Figure 3.5A. The median percentage changes in impedance increase linearly from 12.5-31% with increasing logarithmic alcohol concentrations with a noise threshold of 11%. The impedance signals obtained from the cross-reactive glucose molecules vary between 2.5-10% and lie below the noise threshold. The linearly increasing impedance response obtained from the specific interactions and flat impedance trend obtained from the cross-reactive glucose molecules indicate that the electrochemical signal response in obtained only from the specific interactions of alcohol with alcohol oxidase enzyme biomolecule complex. The response of the glucose sensor to cross-reactive alcohol molecules, as shown in Figure 3.5B, shows an increasing trend in median percentage change in impedance ranging from 22-55% with logarithmic glucose concentrations. The variation in response from the alcohol molecules lies within the range 1-7% and falls below the noise threshold of 14%. Alcohol molecules show a larger spread in impedance response at 50 mg/dL yet, the impedance response from the glucose molecules at 50mg/dL concentration shows a clear separation from the non-specific alcohol molecules. Thus, the combinatorial biosensor is

feasible in distinguishing the non-specific interactions from the specific interactions and keeping the cross-reactions of similar biomolecules within the specified noise threshold.

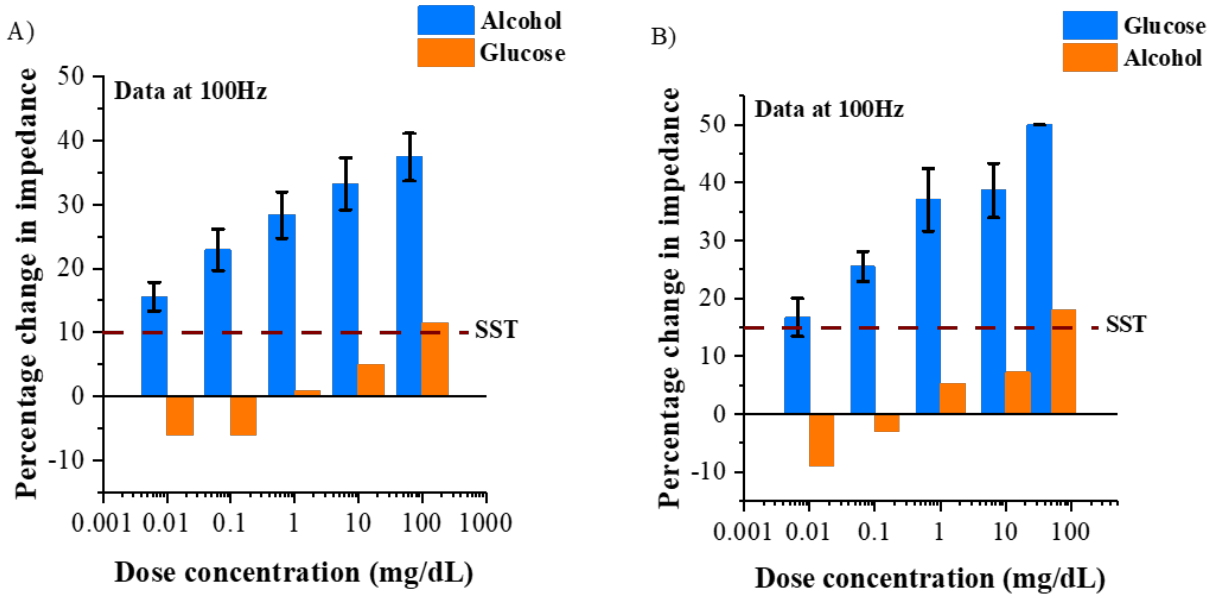

Figure 3.5.(A) Alcohol biosensor selectivity for glucose as the cross- reactive molecule in synthetic sweat on pH 6 (B) Glucose biosensor selectivity for alcohol as the cross-reactive molecule in synthetic sweat on pH 6

3.3.7 Continuous combinatorial monitoring of alcohol in perspired human sweat

The robustness and stability of the combinatorial biosensor was evaluated by performing dynamic continuous monitoring of alcohol in perspired human sweat. The dynamic impedance response of the combinatorial biosensor to alcohol concentrations equivalent to consuming <1-3 standard drinks i.e., 3mg/dL to 125mg/dL alcohol in perspired human sweat obtained at 100Hz is depicted in Figure 3.6A. The rate of change in impedance slopes as a function of drink dose are observed to be 1.7 Ω/min for <1 drink, 42.7 Ω/min for 1 drink, 113. 4 Ω/min for 2 drinks, and 269.8 Ω/min

for 3 drinks. An incremental impedance response is observed with increasing alcohol dose concentrations over a 110-minute duration implying that the rate of change of impedance is entirely drink dependent. This time limited dynamic monitoring of alcohol in human sweat when extended to longer periods as desired in real-world applications, would indicate similar trends in impedance response over time proportional to drink consumed. A polynomial curve was fit to the impedance response and correlation coefficient $R^2 = 0.99$ was obtained.

We have demonstrated for the first time the dynamic interplay in the temporal variations of alcohol and glucose. The dynamic response of the biosensor functionalized with alcohol detection immunoassay was tested to understand the modulation in alcohol levels under the influence of hyperglycemic and hypoglycemic glucose levels. The typical sweat glucose concentrations corresponding to hypoglycemic, normal, and hyperglycemic lie within the range 0.85mg/dL to 5.5mg/dL (Lee et al., 2016). A drink dependent increasing trend in impedance is observed proportional to the alcohol concentration consumed in the presence of hypoglycemic and hyperglycemic glucose levels as shown in Figures 3.6C and 3.6D respectively. The rate of change in impedance slopes as a function of drink dose in the presence of hypoglycemic glucose levels are observed to be 0.05 KΩ/min for <1 drink, 0.52 KΩ/min for 1 drink, 0.9 KΩ/min for 2 drinks, and 1.2 KΩ/min for 3 drinks. The rate of change in impedance slopes as a function of drink dose in the presence of hyperglycemic glucose levels are observed to be 0.06 KΩ/min for <1 drink, 0.68 KΩ/min for 1 drink, 0.73 KΩ/min for 2 drinks, and 1.15 KΩ/min for 3 drinks. The performance of the sensor in terms of their impedance responses suggest its ability to capture only the specific interactions of the alcohol oxidase with alcohol in presence of hypoglycemic (0.85mg/dL) or

hyperglycemic (5.5mg/dL) glucose levels. An R^2 value of 0.99 was obtained for both the polynomial fits.

Continuous monitoring of glucose levels in diabetic individuals with a social drinking lifestyle is essential for diabetes management. Two scenarios representing the effect of evening consumption of alcohol on next morning glucose levels subject to nourishment states are illustrated in Figure 3.1C. The temporal modulations in the glucose levels on drink consumption to simulate real-life situations to control drink consumption is evaluated on the biosensor functionalized with the glucose detection immunoassay. The change in impedance response observed from the varying glucose levels – hypoglycemic (0.85mg/dL), normal (2mg/dL), hyperglycemic (5.5mg/dL) on consuming <1-2 standard drinks in shown in Figures 3.6E and 3.6F over a 120-minute duration. The rate of change of in the slope of impedance response is glucose level dependent. The rate of change in impedance slopes as a function of glucose concentrations in the presence of alcohol equivalent to <1 standard drink is observed to be 27.3 Ω/min for hypoglycemic level, 108.6 Ω/min for normal level, and 395.1 Ω/min for hyperglycemic level. The rate of change in impedance slopes as a function of glucose concentrations in the presence of alcohol equivalent to 2 standard drink is observed to be 40.6 Ω/min for hypoglycemic level, 185 Ω/min for normal level, and 769. 2 Ω/min for hyperglycemic level. The increasing trend in the rate of change in impedance responses observed with increasing alcohol content can be utilized in detecting variations in glucose levels on the consumption of alcohol suitable for wearable applications. Polynomial curves were fit to impedance responses obtained for both cases and an R^2 of 0.99 was obtained.

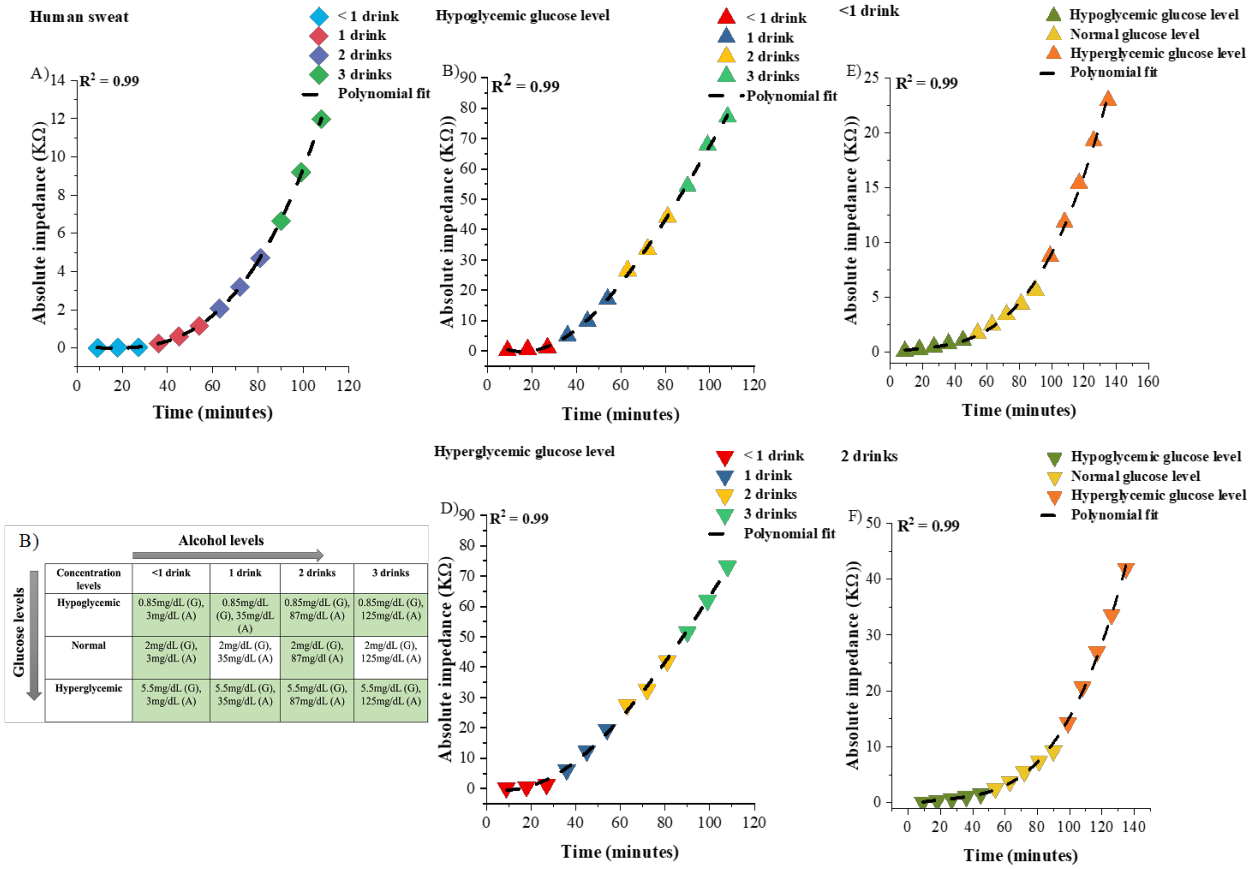

Figure 3.6.(A) Continuous and dynamic monitoring of alcohol spiked in perspired human sweat. (B) Alcohol and glucose dose combination index for combinatorial biosensing. Continuous dynamic monitoring of alcohol in (C) hypoglycemic glucose spiked perspired human sweat (D) hyperglycemic glucose spiked perspired human sweat. Continuous dynamic monitoring of glucose in (E) alcohol equivalent to <1 drink spiked perspired human sweat (F) alcohol equivalent to 2 drinks spiked perspired human sweat

3.4 Conclusion

This work is the first-time demonstration of a biosensor on ultra-low passive perspired human sweat volumes for rapid and dynamic monitoring of alcohol and glucose in a temporal manner

suitable foe wearable IoT applications. A relationship between blood glucose levels and consumption of alcohol has been found to interfere with blood glucose levels and reduce the effectiveness of insulin. Alcohol consumption is prone to increasing diabetes related risks leading to acute hypoglycemia or hyperglycemia depending on the body's nutrition state. To maintain a healthy wellness state, it is imperative to track the fluctuations caused in glucose levels and to limit one's alcohol intake through investigation of human bodily fluids. In this work, we have demonstrated the combinatorial detection of alcohol and glucose in human sweat using electrochemical impedance spectroscopy and CA as a comparative analysis technique. A thorough analysis of effect of pH of the sweat buffers on the combinatorial biosensor's performance in detecting target biomolecules of interest yielded an outcome that the ionicity of buffer plays a key role in giving out reliable and stable sensor output. The biosensor enables users to track the interplay between glucose and alcohol in a "real-time" manner.

The biosensor showed an LOD of 0.01 mg/ dL for alcohol and glucose detection in synthetic buffers using EIS and CA techniques. However, LODs of 0.1mg/dL in human sweat were obtained for alcohol and glucose detection using EIS while lower LODs of 0.01mg/dL were obtained using CA. Shift in linearity of the impedance response and differing LOD's obtained in human sweat are primarily due to the sensitivity of the detection techniques in deconvoluting the specific interactions between the target biomolecules-enzyme biomolecule complex and the non – specific interactions originating from the interferents present in human sweat buffer. The mechanisms underlying the biosensing performance is capacitive double layer modulation from the formation of products and the electron charge transfer processes occurring between the electrode-enzyme complex. Selectivity of the immunoassays functionalized with enzymes on the biosensors specific

to the target biomolecule of interest was established through cross-reactivity studies performed with glucose on alcohol sensor and alcohol on glucose sensor. Negative interactions from the cross-reactive biomolecules yielded responses that lie well within the noise threshold of the biosensor. The combinatorial biosensor's performance in monitoring alcohol and glucose in perspired human sweat in continuous and dynamic manner has been demonstrated towards making it suitable for developing a wearable lifestyle monitor for limiting alcohol intake in the diabetic and pre-diabetic population. The dynamic effects exerted by a chronic cohort of alcohol and glucose molecules on each other are continuously monitored through their impedance responses which indicate an incremental rate of change in impedance response proportional to the biomolecule concentration levels. This work demonstrates a non-invasive, label-free approach towards translation onto portable diagnostic platforms for monitoring vital statistics through analysis of ultra-low volumes of passive perspired sweat.

3.5 Materials and Methods

3.5.1 Materials and reagents

Polyamide substrates (pore size-200nm, thickness-60μm) were obtained from GE Healthcare Life Sciences (Piscataway, NJ, USA). The linker molecule dithiobis succinimidyl propionate (DSP), dimethyl sulfoxide (DMSO), and 1X phosphate buffered saline (PBS) were purchased from Thermo Fisher Scientific Inc. (Waltham, MA, USA). Salt-free streptavidin from Streptomyces avidiini (≥ 13 units/mg protein), alcohol oxidase enzyme from Pichia pastoris (10-40 units/mg protein), glucose oxidase from Asperigillus niger (100,000-250,000 units/g), D-(+)- glucose, absolute ethyl alcohol (≥ 99.5%), and sodium bicarbonate (≥ 99.7%) were purchased from Sigma-

Aldrich (St. Louis, MO, USA). Long arm NHS-biotin was purchased from Vector laboratories (Burlingame, CA, USA). Glucose oxidase antibody was obtained from Abcam (Cambridge, MA, USA). Glucose oxidase antibody was diluted in 1X PBS. Streptavidin was lyophilized in 1X PBS and biotin was dissolved in DMSO. Alcohol oxidase enzyme was biotinylated using the protocol stated in Du *et. al*[57]. Synthetic sweat was prepared as per the recipe described in M.T. Mathew *et. al*[56]. The pH range was varied by varying the concentrations of the constituents. Single donor human sweat of pH ~6 was purchased from Lee Biosolutions Inc. (Maryland Heights, MO, USA). No preservatives were added to this product, and it was stored at -20°C. All alcohol and glucose dilutions were made in synthetic and human sweat buffers.

3.5.2 Sensor fabrication

The combinatorial biosensing stack deposited on flexible nanoporous polyamide substrate is shown in Fig 1A. The biosensing stack comprises of gold electrodes and a ZnO active sensing region. Fabrication of the combinatorial biosensing stack consists of two steps: (1) Deposition of ~150nm gold electrodes on the substrate using a Temescal e-beam evaporator tool (Ferro Tec, Livermore, CA, USA). (2) Sputtering of ZnO thin films in the central region between the two gold electrodes using AJA Orion RF magnetron with a 99.999% ZnO target (Kurt J. Lesker) at room temperature. The thickness of the film is measured to be ~100nm using a Veeco Dektak 8 profilometer.

3.5.3 Sensor calibration in synthetic sweat and perspired human sweat for alcohol detection

The immunoassay developed on the combinatorial biosensor towards detection of alcohol in synthetic sweat and human sweat buffers are shown in Figure 1B. The biosensor was functionalized with 10mM DSP thiol-cross linker diluted in dimethylsulfoxide (DMSO) by dispensing 3uL of sample volume on the ZnO sensing region for 3 hours in dark. Sample solutions were dispensed on the side behind the electrode fabricated region of the sensor. 1 mg/mL of streptavidin in 1X PBS was incubated on the sensing region for 60 minutes. After immobilizing streptavidin, biotinylated alcohol oxidase enzyme was incubated on the sensing region for 15 minutes. The enzyme biotinylation procedure was carried out as outlined in Du *et. al*. Synthetic sweat solution of 3uL volume was dispensed on the sensing region depending on the detection buffer. This step was the baseline measurement for computing impedance changes. Pure alcohol was diluted in synthetic sweat buffers in a logarithmically increasing concentration range between 0.01mg/dL to 100 mg/dL. Alcohol dilutions in sweat were dispensed on the sensor in increasing dose concentrations and incubated for 10 minutes each. EIS and CA measurements were performed after every immobilization step. Single frequency EIS measurements recorded the impedance measurements over 5 minutes and were taken using a potentiostat (Gamry Instruments, Warminster, PA, USA) after applying an AC excitation signal of $10mV_{rms}$ at 100Hz frequency. All measurements were performed in dark and under ambient temperature conditions [See Figs S1-S4 of [80]]. CA measurements were carried out using the same potentiostat after applying a constant step voltage of 600mV for 1 minute. Similar protocols as followed for detection of alcohol

in synthetic sweat were followed for detection of alcohol in human sweat buffer solution [See Figs S4-S8 of [80]]. All data is represented as mean± standard error of mean (SEM).

The calibration dose responses (CDR) for synthetic and human sweat buffers obtained using EIS and CA were calculated for N= 3 replicates. The combinatorial biosensor's EIS response is represented as the percentage change in impedance between the baseline step and the dose concentration step. The percentage change in impedance is the change in impedance observed in response to the target biomolecule concentration with respect to the baseline in the absence of target biomolecule and is calculated using the expression (100*(baseline impedance – spiked biomolecule concentration impedance)/ baseline impedance). The limit of detection (LOD) described as the smallest concentrations of target biomolecules that is reliably detected beyond the specific signal threshold (SST). The chronoamperometric CDRs obtained in synthetic and human sweat buffers are plotted in terms of change in average steady state current of the dose concentration step with respect to the average steady state current obtained for the baseline measurement step. SST for CDR's obtained using both the techniques are computed using a signal to noise ratio (SNR) of 3 [refer to supplementary information of [80]] (Armbruster and Pry, 2008).

3.5.4 Sensor calibration in synthetic sweat and perspired human sweat for glucose detection

The glucose detection immunoassay as shown in Figure 1B developed on the combinatorial biosensor was adapted based on the protocol described in Munje *et. al* [51] . Glucose dilutions of concentrations from 0.01mg/dL to 50 mg/dL were made in synthetic sweat and human sweat buffer solutions. The calibration dose responses using EIS and CA techniques were obtained for N= 3 replicates [See Figs S8-S16 of [80]]. Sensor response metrics such as percentage change in

impedance, average change in steady state current, specific signal threshold, and LOD were computed similarly as done for sensor calibration in synthetic and human sweat for alcohol detection [See Table S1-S4 of [80]].

3.5.5 Evaluation of cross reactivity on alcohol and glucose biosensors with interferents in synthetic sweat of pH 6

The specificity of the combinatorial biosensing system was tested through the sensor's cross reactivity of glucose biomolecules on the alcohol sensor and alcohol biomolecules on the glucose sensor. All alcohol and glucose dilutions were made in synthetic sweat buffer of pH 6. Cross reactivity study on the alcohol biosensor for N= 3 replicates was performed by dispensing varying glucose concentrations in the range 0.01mg/dL to 100 mg/dL on the sensing region functionalized with alcohol detection immunoassay. Similarly, cross reactivity of the glucose sensor to alcohol was examined for N= 3 replicates by dispensing alcohol concentrations varying from 0.01mg/dL to 50 mg/dL on the sensing region functionalized with glucose detection immunoassay. Percentage change in impedance captured at 100Hz is computed as described in the above section.

3.5.6 Continuous monitoring of alcohol in perspired human sweat

Continuous, dynamic monitoring of alcohol in perspired human sweat was performed by dispensing 3µL of sweat alcohol dose concentrations in the range 3mg/dL to 125 mg/dL (≈ <1-3 drinks) for 9 minutes on the ZnO sensing region in succession over a 110-minute duration. Alcohol concentrations of 1mg/dL and 10 mg/dL were prepared by spiking alcohol in human sweat. 1mg/dL alcohol dose was dispensed on the sensing region three times in progression to simulate the ingestion of <1 drink condition. Following this, nine doses of 10mg/dL alcohol concentration

were applied successively to simulate the ingestion of 1-3 standard drinks. The dynamic impedance response of the biosensing system for continuous sweat alcohol monitoring was measured using a potentiostat on the application of an AC excitation signal of $10mV_{rms}$ (Root mean square) at 100Hz frequency.

3.5.7 Continuous, dynamic monitoring of the effect of hypoglycemic and hyperglycemic glucose levels on perspired human sweat alcohol content

The effect of hypoglycemic glucose levels on sweat alcohol content was monitored in a continuous manner over a 120-minute window by dispensing 3µL solution of glucose and alcohol spiked in human sweat onto the ZnO sensing region functionalized with alcohol detection immunoassay. Two hypoglycemic cocktail solutions were made: (1) Hypoglycemic glucose concentrations of 0.85mg/dL combined with alcohol concentration of 1mg/dL in human sweat buffer. (2) Hypoglycemic glucose concentration of 0.85mg/dL combined with alcohol concentration of 10mg/dL in human sweat buffer. Cocktail solution 1 was dispensed three times on the sensing region successively every 9 minutes to simulate the effects of hypoglycemic glucose levels on sweat alcohol post consumption of <1 standard drink. Subsequently, cocktail solution 2 was dispensed nine times on the sensing region successively every 9 minutes to simulate the effects of hypoglycemic glucose levels on sweat alcohol post consumption of 1-3 standard drink.

Two hyperglycemic glucose cocktail solutions were prepared by spiking human sweat with 5.5 mg/dL glucose concentration in combination with 1mg/dL and 10mg/dL alcohol concentrations. Similar procedure as described above was followed to monitor the effect of hyperglycemic glucose levels on sweat alcohol content. All impedance responses were captured at 100Hz.

3.5.8 Continuous, dynamic monitoring of perspired sweat glucose on consumption of <1-2 standard drinks

The effect of consuming alcohol equivalent to <1-3 drinks on the sweat glucose content was continuously monitored over a period of 120 minutes. Cocktail solutions were prepared by spiking glucose and alcohol in human sweat buffer solution. Glucose solutions of concentrations 0.85 mg/dL, 2 mg/dL, and 5.5 mg/dL were made in human sweat. Alcohol solutions of concentrations 3mg/dL (<1 standard drink) and 87mg/dL (2 standard drinks) were made in human buffer solution. Combined concentration of glucose and alcohol solutions were made in six combinations as shown in Figure 5B. The cocktail combinations were dispensed five times on the ZnO sensing region functionalized with glucose detection immunoassay in 3µL volume every 9 minutes. Individual dynamic impedance responses were obtained at 100Hz for glucose levels combined with alcohol concentration equivalent to <1 drink and for glucose levels combined with alcohol concentration equivalent to 2 drinks.

3.6 Acknowledgements

Funding for this research was supported by the National Institute on Alcohol Abuse and Alcoholism of the National Institutes of Health (R43AA026114). We acknowledge the contributions of Ankita Rugi and Amreek Saini for assisting in performing the experiments. The authors thank Saigautam Sirivella for helping with the schematics. The authors would like to thank Richard Willis for programming the data compilation software. We also thank Ambalika Tanak and David Kinnamon for their help in proofreading this document.

3.7 Prior publication

Ashlesha Bhide performed the experiments and compiled the data from all the studies. Ashlesha Bhide fabricated the sensors and analyzed the data. Sriram Muthukumar and Shalini Prasad conceived the design of the sensor stack and guided the experimental design. Ashlesha Bhide, Sriram Muthukumar, and Shalini Prasad interpreted the data and co-wrote the manuscript. This article was published in Biosensors and Bioelectronics in 2018. This article has been reproduced by permission from Elsevier publishing company and the link to this article is: doi: 10.1016/j.bios.2018.06.065

CHAPTER 4

ON-DEMAND LACTATE MONITORING TOWARDS ASSESSING PHYSIOLOGICAL RESPONSES IN SEDENTARY POPULATIONS

4.1 Abstract

Identification of diseases in sedentary populations on a timely basis before reaching a critical stage is a continuing challenge faced by emergency care centers. Lactate is a key biomarker for monitoring restricted oxygen supply essential in assessing the physiological responses of the user for clinical diagnostics. The novelty of this work is the development of a non-invasive, mediator-free, stick and remove biosensor for the on-demand measurement of lactate in passive sweat targeted towards sedentary populations. The conformable interface of the biosensors with skin can be engineered to extract relevant biochemical signals and quantify the in-situ sweat biomarker levels. In this work, we demonstrate a highly sensitive and specific on-demand biosensor with a fabricated hybrid nanotextured Au/ZnO electrode stack embedded within a flexible nanoporous material to capture the temporal dynamics of passive sweat lactate. The biosensor exhibits a lactate specific response in human sweat with a 1mM lower limit of detection and a wide dynamic detection range of 1-100 mM (R^2 = 0.98). The proposed biosensor yields a sensitivity of 8.3% mM^{-1} while selectivity studies reveal negative interactions with non-specific molecules. The sensor stability studies showed a ~30% degradation in the lactate biosensing response over 4-day duration stored under 4°C. Non-faradaic electrochemical spectroscopy is employed as the detection modality to quantify the enzymatic catalysis of sweat lactate at the electrode-sweat interface. Spectroscopic characterization techniques confirm the enzymatic assay binding efficacy on a qualitative scale.

4.2 Introduction

Geriatric and pediatric populations are vulnerable to unforeseen circumstances that demand the identification of technologies that can prolong the lives of these sedentary population subsets. Thus, facile care approaches are required to monitor the health parameters of sedentary populations calling for the need of developing on-demand, single- use platforms for point-of-use testing. Early screening and diagnosis provide initial heath intervention through safe, non-invasive, and potentially inexpensive methods for detecting the onset and progression of diseases. Progression of diseases into an advanced stage causes delay in procuring effective treatment consequently requiring laborious invasive, immunological, imaging, and genomic diagnosis procedures[83]. The invasiveness of conventional diagnosis techniques requires frequent painful testing procedures posing a challenge for regular screening of disease progression in elderly and infants. Biomarkers have the enormous ability to assess and characterize the extent of disease towards the development of next-gen non-invasive diagnostic devices without the requirement of expensive and bulky equipment[84]. Increase in blood lactate levels are related to increased production or decreased lactate clearance further leading to conditions such as tissue hypoxia and subsequently leading to septic shock in extreme conditions[85]. Hence, an on-demand, point-of-use, stick and remove biosensor can be used for initial quantification of lactate levels further prompting clinicians to initiate immediate medical actions.

For years, eccrine sweat has been a neglected diagnostic bodily fluid but with the advent of flexible sensing, sweat sampling has become an extremely promising non-invasive diagnostic approach for biomarker analysis. Most efforts have been focused on the detection of sweat metabolites such as lactate, glucose, and uric acid as they are present in higher detectable

concentrations while the protein concentrations are in lower ranges. Low tonicity and acidic pH of sweat allows of more accumulation of biomarkers in sweat[17]. Eccrine sweat is a valuable source of proteins, metabolites, electrolytes, lipids, and other non-invasive biomarkers with less susceptibility to fouling making it a critical tool for frequent monitoring of disease states in sedentary populations[86]. Sweating occurs as a response to maintain thermoregulation when there is an excess rise in core body temperature. Higher sweat volumes can be achieved by inducing sweating through stimulation in healthy subjects. The quality and quantity of the biomarkers is highly depending on the type of glands and the region of sweat sampling on the body. Eccrine sweat is present on the body's skin with an average density of 100-200/cm^2 on the surface area of the body with its appearance on the body's surface allowing for non-invasive biomarker detection[87]. Advancement in passive sweat sampling and iontophoretic sweat stimulation techniques have unlocked new opportunities for sweat analytics-based screening devices with the potential to provide the continuous feedback on health and disease status. Lactate levels in eccrine sweat are found to be higher than in blood ranging from 4mM to 25mM in healthy individuals to 50-100mM after exhaustive exercise rendering sweat lactate detection to be a viable alternative for monitoring clinical conditions[88]–[91]. Most sweat based sensors rely on localized pilocarpine stimulation of sweat glands so as to achieve 10-100µL of sweat volume required for biomarker detection[26],[92]. Studies have shown that sweat stimulation induced using pilocarpine did not significantly show a change in lactate levels before exercise and during exercise in the exercise group in comparison to the non-exercising group[93]. Previously, our group has demonstrated dynamic continuous monitoring of lactate in ultra-low volumes of passive perspired sweat on a graphene biosensing platform[94]. Recent studies reporting real-time lactate biosensing

require high sweat volumes and the use of redox mediators to widen their dynamic range of detection (see supplementary Table S1 of [95])[26], [92], [96]–[100]. Most of the efforts report a dynamic range up to ~70mM with the use of redox probes. However, in our work, we report a non-faradaic, mediator-free lactate sensing strategy with an extended dynamic detection range up to 100mM by leveraging the properties of a porous substrate.

Porous substrates such as polyamide offer higher current density and capacitance due to the enlarged surface area to volume ratio in comparison to flat substrates. The dimensionality of the electrode materials also enhances the kinetics of electrochemical reactions. Nanoporous membranes allow for nanoconfinement of biomolecules within small volumes to increase the frequency of interactions with the biomolecules and the functionalized electrode surface[101]. The sensitivity of biomarkers can be enhanced by macromolecular crowding in the nanopores which influences the conformal stability of the protein, enhances the folding process, accelerates enzyme reaction kinetics, and prevents protein denaturation[102]. The specificity in detecting the target biomarker is achieved by excluded-volume effect wherein inert macromolecules crowd the nanopore and reduce the randomness in motion of the target biomolecules[38]. The decrease in the entropy of a crowded solution increases the thermodynamic activity of the solution resulting from the volume exclusion effect thus allowing specific probe-target analyte interactions[103]. Aside from the biocompatibility provided by the polyamide required for integration in flexible devices, another important aspect of using porous substrates is its capability to capture ultralow sweat volumes, drive the passively produced local sweat from the epidermis to the functionalized electrode interface, and provide the user with instantaneous feedback. Experimental studies and simulation done previously by the group have shown that passive eccrine sweat is transported

rapidly through the entire cross-section of the polyamide substrate steadily within 30seconds in a radial profile through capillary action[104].

Zinc oxide nanostructures have been explored heavily in recent times for biosensing applications (glucose, H_2O_2, cholesterol) because they offer advantages such as faster response time and sensitivity of detection. The nanotextured surface of ZnO provides greater surface area of probe-target biomarker interaction, biocompatibility, structural and chemical stability, fast electron kinetics, and strong adsorption ability due to its high isoelectric point[105]. The direct charge tunnelling between the ZnO nanostructures, and the active site of the enzyme reduces the need to use a redox mediator[106]. The ZnO surface is positively charged at physiological pH allowing for immobilization of negatively charged proteins to be adsorbed on its surface by electrostatic forces of attraction [28]. The electronic properties of ZnO allow for sensitive detection of biomarkers in small volumes with a wider dynamic range of detection while tailoring the polar termination of ZnO surface enhances the selectivity of the biosensor. The zinc and oxygen terminations of the ZnO nanostructures have been demonstrated to be efficient for the functionalization of antibodies and enzymes through dithiobis succinimidyl propionate (DSP) linker chemistry[107]. This work demonstrates the operation of biosensor with the capability of providing an on-demand measurement to the user for monitoring elevated lactate levels. Highly sensitive and specific lactate detection is accomplished by capitalizing on the interaction between the low volumes of passive sweat entrapped in the pores of the substrate and the nanotextured hybrid Au/ZnO electrodes aiding in signal amplification for ultra-sensitive lactate detection.

4.3 Results and Discussions

4.3.1 Enzymatic assay functionalization and structural characterization of the biosensing substrate

Lactate detection in eccrine sweat is achieved by the catalytic oxidation of L-lactate into pyruvic acid and H_2O_2 through lactate oxide (LOx) embedded within the nanopores and immobilized on the nanostructured ZnO active sensing region by a crosslinker as shown in Figure 4.1A. The production of H_2O_2 contributes to the impedance changes which are monitored by electrochemical impedance spectroscopy. The fluid wicking profile of the nanoporous substrate on contact with 3µL of passive sweat is shown in Figure 4.1B. The sweat is introduced into the pores through the face opposite to the sensing region and is transported through the pores to interact with enzyme. The mechanism guiding the fluid transport is a function of pore diameter, thickness, contact angle, packing density and pore arrangement which drives the transport of sweat across the membrane and influences the biosensor metrics. The SEM image in the inset provides evidence of the intercalated pore structure that aids in navigation of the passive sweat expressed from the epidermis to the detection region by lateral diffusion.

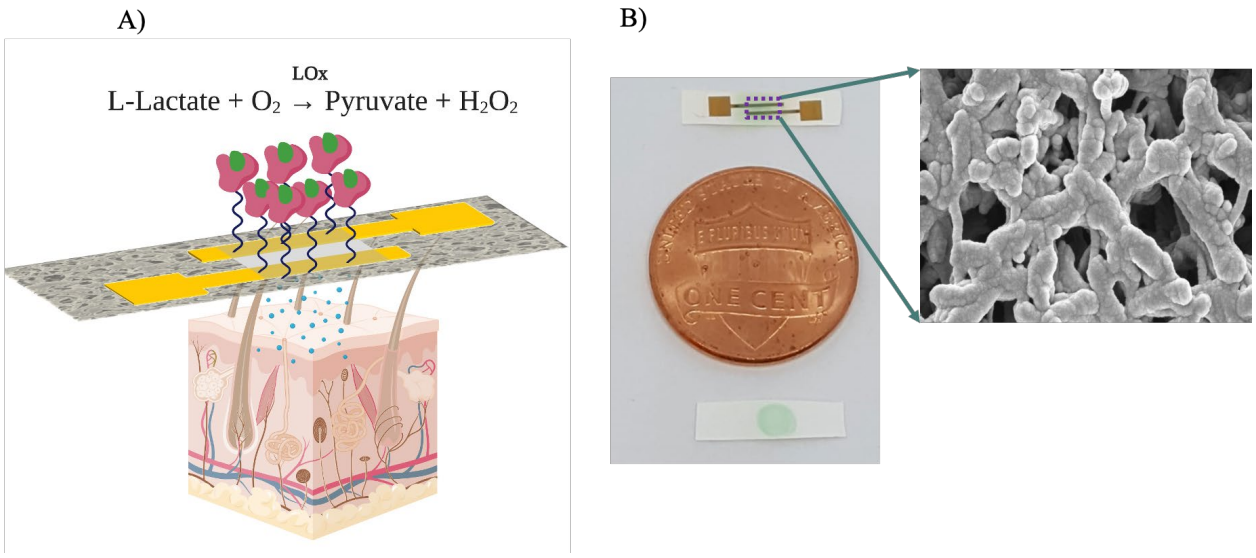

Figure 4.1.(A) Enzymatic assay chemistry immobilized on the ZnO active sensing region for the detection of L-lactate. Created using BioRender.com (B) Fluid wicking profile of the nanoporous polyamide substrate. Inset shows the SEM image of the substrate

4.3.2 Surface characterization for confirmation of enzymatic assay functionalization on lactate biosensing platform

Attenuated total reflectance (ATR) spectroscopy provides a detailed insight of the protein interactions occurring at the electrode-electrolyte interface. The interactions between the various layers of the enzymatic assay chemistry are characterized by a unique spectral fingerprint which is associated with the appearance or shift in certain absorption peaks. The ATR-FTIR spectra for nanostructured ZnO surface modified with DSP and DSP-LOx chemistry within the spectral range 600-4000cm^{-1} is shown in Figures 4.2A and 4.2B respectively. The peak related to ZnO nanotextured surface appears at 587 cm^{-1} and is shown in supplementary figure S1b. DSP linker is an amine-reactive crosslinker consisting of NHS-ester groups at the ends of its spacer arm and

a cleavable disulfide bond. The peaks appearing at 670 cm^{-1} and 705cm^{-1} represents the vibrations of CH_2 bond that form the backbone of DSP. The peaks at 1022 cm^{-1} and 1315 cm^{-1} are assigned to the stretching vibrations of the ester linkage and symmetric C-N-C stretch of NHS present in DSP respectively. Other significant identifier groups present in DSP appear at 1674cm^{-1} representing the asymmetric carbonyl stretch of NHS ester group. The absorption bands at 1407cm^{-1} and 1438cm^{-1} are characteristics of vibrations of the methylene scissors present in DSP. The bending vibrations of alkane stretch (C-H) is indicated by the two peaks at 2915 cm^{-1} and 3000 cm^{-1}. The DSP linker binds to the enzyme at the NHS end by breaking the C=O bond to form a stable amide bond and releasing the succinimidyl group. This process is indicated by appearance of peaks at 1020cm^{-1} (C-N stretch) and 1200 cm^{-1}(C-C stretch) associated with aminolysis of NHS groups in DSP with primary amines in enzyme. The peak at 1044 cm^{-1} indicates the C-O vibrations in LOx. The peaks at 1633cm^{-1} and 1538 cm^{-1} indicates the presence of amide I and amide II bonds of LOx. The amide I band appears from the C-O stretching of the peptide linkage present in the backbone of the protein. The amide II band appears due to the combined stretching of N-H and C-N bonds of the peptide group.

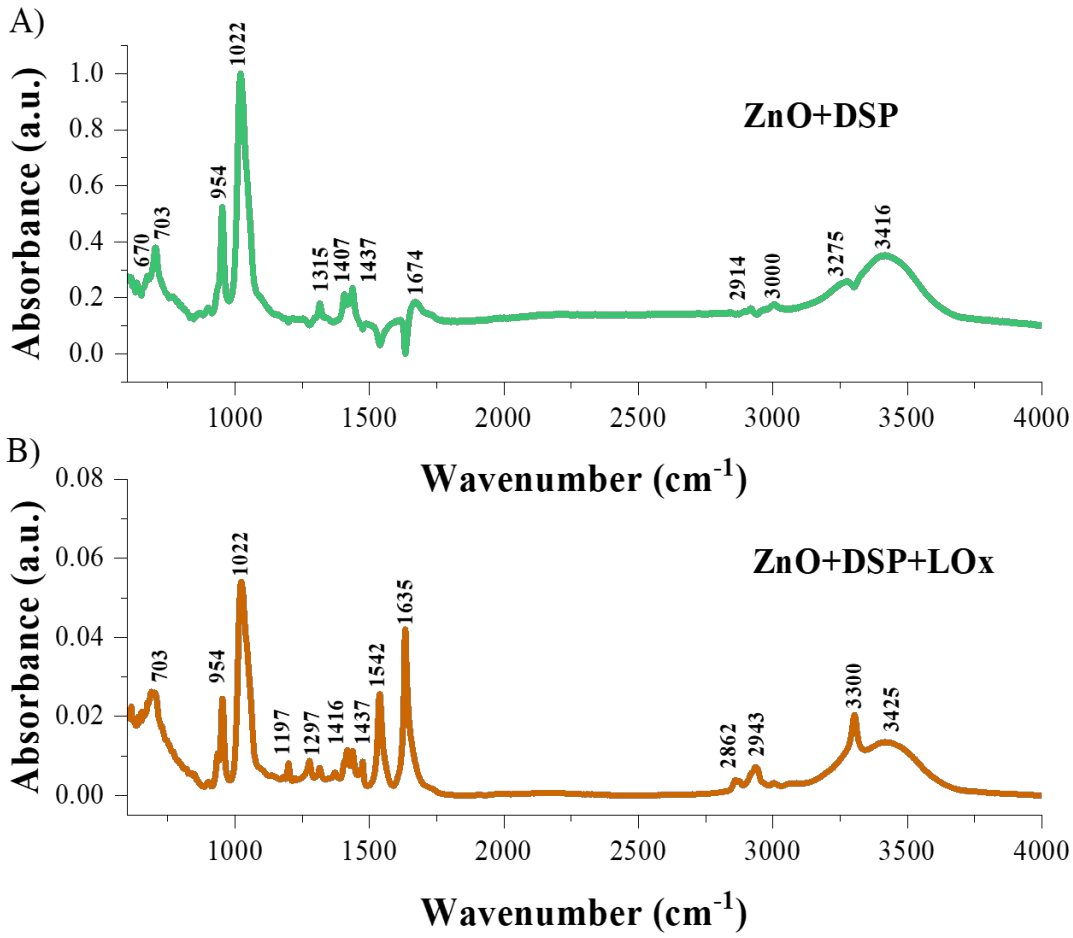

Figure 4.2. (A) ATR-FTIR spectra for ZnO- linker (DSP) binding (B) ZnO- linker (DSP)- enzyme (LOx) binding.

Another surface analysis technique called X-ray photoelectron spectroscopy (XPS) is utilized to get an in-depth understanding of the elemental composition of the interface being probed. XPS analysis was performed to ensure the binding of the thiol crosslinker to the sensing element. Figures 4.3A, 4.3B, and 4.3C show the XPS spectrum of bare ZnO and DSP modified ZnO surface for Zn2p3/2, O1s, and N1s peaks respectively. The Zn 2p3/2 peak for bare ZnO appears at 1021.4eV; it shifts to 1021.8eV for the DSP modified ZnO surface indicating the formation of Zn-S bonds. The O1s peak for bare ZnO observed at 530.8 eV shifts to 531.4 eV and can be attributed

to the C=O group of the NHS terminus. The peak at appearing at 533.4 eV indicates the presence C-O in the NHS terminus of DSP. The N1s peak appears at a binding energy of 400.4eV after modifying the ZnO surface with DSP which is a signature of the nitrogen species present in the NHS ester.

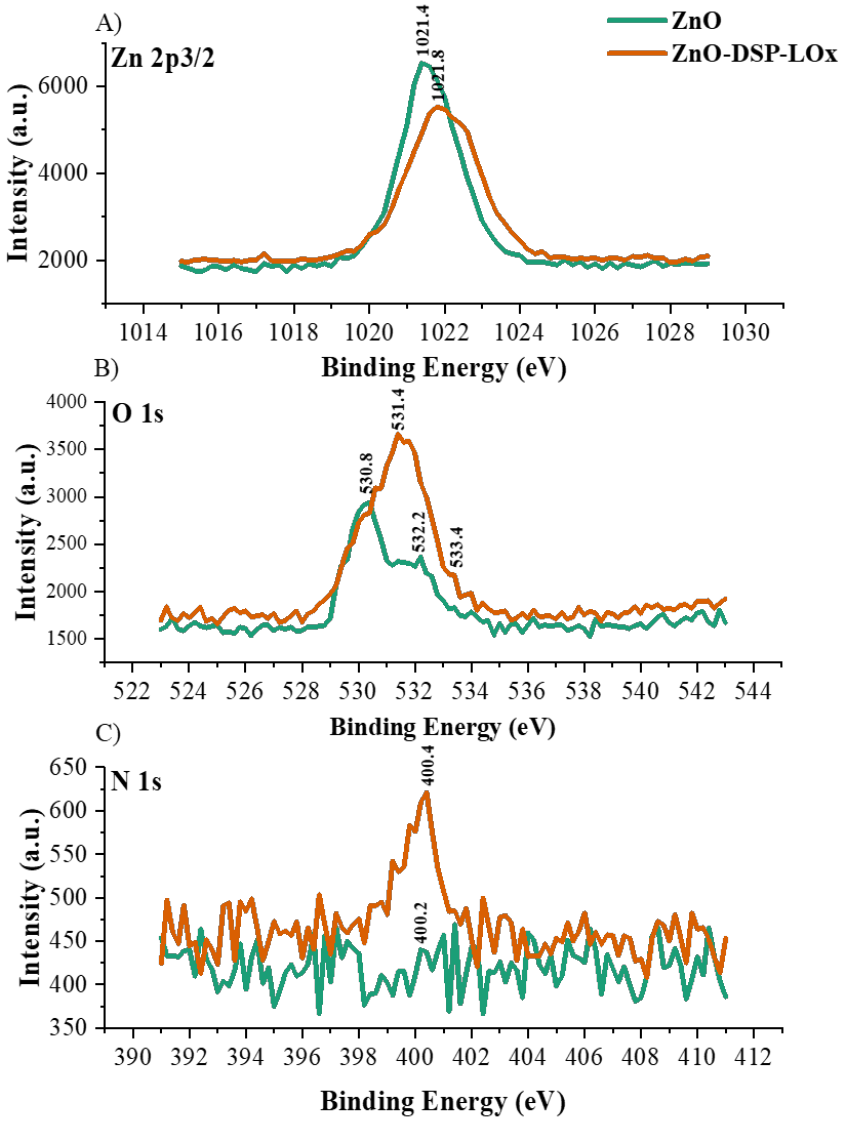

Figure 4.3.XPS spectra for bare ZnO and linker (DSP) modified ZnO surface for (A) Zn 2p3/2 peak (B) O1s peak (C) N1s peak

4.3.3 Zeta potential analysis for investigation of enzymatic assay stability in varying sweat pH buffers

Zeta potential quantifies the effective electric charge present on the surface of a particle. We utilize zeta potential measurements to characterize the electrical double layer formed at the sensing element – sweat interface and the modulations arising at the interface from LOx-lactate interaction. The surface charge states of a particle suspended in a solution is highly dependent on factors such as varying pH, ionic strength, and temperature. Zeta potential of bare ZnO nanoparticles and DSP-LOx functionalized ZnO nanoparticles in contact with sweat of pH 6 and pH 8 is shown in Figure 4.4A. The zeta potentials of bare ZnO nanoparticles in sweat pH 6 and pH 8 are 6.9±0.4mV and 2.55±0.5mV respectively. Higher potential is observed for ZnO particles suspended in sweat pH 6 than pH 8 due to excess H+ ions of the sweat buffer surrounding the ZnO nanoparticles. After DSP-LOx functionalization, the zeta potentials in sweat pH 6 and pH 8 alters to -13.68±0.6mV and -13.45±0.3mV respectively. The zeta potentials of DSP-LOx modified ZnO nanoparticles in varying pH sweat buffers change to negative potentials from positive potentials of bare ZnO nanoparticles. At pH 6 and 8, the positive surface charge of ZnO nanoparticles favors electrostatic coupling of the negatively charged enzymes to its surface[108]. Figure 4.4B shows the zeta potential response of the enzyme functionalized ZnO nanoparticles to increasing lactate dose concentrations in sweat buffer pH's 6 and 8. The zeta potential of zero doses for sweat pH 6 and 8 were -13.46±0.45mV and -13.44±0.6mV respectively. For 1mM lactate concentration, the zeta potentials for sweat pH's 6 and 8 are observed to be -13.11±0.52mV and -13.2±0.45mV respectively. At 100mM lactate concentration, the zeta potentials for sweat pH's 6 and 8 increase to -12.41±0.52mV and -12.39±0.12mV respectively.

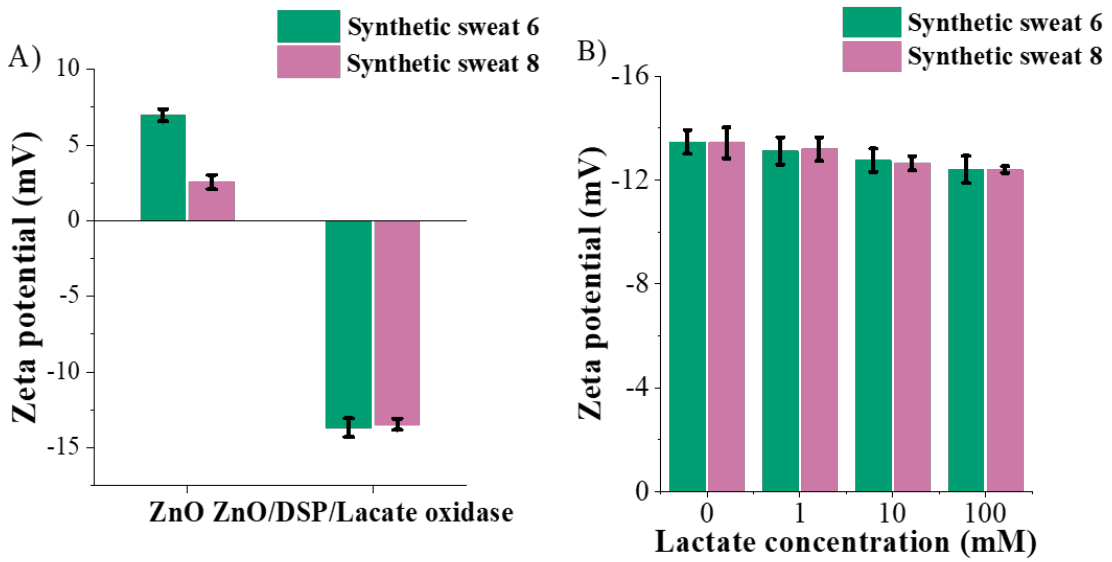

Figure 4.4. (A) Zeta potential for bare ZnO and linker (DSP)-enzyme (LOx) modified ZnO nanoparticles in synthetic sweat pH's 6 and 8 (B) Zeta potential response of the enzyme functionalized ZnO nanoparticles to increasing lactate dose concentrations in synthetic sweat pH's 6 and 8

4.3.4 Electrochemical characterization of the lactate biosensing platform for analytical performance evaluation in synthetic and human sweat

Electrochemical impedance spectroscopy has increasingly gained interest in characterizing protein-protein interactions in complex biological matrices. EIS yields several advantages such as high sensitivity, non-destructive sensing, quantification of the signal registered due to protein interactions from the background noise produced by the complex biological medium, and the capability to discriminate between interfacial and bulk processes[109]. Herein, the impedance spectrum is recorded within a narrow frequency range by applying a small AC perturbation signal and then measuring the AC current produced by the electrochemical changes occurring from the

immobilized biorecognition element – target analyte interactions. The data extracted from EIS analysis can be mapped to distinct frequency regimes consisting of solution resistance (R_s), resistance to charge transfer between the electrode surface and the solution (R_{ct}), resistance to diffusion of species to and from the bulk solution (Z_w), and the double layer capacitance (C_{dl}). The numerical values of these individual frequency dependent impedance parameters can be extracted by fitting the EIS spectrum to the Randle's equivalent circuit [see supplementary figure S2 of [95]]. We have used the non-faradaic mode of EIS for reporting the LOx enzyme-lactate interactions wherein the ionic charges are confined to the electrode and no true charge transfer is observed at the electrode-electrolyte interface making the system more capacitive in nature[110]. The formation of an electrical double layer at the electrode-electrolyte interface is the origin of capacitance in the system. Adsorption of the biorecognition element and its interactions with the target analyte induces a change in the dielectric properties at the electrode-electrolyte interface by displacing water and hydrated ions from the near vicinity, or from the change in protein structure conformation which are detected through capacitance probing. The total double layer capacitance of the system is generated from the capacitances contributed by the semiconducting film, the biorecognition element film, and the target analyte-biorecognition element interactions.

Although, human subject testing is considered ideal validation for performance testing of the lactate detection platform, constraints such as variation in sweating mechanism, sweat collection times and regions in the same subjects can affect the repeatability in measurements during system development and characterization phase of the platform. Hence, synthetic sweat is utilized to standardize the sensing protocol and expedite the development of the platform. We have calibrated the performance of the lactate detection platform for increasing lactate concentrations

0.1mM to 100 mM in synthetic sweat pH 6 and 8 to understand the effect of sweat pH variance on the lactate biosensing. The impedance response is represented as the change in impedance at a given concentration from the baseline impedance at zero dose (sweat devoid of lactate). The percentage change in impedance for increasing lactate dose concentration spiked in sweat is represented by the equation:

$$\%\ \text{change in impedance} = \ 100\ \times \left(\frac{\text{Baseline impedance} - \text{Dose impedance}}{\text{Baseline impedance}}\right)$$

The signal detection frequency was chosen to be 10Hz as maximum signal to noise response was obtained within the 1Hz to 100Hz regime with stable noise variation. The percentage change in impedance for lactate spiked in synthetic sweat pH 6 (SS6) from 0.1mM to 100mM varied from 4.5±2.2% to 37.6±3.3% as shown in Figure 4.5A. The specific signal threshold (SST) calculated using an SNR of 3 was computed to be 9.5%. Limit of detection of lactate in synthetic sweat pH 6 was found to be 1mM with an R^2 of 0.98. The percentage change in impedance for lactate spiked in synthetic sweat pH 8 from 0.1mM to 100 mM varied from 4.8±4.5% to 35.1±1.8% as shown in Figure 5B. The limit of detection was found to be 1mM as the percentage impedance change recorded from 0.1 mM lactate in synthetic sweat pH 8 falls under the 8.6% signal threshold level. The coefficient of determination R^2 was found to be 0.97. The dynamic range for lactate detection in synthetic sweat pH 6 and 8 was found to be 1mM to 100 mM. The overall percentage change in impedance for lactate dose concentrations in synthetic sweat pH 6 and 8 varies between ±1-4%. The Nyquist plots for target lactate dose concentration range 0.1mM to 100 mM spiked in synthetic sweat pH 6 and 8 are shown in supplementary figures S3a and S3b of [95] respectively. The imaginary impedance increases concomitantly with increasing lactate concentrations resulting from the charge storage capacitive properties of the double layer. These modulations arise from

the permittivity changes within the double layer which quantifies the LOx enzyme-lactate interactions at the electrode-sweat electrolyte interface and can be validated from the extracted capacitance values obtained from fitting the experimental Nyquist plot to the Randle's circuit as shown in Figure 4.5D. The double layer capacitance values demonstrate a dose dependent increase in response with increasing lactate concentrations. For 0.1mM to 100mM lactate dose concentrations, the Cdl values vary from 0.5µF to 0.96µF for synthetic sweat pH 6 and 0.44µF to 1.2µF for synthetic sweat pH 8. Figure 4.5C shows the calibration dose response curve for the detection of lactate in human sweat. The variation in percentage change in impedance from 0.1 mM to 100mM lactate concentration was found to be 0.4±0.28% to 27±2.2%. The sensitivity of the biosensor is calculated to be 8.3±0.92%/mM. The selectivity of the immobilized LOx enzyme in specifically detecting lactate molecules specifically in a complex human bodily fluid was established through cross-reactivity studies. The cross-reactive study was performed with cortisol as the detection molecule on the lactate biosensing platform. The percentage change in impedance obtained from the cross-reactive interactions of cortisol with the LOx enzyme was found to be 1.1±3.6% to 6.8±3.4% from 0.1mM to 100mM cortisol concentrations. The impedance responses obtained from 0.1mM lactate and cortisol overlap while the responses obtained from non-specific cortisol concentrations from 1mM to 100mM lie below the responses obtained from specific lactate interactions giving a confirmation that the developed enzymatic assay is specific to the target analyte lactate. The signal threshold was calculated to be 4.3% and smallest detectable lactate concentration (LOD) was found to be 1mM making the biosensor capable of detecting lactate within the established physiologically relevant range of 4mM to 80 mM in human sweat[111]. The Nyquist plot for increasing lactate dose concentrations in human sweat is shown in supplementary

figure S3c of [95]. The extraction of double layer capacitance varies from 0.38μF to 0.46μF for 0.1mM to 100mM lactate dose concentrations as shown in Figure 4.5D. The variations in charge transfer resistance resulting from the increased lactate binding in synthetic sweat of varying pH's and human sweat is shown in supplementary figure S3d of [95]. The performance calibration outcomes of the lactate biosensing platform demonstrate reliable and specific detection of lactate within the physiologically relevant range present in human sweat primarily originating from the permittivity changes within the double layer. The enhanced sensitivity of detection can be credited to the nanoporosity of the flexible membrane used for detection which influences transport kinetics, reduces diffusion time, and provides high surface area to volume. The macromolecular confinement stabilizes protein, retains protein conformation, and enhances protein-bioreceptor interactions. Selectivity is achieved by leveraging the size-based exclusion feature of the membrane that rejects interfering lipid and ions present in human sweat allowing for small molecule detection[112].

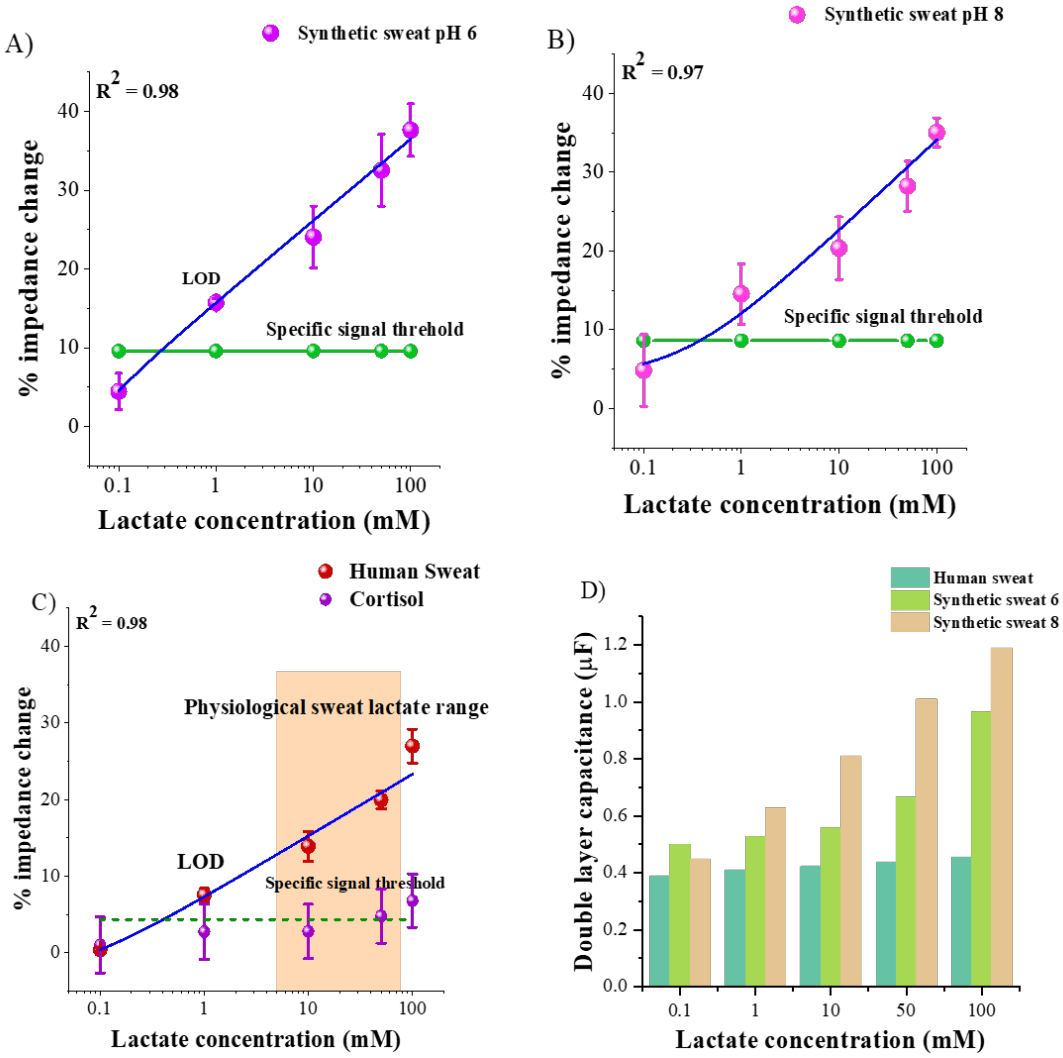

Figure 4.5.Calibration dose response of lactate in (A) synthetic sweat pH 6 (B) synthetic sweat pH 8 (C) human sweat (D) Extracted double layer capacitances for 0.1mM – 100mM lactate concentrations in synthetic sweat pH 6,8, and human sweat

4.3.5 Sensor stability and continuous lactate monitoring

Majority of the biosensing platforms suffer from instability as the immobilized proteins or enzyme are liable to undergo alterations under inappropriate storage conditions further affecting the biosensor's sensitivity. The evaluation of the biosensor's stability is crucial for the assessment its

of performance metric particularly in the use of single-use, disposable sensors. The stability metric gauges the retainment of the biosensor's activity when stored under specific conditions to avoid performance degradation[113]. The biosensor strips were immobilized with LOx enzyme at room temperature and the performance of the lactate biosensor stored at 4°C until use was measured over 4 days as shown in Figure 4.6A. Each day a new biosensor strip was taken out from 4°C to measure the impedance response of varying lactate concentrations spiked in human sweat. The mean % impedance changes produced over 4 days for 1, 10, 100mM lactate were found to be 11.9±0.96, 18.4±2.05, 27.0±2.0 respectively. The lactate biosensor's performance diminishes by ~30% over the 4-day period while the % coefficient of variation in this duration was computed to be well within 20% variation limit as set by CLSI standards indicating stable sensor operation.

It is imperative to understand the long-term sensing performance of the biosensing platform making it essential to establish the passive sweat patterns in average people during sedentary phases. The average passive sweating rate of one consenting sedentary subject were recorded using a commercial sweat rate sensor (VapoMeter, Delfin Technologies, Ltd.) over a 60-minute duration. The average passive sweat rate in the sedentary phase was recorded to be 19.7± 3.2g/m^2h as shown in the inset of Figure 4.6B. The passive sweat volumes calculated from the sweat rates of the three subjects are calculated to be 0.03 – 0.05µL/cm^2min. Considering a sweat gland density of ~200/cm^2 present on the forearm, the passive sweat volume rates can be translated into 3-6µL sweat volume which is adequate for on-demand, single- use biosensing. The response of the platform to continuous benchtop dosing of lactate spiked in human sweat to mimic the continuous mode of passive sweat based-lactate detection in real-time is shown in Figure 4.6B. The biosensor was dosed with 3 µL lactate concentrations in the range 20mM to 80mM in a 5-

minute loading interval with an incremental percentage change in impedance observed for every dose loading step. The output percentage impedance increases from 5-22%, 32- 45%, 47-49% for 20,40, 60mM lactate loading respectively. At 80mM, the sensor begins to reach an inflection point at 56% owing to excess lactate ions causing charge screening. The developed lactate biosensing platform is responsive to accumulative lactate concentrations up to 80mM in passive human sweat over a 45-minute duration before the sensor begins to show signs of saturation.

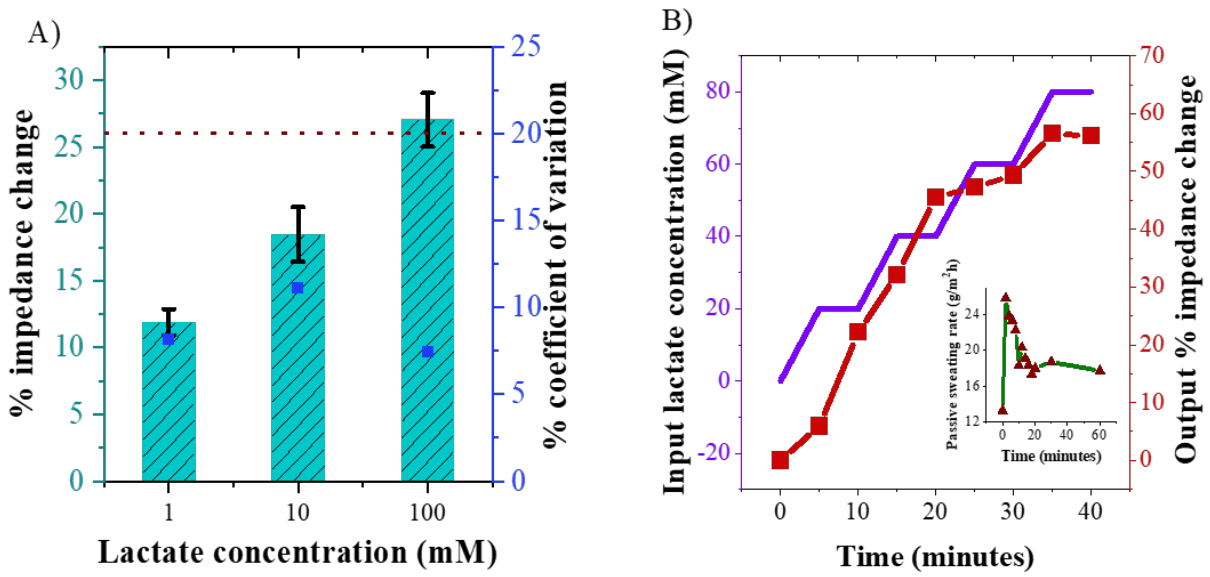

Figure 4.6 (A) Stability performance of the lactate biosensing platform over a 4-day duration. Dashed line at 20% represents the acceptable variation limit as set by CLSI standards (B) Continuous detection of lactate in passively expressed human sweat. Inset shows the passive sweat evaporation pattern in an average person during a sedentary phase.

4.3.6 Human subject on-demand evaluation of lactate biosensing platform

The translation of the lactate biosensing platform from a benchtop environment to its utility as an on-demand platform for sedentary lifestyle can be studied by characterizing its performance when placed in close proximity to the human epidermis such that there is direct interaction with the sweat biomarker of interest. The underlying idea is to capture the temporal dynamics of sedentary lifestyle in its entirety from inactive state to less active state yet producing passive sweat. The electrochemical performance of the developed lactate biosensor was evaluated to estimate the lactate levels from three consenting human subjects recruited as per IRB compliant protocols. Eccrine sweat glands play an important role in thermoregulating the temperature of the body when sweat is produced in response to activity. The eccrine gland density present on the forearm region is 225±25 glands/cm^2 and is chosen to be an ideal location for placing the sensor[114]. The lactate levels were extracted after a 60-minute duration of being sedentary or a lightly intense active phase by correlating the obtained impedances to the impedance ranges obtained from the constructed calibration dose response curves (see materials section for detailed protocol). Signals generated from the interaction of the lactate produced in human eccrine sweat with the LOx enzymatic assay are authenticated by simultaneously testing for lactate on a control sensor without any LOx functionalized on it. Figure 4.7A shows the impedance values extracted from the human subjects before and after activity on the LOx functionalized and control sensors respectively. The impedance response generated before and after activity from the catalytic interaction of the lactate produced in human sweat with the LOx enzyme lie within ranges 28.5-29.5KΩ and 26.9-27.4KΩ respectively while the impedance ranges produced by the control sensor before and after activity are found to be 44-193KΩ and 23-41KΩ. Additionally, the transition in the phase response from

a resistive phase angle prior to activity to a capacitive phase angle post activity confirms our claim of double layer capacitance modulation occurring on enzymatic catalysis of lactate [see supplementary figures S4a, 4b, and 4c of [95]]. A significant difference is found in impedance levels registered by the lactate sensor pre and post activity with a p-value of 0.017 (assuming $p<0.05$). The decrease in the impedance after the catalytic interaction of the lactate with the LOx enzyme corroborates with our observations made in human sweat calibration studies. The percentage changes corresponding to the extracted sweat lactate levels produced by the lactate sensor lie within the 10-18% range. As shown in Figure 4.7B, the sweat lactate levels extracted from the percentage impedance changes observed on LOx functionalized sensors for subjects 1, 2, and 3 were found to be 4.87 mM, 9.07 mM, and 21.2 mM respectively validating the catalysis of sweat lactate by the immobilized LOx on the sensor surface. The responses generated by the enzymatic and non-enzymatic control sensors indicate that the biosensing platform is selective to detecting only lactate present in sweat over other sweat constituents. Table 4.1 provides the detailed summary about the activity of the human subjects and the ranges of their vital parameters. Factors that affect the sweat lactate production in human subjects depend on the sweat rates, intensity of the exercise, lactate excretion, and the heart rate[115].

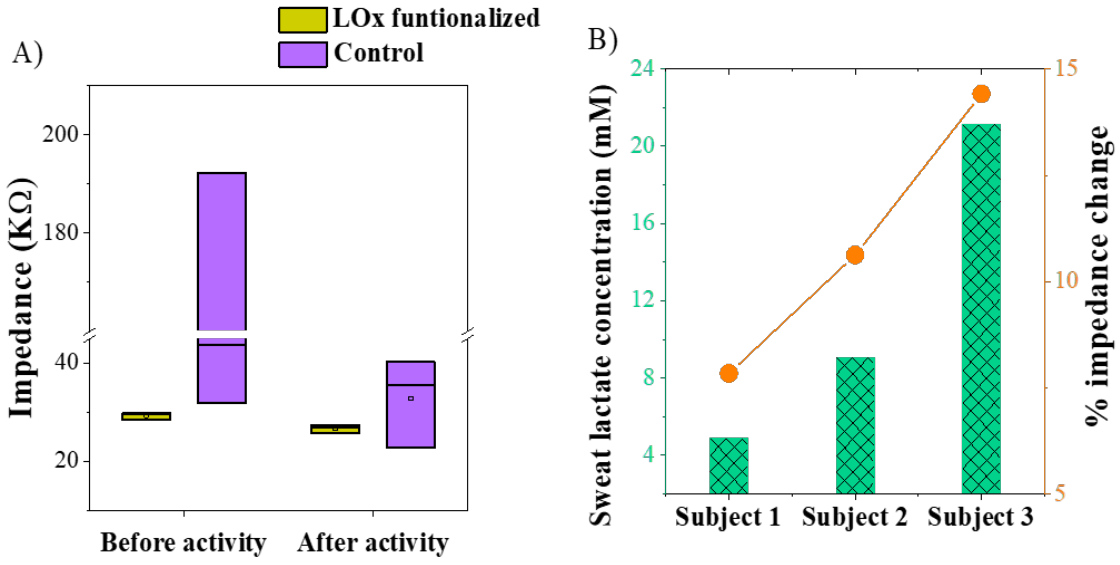

Figure 4.7.(A) Extracted impedance values from human subjects before and after activity on LOx functionalized and control sensors (B) Sweat lactate levels of human subjects extracted after activity on LOx functionalized sensors

Table 4.1. Summary of the activity of the human subjects and the ranges of their vital parameters

Subject 1	Sedentary
Subject 2	Sedentary
Subject 3	Light activity
Heart rate	110-120bpm
Temperature	36-37.5°C
spO2	95-100%
Blood pressure	120/80-135/80

4.4 Experimental section

4.4.1 Materials and reagents

Polyamide substrates of pore size 200nm and thickness 60µm were obtained from GE Healthcare Life Sciences (Piscataway, NJ, USA). The linker molecule dithiobis succinimidyl propionate

(DSP), dimethyl sulfoxide (DMSO), and 1X phosphate buffered saline (PBS) were purchased from Thermo Fisher Scientific Inc. (Waltham, MA, USA). Sodium L-lactate (~98% purity) and ZnO nanopowder (<100nm) was purchased from Sigma-Aldrich (St. Louis, MO, USA). Lactate oxidase (80U/mg) was purchased from Toyobo USA. α-cortisol antibody and hydrocortisone were purchased from Abcam (Cambridge, MA, USA). Synthetic sweat was prepared from the recipe described in M.T. Mathew et. al[56]. The pH range was adjusted by varying the concentrations of lactic acid and ammonia. Single donor human sweat of pH ~6 was purchased from Lee Biosolutions Inc. (Maryland Heights, MO, USA). No preservatives were added to this product, and it was stored at -20°C. All lactate dilutions were made in synthetic sweat pH 6, 8, and in human sweat.

4.4.2 Sensor fabrication

The fabrication process of the lactate biosensor involves thin film deposition of 150nm thick gold interdigitated electrodes on a flexible nanoporous polyamide membrane using a Temescal e-beam evaporator tool (Ferro Tec, Livermore, CA, USA). Further, a 100nm thick semi-conducting ZnO thin film was sputtered onto the overlap region between the interdigitated gold electrodes using AJA Orion RF magnetron with a 99.999% ZnO target (Kurt J. Lesker, Pittsburgh, PA, USA).

4.4.3 Lactate biosensor calibration

3-5µL volume of 10 mM DSP linker was diluted in DMSO and incubated on the sensor surface for 3 hours. All solutions are dispensed from the backside of the sensor. 3-5µL PBS wash was carried out to remove any unbound linker. The linker functionalized surface was treated with

4mg/mL of lactate oxidase and incubated for 90 minutes. Lactate-free synthetic sweat was applied to the sensing region to obtain baseline impedance measurement. Further, lactate dilutions of concentrations – 0.1, 1, 10, 50, 100mM were made in synthetic and human sweat buffers. The lactate doses were incubated on the sensor surface for 5 minutes to allow for catalysis reaction to occur. The lactate doses were applied serially from low to high concentrations to construct the calibration response curve. The cross-reactivity study was performed in a similar manner with cortisol dose concentrations- 0.1, 1, 10, 50, 100mM made in human sweat buffer being introduced serially on the sensing surface. EIS measurements were recorded using a potentiostat (Gamry Instruments, Warminster, PA, USA) after the application of a 10mV AC excitation signal with a frequency sweep of 1Hz to 1MHz. All measurements were carried out in under ambient temperature conditions. All data is represented as mean± relative standard deviation (RSD). A sample set of N= 3 was used throughout this research for building CDRs in synthetic and human sweat buffers.

The stability study was performed by immobilizing the lactate oxidase enzyme on four sensors and storing it in 4°C until usage. Each day a new sensor was tested by serially applying 1, 10, 100mM lactate doses made in human sweat and EIS measurements were recorded at 10Hz. The continuous dosing study was performed by dispersing 20, 40, 60, 80mM lactate doses made in human sweat on the sensor successively. Each lactate dose concentration was added twice at the rate of 3μL every 5 minutes over a total duration of 45 minutes. Single frequency EIS response was recorded at 10Hz.

4.4.4 ATR-IR spectroscopy

The infrared spectra collected to establish the successful functionalization of the lactate detection enzymatic assay was captured using Thermo Scientific Nicolet iS-150 FTIR (Waltham, MA, USA) in Attenuated Total Reflectance (ATR) mode. The tool consists of a KBr window and deuterated triglycine sulphate (DTGS) detector. A Harrick VariGATR sampling stage with a 65° germanium crystal was used to obtain the spectra. The spectra were collected with a resolution of 4 cm^{-1} for 256 scans in a wavelength range of 4000 cm^{-1} to 600 cm^{-1}. The ATR-IR samples were prepared on ZnO deposited polyamide membrane by functionalizing the lactate detection enzymatic assay.

4.4.5 X-Ray Photoelectron Spectroscopy

XPS spectra was obtained by using a PHI 5000 Versa Probe II (ULVAC-PHI, Inc., Methuen, MA, USA) with a monochromatic Al Kα radiation (hν = 1486.6 eV) at a 45° takeoff angle with respect to the sample surface. All spectra were obtained with a 0.2 eV step size and 23.50 eV pass energy. The base pressure in the analysis was maintained at 1.6 × 10−8 Torr. Sample preparation was carried out on a silicon wafer by functionalizing the lactate detection enzymatic assay. Further, the prepared samples were dried in a vacuum chamber. All binding energies were corrected for the charge shift using the C1 s peak of graphitic carbon (BE = 284.8 eV) as a reference.

4.4.6 Zeta potential study

Zeta potential measurements were carried out in synthetic sweat pH 6 and 8 to validate the enzymatic assay functionalization on the ZnO sensing surface by using Malvern ZetaSizer Nano ZS (Malvern Panalytical, Malvern, UK). The zeta potential was calculated from the measured electrophoretic mobility using the Smoluchowski approximation:

$$\mu = (\varepsilon.\zeta)/\eta$$

where μ is electrophoretic mobility; ε is the dielectric constant; ζ is the zeta potential; and η is the viscosity of solution. Initially, the zeta potential of the zinc oxide nanoparticles suspended in synthetic sweat pH 6 and 8 were measured. Further, 10μL of ZnO nanoparticles, 10μL of DSP made in DMSO, and 10μL of lactate oxidase enzyme was incubated for three hours at room temperature followed by the addition of 970 μL of synthetic sweat pH 6 and 8. All measurements were performed in triplicate measures. The zeta potentials for lactate concentrations- 0, 1, 10, 100 mM made in synthetic sweat pH 6 and 8 were recorded to ensure the functionality of the enzymatic assay immobilized on the ZnO surface.

4.4.7 Vapometer sweat rate measurements

One healthy volunteer (age: 20-30 years) was recruited for sweat rate measurement study using an FDA approved commercial device VapoMeter (Delfin Technologies, Ltd., Kuopio, Finland) that measures transepidermal water loss and sweat evaporation rate. The subject was asked to wear a trimmer band on the forearm at the site of sweat rate measurement to induce passive sweat. Measurements was carried out every 2 minutes for 60 minutes. Written and informed consent was obtained from the subject prior to the study. All trials were conducted with strict compliance to the IRB protocol (#19-23) approved by the Institutional review board of University of Texas at Dallas

4.4.8 Human subjects testing

Three healthy volunteers (age: 20- 30 years) were recruited for this study. Written and informed consent was obtained from the subjects prior to the study. All trials were conducted with strict

compliance to the IRB protocol (#18-116) approved by the Institutional review board of University of Texas at Dallas. The study conducted involves less than minimal risk. The recruited volunteers had no history or existing heart condition, diabetes, or muscular pain. The site of sensor placement on the forearm was cleaned with alcohol wipes prior to securing the control and the LOx functionalized sensors with a medical grade adhesive. The volunteers were asked to wear a trimmer belt on their arm to induce sweating for the 60-minute duration of being sedentary or during the light activity phase. The impedance baselines of the control and LOx functionalized sensors were measured prior to human subject trials. After the 60-minute duration, the sweat lactate levels were extracted by connecting the sensor to the Gamry for impedance measurements. The instantaneous lactate levels were extracted by measuring the percentage change in impedance before and immediately after 60 minutes. The sensors were carefully unmounted from the forearm of the volunteers and the impedance data was recorded using a potentiostat (Gamry Instruments, Warminster, PA, USA) at 10Hz frequency.

4.5 Conclusions

The timely recognition of diseases by means of non-invasive fluids such as eccrine sweat would be critical in providing rapid treatment and improving the survival rates for patients that further develop complications. Design and development of on-demand, point-of-use sensing platforms will aid in measurement of biomarker levels for better care of sedentary population. Lactate detection has grown out of the stage of infancy to become a molecule of interest in health and disease monitoring. Emergent flexible sensing technologies have shifted their focus from fitness tracking towards real-time physiological biomarkers in non-invasive bodily fluids for disease detection. Aside from being a workhorse biomarker for endurance testing in the sports arena,

increased lactate production is indicative of clinical conditions caused by restricted oxygen supply. The key highlight of this work is the epidermal functionality and performance of a sweat lactate sensor on a surface engineered nanoporous platform with low volume detection capability for on-demand measurements. Semiconducting properties of nanotextured zinc oxide films have been leveraged for the sensitive detection of lactate in a complex human sweat buffer through non-faradaic EIS technique. EIS gives a microscopic understanding of the enzyme-target analyte interaction dynamics characterized by the charge perturbations occurring in the double layer. The lactate biosensor exhibited an LOD of 1 mM and a dynamic detection range of 1-100 mM in human sweat. A highly specific response to lactate was observed with minimal cross-reactivity from non-specific molecules present in human sweat. Stability and continuous dosing studies indicate the robustness and the long-term capability of the biosensing platform in detecting lactate in human sweat. The on-demand feature of the biosensing platform provided a rapid quantification of sweat based-lactate levels when placed on human subjects. ATR-FTIR and XPS analysis gives a confirmation on the enzymatic assay immobilization on the ZnO sensing surface. The modification in surface charge at the electrode-electrolyte interface as a consequence of enzymatic assay binding and synergistic interactions between enzyme-lactate is characterized by the zeta potential.

4.6 Acknowledgements

The authors would like to thank John Craven for helping with the scanning electron micrographs.

4.7 Prior publication

Ashlesha Bhide performed the experiments and compiled the data from all the studies. Kai-Chun Lin performed the XPS and zeta potential experiments. Ashlesha Bhide fabricated the sensors and

analyzed the data. Sriram Muthukumar and Shalini Prasad conceived the design of the sensor stack and guided the experimental design. Ashlesha Bhide, Sriram Muthukumar, and Shalini Prasad interpreted the data and co-wrote the manuscript. This article was published in Analyst in 2021. This article has been reproduced by permission from the Royal Society of Chemistry publishing company and the link to this article is: https://doi.org/10.1039/D1AN00455G

CHAPTER 5

POINT-OF-USE SWEAT BIOSENSOR TO TRACK THE ENDOCRINE-INFLAMMATION RELATIONSHIP FOR CHRONIC DISEASE MONITORING

5.1 Abstract

When the body is under stress, a lot of physiological processes work towards bringing the body back to its normal state. The Hypothalamic-Pituitary-Adrenal (HPA) axis is involved in maintaining homeostasis by engaging with the parasympathetic nervous system. During the process of chronic disease affliction, this relationship is disturbed and there is an imbalance driven response observed. Cortisol, a stress hormone and TNF-α, a protein related to inflammation, are direct products of these physiological processes. By monitoring the two key components involved in these pathways, cortisol and TNF-α, the manifestations of chronic stress on the homeostasis of the body can be evaluated in a comprehensive manner. The goal of this work is the demonstration of a biosensor that is capable of tracking these molecules in human sweat. This work highlights the development of an electrochemical detection system for the two biomarkers through human sweat. The limit of detection and dynamic ranges are 1ng/mL, 1ng/mL to 200ng/mL for cortisol and 1pg/mL, 1pg/mL to 1000pg/mL for TNF-α. The significance lies in simplifying disease diagnostics, i.e., to detect and monitor diseases. This system is designed to be a wearable that will track the levels of cortisol and TNF-α and use it as an indicator of the user's health status.

5.2 Introduction

Understanding the relationship between the endocrinal pathway for stress regulation and the inflammation pathway is key to understanding the physiological effects and the extent of damage

inflicted during periods of exposure to stress. The HPA axis is a prime component of the endocrinal system to prepare the body to react to a stressful episode. The response to stressful stimuli is non-voluntary and is aimed at bringing the body back into homeostasis via a process known as allostasis. A detailed summary of the response to stress is illustrated in Figure 5.1A. The signal originates in the hypothalamus, specifically in the hypothalamic paraventricular nucleus. The neurons in response to this produce Corticotropin releasing hormone. Corticotropin releasing hormone production signals the pituitary gland to release Adrenocorticotropic hormone into the blood stream. Once in the blood stream, as the name of the hormone suggests, it activates the receptors present in adrenal gland – specifically in the adrenal cortex. This houses cells that are capable of steroidogenesis and with the adrenocorticotropic hormone-mediated activation, start producing Glucocorticoids, like cortisol. Cortisol is an anti-inflammatory corticosteroid, which is responsible for performing allostasis by activating various pathways responsible for a decreased inflammatory response in the target organs. One of the pathways functions by reducing the adaptive immunity effector cells i.e., T-cells, by apoptosis and the other pathway performs tightening of the tight junctions in endothelial cells to prevent transport of peripheral immune cells from entering the blood-brain barrier. However, the main response of cortisol mediated control of inflammation is through the glucocorticoid receptor (GR) controlled genomic immunosuppression, which reduces the production of pro-inflammatory cytokines like TNF-α[116], [117]. There is a presence of a negative feedback mechanism that is controlled by the affinity of corticosteroids to GRs. After sufficient production, the receptor is saturated and signals the HPA axis components to stop production of GC activating hormones. With the production of cortisol as a response to stress, the inflammation pathway is stimulated as demonstrated in Figure 5.1B. The glucocorticoid

receptor has a major role in the processes responsible for cell homeostasis. There are various modes of action by which the GC receptors operate. In this research, we focus on capturing the pathway that is responsible for controlling the production of TNF-α. Normally, GR is present in the cytoplasm; once activated with corticosteroid, the bound proteins dissociate, and it enters the nucleus. Figure 1 depicts a red cylinder, which is the HSP90 chaperone protein, and the two circles are the other accessory proteins involved with activation and transport of the GR from the cytoplasm to the nucleus. The GR regulates genomic expression by dimerizing to glucocorticoid response elements in the target genes and affecting the transcription/translation of the mRNA to produce cytokines. Due to this effect, the production of pro-inflammatory cytokines like TNF-α, IL-6, and IL-1β are decreased and the production of anti-inflammatory cytokines such as IL-10 and TGFβ is increased[118], [119]. The interconnection of these two pathways is of diagnostic importance to many disorders. An impairment of these regulation pathways is highly associated with mortality. In case of patients suffering from Crohn's disease, findings suggest that the inflammation pathway is disturbed and there is an overexpression of TNF-α. Similarly, in the case of IBD (irritable bowel disease) there is an imbalance in the sympathetic control of the adrenal gland activity. The triggers for generating severe symptoms in both these conditions were observed to affect the HPA axis functioning first, thus resulting in lower cortisol production[120]. A report also suggests that the elevation of pro-inflammatory cytokines and corticosteroid levels has negative effects on the cognitive functioning and hippocampal structure of older adults [121]. All these examples highlight the interconnectivity of the two pathways and the need to monitor the direct products from a chronic disease diagnostics and monitoring aspect. The effective solution for offering a convenient platform for self-monitoring is using sweat for biomarker quantification.

Human sweat based sensing platforms offer significant advantages over traditional and gold standard methods of detection. Physiologically, cortisol and TNF-α are expressed in sweat in the ranges of 8ng/mL to 141ng/mL and 9pg/mL to 362pg/mL respectively[122], [123]. There have been significant advances in the field of developing sweat-based cortisol sensors for investigation into the effects of stress on the body. TNF-α has been explored as a key to understanding the regulatory processes in the body upon the onset of inflammation. Table 5.1 describes the different biosensors developed for tracking TNF-α and cortisol in various biofluids, which are aimed towards eventually becoming wearable technology. TNF-α detection in sweat has not yet been extensively researched and is an upcoming area of interest amongst the researchers in the field of wearable diagnostics. However, in the past few years, researchers have looked at understanding the fluctuation of cortisol and TNF-α levels in blood/serum towards characterization of phenotypes of multiple diseases[124], [125]. The levels of cortisol have been known to correlate with the sweat levels with levels being independent of sweating rate[126]. Similarly for TNF-α, it has been reported that sweat biomarker levels closely mirror the blood/serum levels and can be easily detected using wearable patches[123]. By tuning the sensor to capture changes in the biomarker levels withing the physiologically relevant levels of cortisol and TNF-α, this platform offers a novel approach towards understanding the effect of circadian dysregulation on the inflammatory response of the body. This would also enable early detection of circadian dysregulation and understanding its connection with the etiology and pathophysiology of disorders.

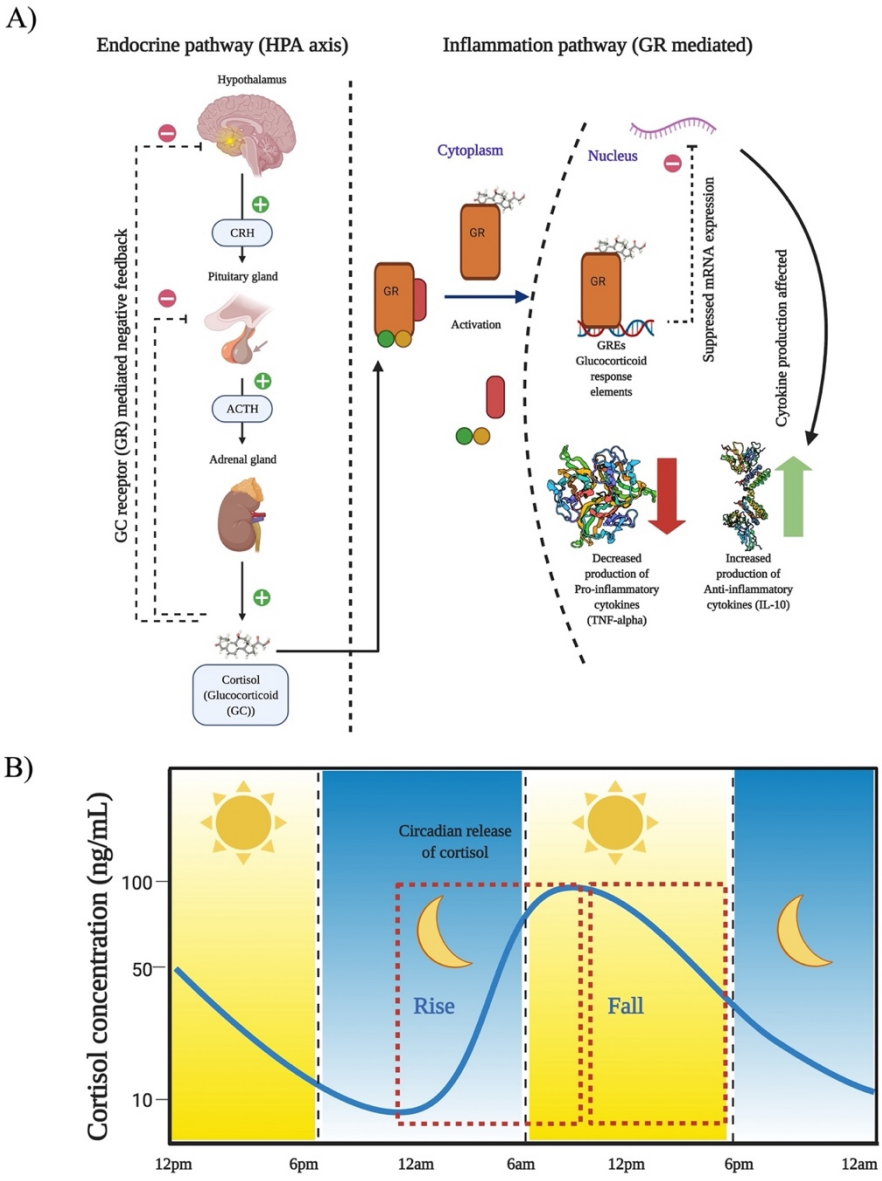

Figure 5.1.(A) Figure depicting relationship between the Endocrinal HPA(Hypothalamic-Pituitary-Adrenal) axis pathway and Inflammation pathway (TNF-α) (B) Schematic depicting diurnal cycling of cortisol over the period of 24 hours. Created using BioRender.com

Table 5.1. Biosensor technologies for detection of TNF-α and cortisol

Sensor description	Biomarker and biofluid	Type of detection	Limit of Detection (LOD)	Reference
Polypyrrole based gold screen printed electrode (enzyme labelled)	TNF-α, bovine calf serum	Potentiometric	10pg/mL, compared with commercial ELISA	[127]
Gold interdigitated electrode capacitor arrays	TNF-α, Phosphate Buffered Saline (PBS)	Label free capacitance measurements	32pg/mL	[128]
Affinity based gold electrode functionalized using carboxymethylaniline (CMA)	TNF-α, artificial saliva, human saliva	Chronoamperometry	1pg/mL	[129]
Stretchable and disposable 3D micropatterned elastomer-based electrode	TNF-α, human serum	Electrochemical (potentiometric and impedimetric)	100fM	[130]
Label-free chronobiology tracking system	Cortisol, sweat	Impedimetric	1ng/mL	[104]
Molybdenum disulphide ($MoS_{2)}$ nanosheet based flexible electrode	Cortisol, sweat	Impedimetric	1ng/mL	[131]

Multiplexed biomarker detection has gained considerable visibility in point-of-use testing arena in the recent years, owing to its capability in enhancing the diagnostic detection process of an underlying condition with precision and efficiency through rapid on-site analysis of bodily fluids[132]. Multi-biomarker detection platforms provide an in-depth clinical understanding of the processes occurring within the body with a certainty that a condition is indeed present in an individual; single biomarker analysis may not prove to be effective in providing accurate diagnosis

[133], [134]. Multiplexed point-of-care testing, through its capabilities, has paved the way for home-based, personalized patient centric systems for the management of chronic and acute diseases in resource limited settings[135]. Conventional testing methods are tedious, constrained to laboratory and hospital setups, require trained personnel, and require prolonged analysis times [136]. Wearable technology is expected to show a global growth rate of 38% in the next decade and will continue to evolve with the advent of smart-watches, patches, clothing, and fitness trackers[3]. Real-time, continuous health monitoring is one important feature that is being explored in the research space of multiplexed biomarker detection to provide an account of an individual's health status for the healthcare provider to administer accurate treatment and drug therapy. Herein, we describe a proof-of-concept multiplexed detection of stress biomarker cortisol and inflammatory cytokine TNF-α on flexible, body conforming substrate towards integration on a wearable platform. The choice of substrate is a key parameter to be considered while designing flexible biosensing platforms. The desired features of the selected substrate are bendability, foldability, stretchability, portability, skin-conformability, disposability, and being lightweight[137]. We have utilized a nanoporous polyamide membrane that allows for sweat wicking through its intercalations, sensitive detection due to enhanced charge storage through its nanoconfinement properties, and selective detection of target biomolecules from the biomolecular sieving properties[37].

In this work, we have demonstrated the functionality of biosensing platform in detecting dual biomarkers – cortisol and TNF-α in human sweat towards the development of a multiplexed point of use device. Additionally, the long-term temporal stability of the cortisol biosensor in detecting the simulated rise and fall in cortisol levels through the 6-hour sleep cycle has been

demonstrated. Furthermore, COMSOL Multiphysics simulation highlight the electrode design features and fluid wicking pattern of membrane for design optimization of the sweat based platform. The cross-reactivity performance demonstrates that the sensor is highly specific for the target biomarker. Thus, this novel platform shows the feasibility of tracking the endocrine-inflammation relationship towards chronic disease diagnostics using sweat.

5.3 Results and Discussions

5.3.1 Sensor substrate characterization

The focus of this work is to demonstrate the functionality of a novel, flexible sweat based sensing platform for quantifying the concentrations of biomarkers, cortisol and TNF-α. The substrate employed to make this platform is a nanoporous polyamide membrane. A two-electrode interdigitated system is chosen as the electrode design and fabricated using thin film gold deposition. The physical properties of the nanoporous membrane are highlighted in Table S1 of [138]. Nanoporous platforms offer significant advantages over porous materials. They increase the overall surface area of interaction between the target molecule and receptor i.e., capture probe. This work is based on an affinity sensing mechanism by using electrochemical detection modality. The gold electrode surface is treated to immobilize the detection probe i.e., the antibody, using a thiol linker chemistry. The analyte present in sweat is introduced on the sensor surface and it wicks through the membrane to interact with the bioactive components and generate a signal response. The advantage of having a nanoporous membrane is that it provides selective molecular confinement based on size and diffusion kinetics[139]. A schematic of this phenomenon is presented in Figure 5.2A. The schematic describes the process of detection of target biomarker in

a complex biofluid sample matrix, which in this case, is human sweat. Sweat is a complex mixture of proteins, steroids, hormones, electrolytes, and other interferent molecules. The blue droplet of sweat is loaded on to the functionalized sensor surface, with the antibodies concentrated on the gold surface of the sensor. The sensor surface depicted as a grey matrix in the figure is a magnified cross-section of the sensing membrane. With the nanopore based filtration, there is enhancement in the selectivity of the sensor response. Also, this reduces the overall noise of the system and improves the selectivity and sensitivity. The principle of wicking in this nanoporous membrane is capillary imbibition. Two main factors contribute to it, one is the transport of biomolecules normally a function of permeability and retention factor of the membrane, and second is biomolecular confinement, which is associated with the pore packing structure of the membrane. The retention factor describes the affinity of the dye to the solid phase, which is the nanoporous polyamide membrane. Zone separation of a liquid solute during wicking through the nanoporous membrane highlights the ability of the membrane to filter the different components in the liquid phase. The red dye solution has approximately four components, thus the formation of three or more separation zones indicates that the chosen substrate is able to perform density dependent separation of the mixture. The formation of zones of separation highlighted in Figure S1 of [138] and shows the density-dependent filtration performed in the membrane. The biomolecular transport is a function of pore size, thickness, contact angle and pore diameter, whereas the confinement is driven by pore packing arrangement and density. Both of these factors are important measures while choosing a substrate to ensure maximum sweat wicking occurs during sample collection[104]. Permeability of the membrane drives the fluid transport across the membrane and influences biomolecule interaction. The goal is to leverage maximum lateral

transport towards enhancing of biosensing outcomes of a detection platform, namely, limit of detection (LOD), sensitivity and range of operation[82]. The permeability calculated for the polyamide membrane was approximately 0.04 cm^2 per second and the fluid coverage was identified to be 0.16 mm^2 per second. The wicking profiles have been generated using COMSOL Multiphysics simulations, which highlights the rapid lateral transport of polyamide membrane. These profiles have been used to further calculate the optimal rate and time for fluid loading. From these calculations, the optimal time for complete sensor area coverage will be 16 seconds. Rapid wicking facilitates fast sample collection especially using a passive sweat collection method. Herein, no external stimulation is required by the user to generate a sample. Eccrine sweat volumes between 3-5 nL per gland per minute are produced passively by the sweat glands. Thus by employing this hydrophilic, rapid wicking membrane, this system can perform detection using ultralow volumes i.e. 3 μL of human sweat[140]. All the conditions mentioned above are applicable to sweat based detection systems only if the surface is hydrophilic. This is because sweat is aqueous in nature. Contact angle studies illustrated in Figure 5.2B show the contact angles of de-ionized (D.I.) water and human sweat on the surface of the polyamide membrane. The contact angle was measured to be 20.23° for de-ionized water and 18.11° for human sweat. These studies were carried out at room temperature. Evaluation of contact angle, i.e. the angle measured between the tangents of a liquid-solid interface indicates the degree of wetting of the substrate[141]. A contact angle less than 90° indicates that the surface is hydrophilic. The acute angle results in this case confirm the hydrophilicity of the membrane, which also corresponds to high wettability. This is advantageous for developing wearable platforms as it facilitates rapid wicking of sweat throughout the membrane. Therefore, by employing this nanoporous membrane

in the platform development, the dynamic range is extended due to optimal filtration, better signal resolution is promoted, bulk solution effects are reduced, and higher sensitivity is observed. A picture of the sensing system, highlighting the flexibility aspect has been presented in Figure 5.2C.

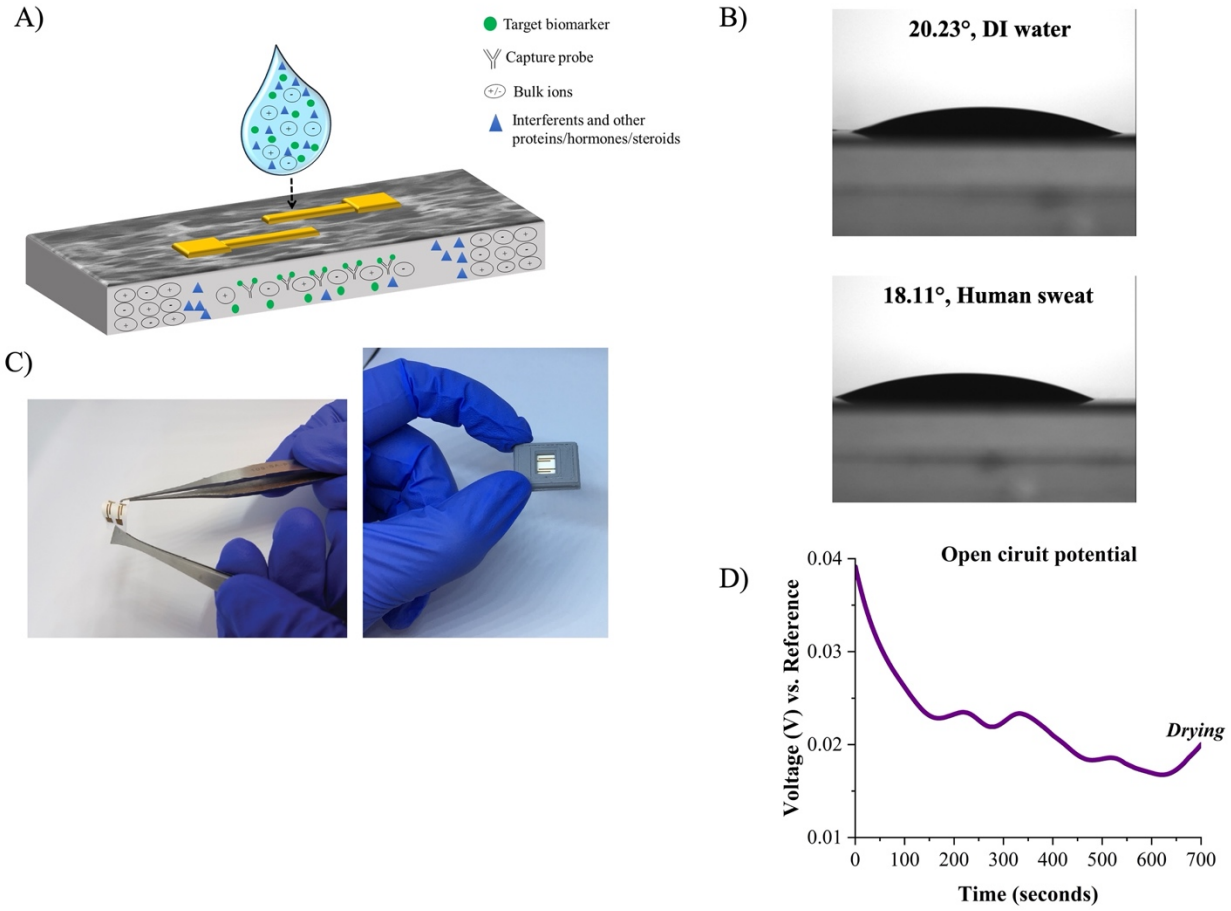

Figure 5.2.(A) Schematic depicting the wicking of sweat with target biomarkers (cortisol and TNF-α) on the nanoporous membrane highlighting selective molecular confinement (B) Contact angle studies using DI water (top) and human sweat (bottom) on membrane (C) Sensor pictures to highlight flexibility of platform and sensor prototype with case (D) Open circuit potential for electrochemical stability.

5.3.2 Sensor stability

The electrochemical stability of the sensor is determined using open circuit potential. This is used to evaluate the inherent baseline potential and the potential fluctuations in the bare, non-functionalized electrode system[74]. The inherent potential can then be used to remove the offset created by the bare system during active measurement and determine the true binding responses from a normalized system. The potential of this system is averaged at 2.7 mV, which is stable and has very low susceptibility for corrosion as shown in Figure 5.2D. The sensor system does not show any sharp peaks or sudden rise and fall in the system. The study is performed by drop-casting phosphate buffered saline solution on the sensor surface. Following 600 seconds, the membrane starts drying, which is characterized by the increase in the potential seen in the graph. Overall, the system indicates that it is electrochemically stable, not prone to corrosion, and will not drive the electrochemical response.

5.3.3 Sensor design and substrate simulations using COMSOL Multiphysics

Finite Element Analysis (FEA) helps in visualizing the distribution of simulated electrochemical conditions. It can also be used to characterize the wicking pattern of the nanoporous substrate used in this work. Figure 3 demonstrates the various FEA results that were performed on the sensing system. Figure 5.3A highlights the geometry of the interdigitated electrode along with the appropriate boundary conditions. The sensor has two electrodes (RE-Reference electrode and WE-Working electrode) interdigitated geometry created by thin film deposition of gold. The working area is simulated by using a layer of Phosphate saline buffer as an electrolyte for maintaining controlled conditions. The equations governing the simulations have been described in the

supplementary section 1 of [138]. A 10mV bias is applied to the working electrode and the distribution of electrolyte potential and current density was simulated. This is illustrated in Figures 5.3B and 5.3C. The distribution of electrolyte potential has been plotted as a multi-slice graph showing the cross-section view of the electrolyte. The maximum potential is concentrated around the working area with the gradient being created as we move from working to reference electrode area. The interdigitated electrode design is known to increase the overall capacitance of the system due to the increased surface area. Also, it provides enhanced sensitivity, lower detection limits, ability to operate with lower sample volumes, and ease of fabrication[142]. The current density was extracted and plotted as a line plot extending from working to reference electrode. There is a sharp drop in the current density from 5.4 Am-2 to 1.0 Am-2, highlighted by the current gradient present in Figure 5.3C. There are minimal parasitic current peaks indicative of an electrochemically stable sensing system. Substrate optimization is of prime importance while designing optimal sweat based detection platforms. The substrate used for this study is a hydrophilic polyamide membrane. The membrane is designed to offer rapid wicking of sweat which enables instant sample collection and optimal interaction time between analyte and detection probes in the sensor system. Table S1 of [138] summarizes the properties of this membrane. The surface capacitance has been presented as Figure S2 of [138]. The uniform distribution and value of inherent capacitance (values ranging in the pico farad range) contributed by the membrane indicates that the membrane will not drive the capacitive behavior of binding. This is ideal, as the response is mapped as capacitive modulations and will be a direct function of binding between the target and detection probe. Another component related to simulations presented is performing FEA analysis to determine the wicking pattern and speed according to the

given porosity of the membrane. This helps in optimizing the sample loading time and volume. Figures 5.3D,5.3E, and 5.3F highlight the lateral flow wicking profile of the polyamide membrane strip generated using COMSOL Multiphysics. It shows the progression of transfer of a dilute medium going from 0 $molm^{-3}$ to 1 $molm^{-3}$ in a period of 20 seconds. This capillary wicking has been simulated using principles of Darcy's law and diffusion kinetics[143]. The equations regarding the transport have been added to the supplementary section 1 of [138]. The assumptions related to the flow in the membrane strip model are also listed in the supplementary data of [138]. The flow is modelled to be a bulk flow from one end of the strip to the other. It can be observed that rapid wicking occurs within the first 5 seconds and then once the membrane nanopores start saturating by filling up, the transport slows down. Within 20 seconds, it can be observed that there is transport of solute halfway through the membrane strip. The driving forces are capillary flow due to the pressure gradient created by the volume of liquid in the filled spaces versus the empty spaces. This is modelled using the Lucas Washburn equation, which describes the capillary wicking in a channel inside a nanoporous membrane[144]. Due to these fluid transport properties, the sensing system can successfully perform detection using ultralow sample volumes such as 3µL. This is conducive to passive sampling for detection instead of active stimulation of sweat. Moreover, some of the other advantages of using this nanoporous membrane is that it reduces the biofouling that occurs at the electrode surface. Also being biocompatible, it nests with the user's epidermis and does not create any local irritation at placement site.

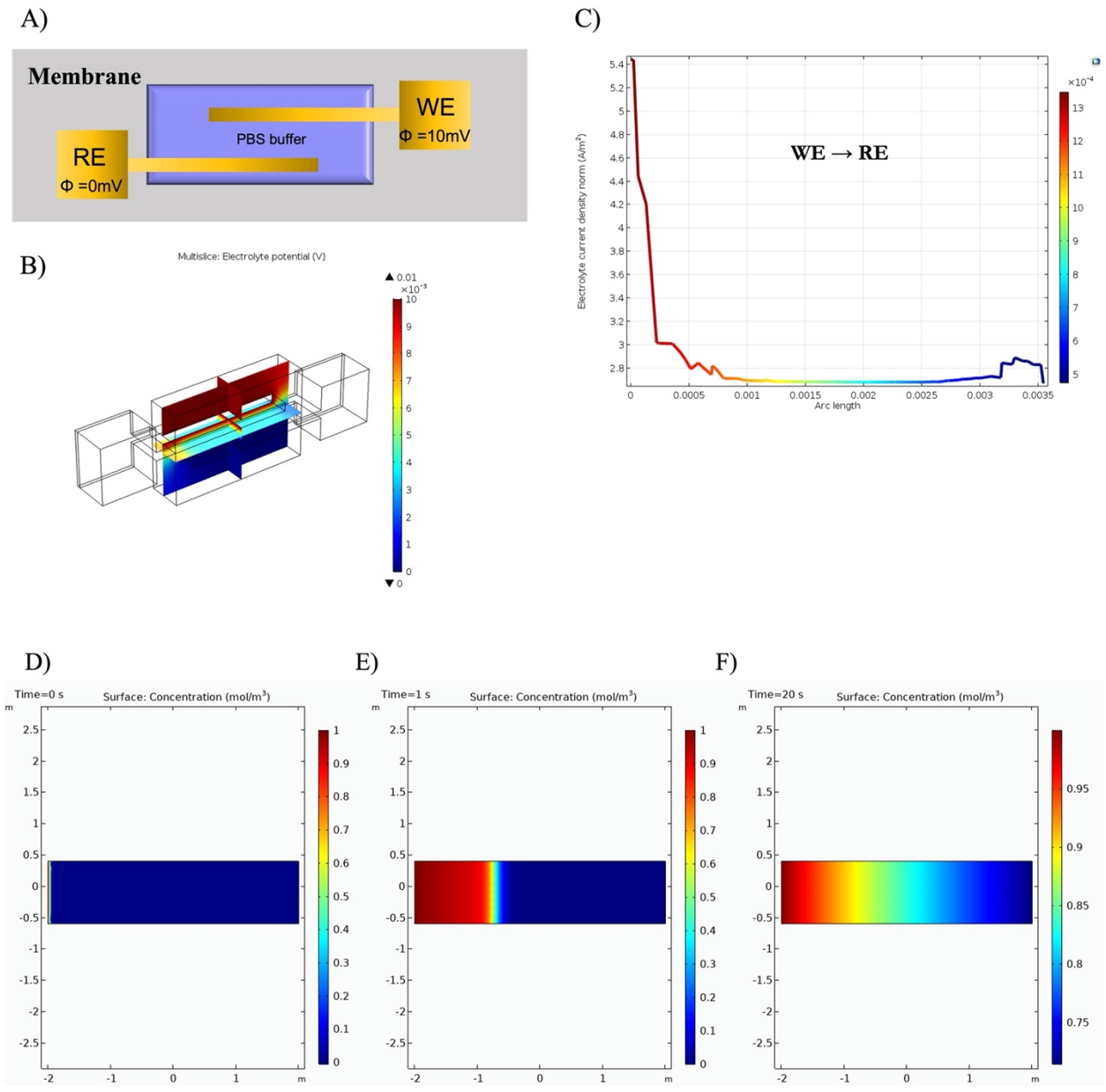

Figure 5.3.(A) Electrode schematic depicting conditions for COMSOL simulations (B) Multislice 3D graph depicting electrolyte potential distribution (C) 1D line plot illustrating the current density distribution from working (WE) to reference electrode (RE). Simulation for wicking of solute over porous membrane at (D) 0s (E) 1s and (F) 20s.

5.3.4 Binding chemistry characterization

ATR-IR analysis was performed to characterize the binding interaction of the capture probe antibody with thiol bound DSP linker between 1000 and 3500 cm^{-1}. Figure 5.4A shows the peak observed at 1310 cm^{-1} of DSP before antibody incubation indicating the symmetric C-N-C (Carbon-Nitrogen-Carbon) stretch of DSP. The peak observed at 1738 cm^{-1} in Figure 5.4B indicates the presence of free carboxylic acid in DSP. After antibody incubation, antibody conjugation to DSP occurs by breaking of carbon-oxygen bond within N-hydroxysuccimide (NHS) ester of DSP. Amine-reactive NHS ester reacts with primary amine of the antibody to form a stable amide bond. This occurrence is observed by the disappearance of peak at 1738 cm^{-1} due to breaking of C-O bond of NHS ester in the DSP. The appearance of 1655 cm^{-1} representing amide I band associated with C=O indicates the conjugation of Cortisol and TNF-α antibody to DSP functionalized gold surface. The C-N-C stretching mode also shift from 1310 to 1316 cm^{-1} after antibody incubation suggesting that Cortisol and TNF-α were successfully conjugated to the thiol linker (Figure 5.4A). Additionally, the broad O-H stretch at 3400 cm^{-1} confirms the Cortisol and TNF-α were successfully bound to DSP immobilized linker substrate (Figure 5.4C).

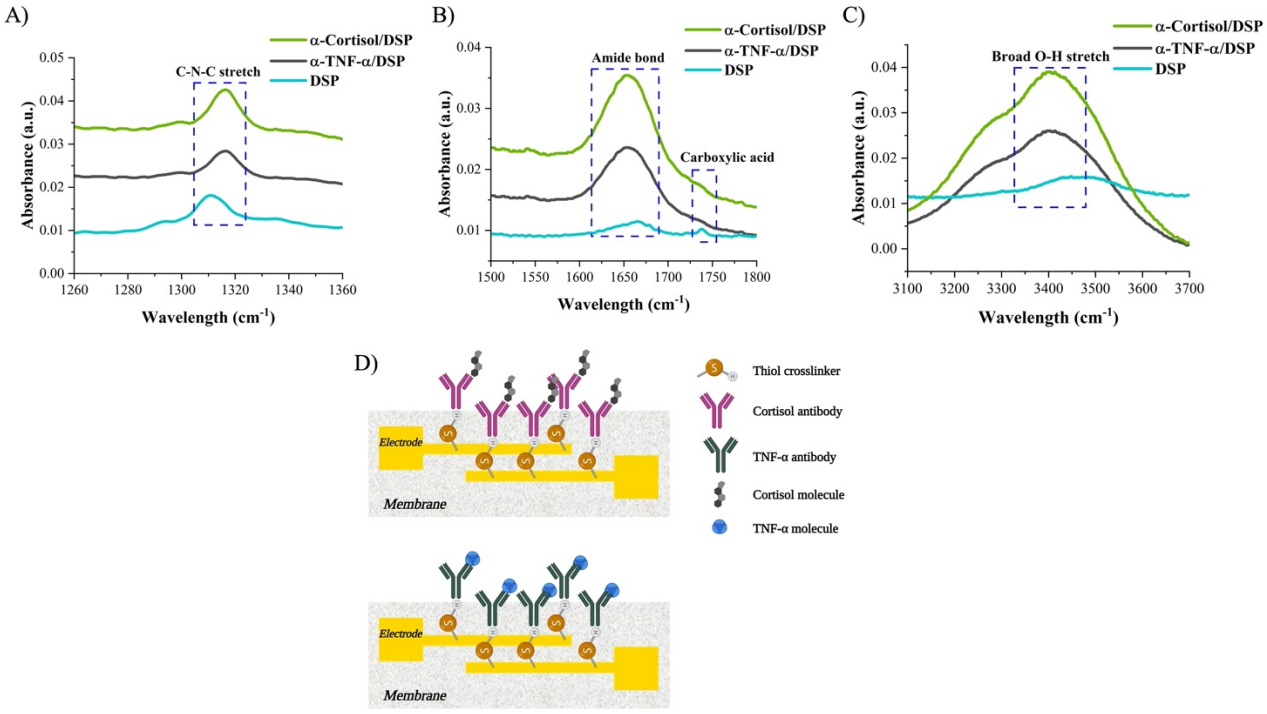

Figure 5.4.FTIR spectrums validating the binding chemistry (A) C-N-C stretch for DSP immobilization, (B) Amide bond and carboxylic acid highlight for protein immobilization, (C) Broad O-H stretch for antibody immobilization, and (D) schematic depicting the immunoassay employed for performing affinity-based detection for cortisol and TNF-α.

5.3.5 Dose dependent response of sensing platform

The performance of the affinity biosensor was characterized by building a calibration dose response curve (CDR) for varying concentrations of cortisol and TNF-α in human sweat. The CDR is represented as percentage change in impedance obtained for a given analyte concentration from a baseline concentration (without the presence of the target analyte) at 100Hz. The analysis frequency is chosen to be 100Hz due to maximum signal response and stable noise factor obtained within the frequency regime of interest. The calibration sensor responses of cortisol and TNF-α in

human sweat are shown in Figures 5.5A and 5.5B, respectively. As demonstrated in Figure 5.5A, the percentage change in impedance varies from 37.2± 0.03% and 82.3±0.5% for 1ng/mL to 200ng/mL cortisol concentrations with a specific signal threshold (SST) of 10%. The specific signal threshold is calculated with an SNR of 3 with the lowest detectable dose concentration 1ng/mL lying above the SST and thus can be regarded as the LOD. We have achieved a linear dynamic range of 1ng/mL to 200ng/mL which encompasses the physiological relevant range of cortisol present in human sweat and reliably distinguishes between low and elevated cortisol levels with a p-value of less than 0.001. The constructed CDR for increasing TNF-α concentrations 1pg/mL to 1000pg/mL is shown in Figure 5.5B. The variation in percentage impedance changes is observed to be 2.5±0.3% and 24.6±2.4% from 1pg/mL to 1000pg/mL TNF-α. The SST is computed to be 1.85% with an LOD of 1pg/mL. The linear dynamic range is found to be 1pg/mL to 1000pg/mL. The established LDR comprises of physiological TNF-α ranges found in human sweat with an ability to distinguish between low (10pg/mL), normal (100pg/mL), and elevated (300pg/mL) levels of TNF-α (p-value <0.001). The mechanism underlying the biosensing of cortisol and TNF-α in a complex medium such as human sweat is the charge modulations arising within the electrical double layer (EDL) formed at the electrode – sweat interface because of antibody-target analyte binding. The charge modulations induce an impedance change which can be attributed to either the charge-transfer resistance or the double layer capacitance. Here, the biosensing in capacitance dominated and the enhanced signal response obtained from the antibody-target analyte binding is due to the high charge storage capability of the double layer[145]. Typically in affinity-based assays, the double layer capacitance is enhanced due to interlinking of biomolecules of the immunoassay which causes charge modulation within the EDL[78], [146].

The capacitance of the EDL increases with increasing target analyte concentrations and can thus be used to quantify sensor response.

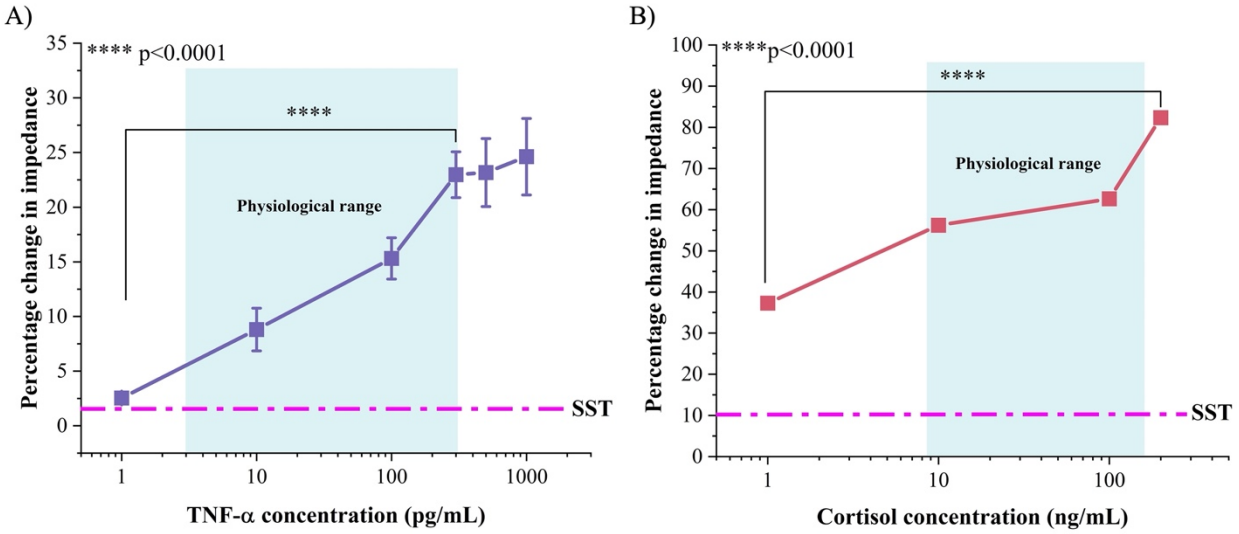

Figure 5.5.(A) Calibrated Dose Response (CDR) curves for cortisol (B) CDR curve for TNF-α. Significance ****p<0.0001, SST- Specific Signal Threshold

5.3.6 Long term study and temporal response of sensing platform

Continuous monitoring of biomarker levels is of paramount importance in maintaining a healthy lifestyle with an intent of providing the user with an assessment of their health status from time to time. Herein, we have demonstrated the temporal response of varying levels of cortisol on polyamide to mimic the rise and fall of cortisol as represented by the diurnal cortisol curve over a 1-hour duration to assess the feasibility of continuous, dynamic monitoring of cortisol in human sweat. The cortisol biosensor was subjected to three low (1ng/mL) and three elevated (100ng/mL) cortisol doses spiked in human sweat to simulate the cortisol rise level; subsequently the biosensor was loaded with three intermediate (10ng/mL) cortisol concentration to simulate the fall of cortisol level. The input cortisol dose concentration profile presented to the biosensor as accumulated dose

concentrations in the 1-hour window with a sampling interval of 5 minutes is shown in Figure 5.6A. The percentage change in impedance from baseline obtained in response to the accumulated dose concentrations in human sweat, as shown in Figure 5.6B, indicated a change from 7.5% to 28% for the rise cycle while the percentage change observed for the fall cycle was 28% to 31%. In temporal accumulative dose response studies, the dynamic differential signal (DDS) change is an appropriate method to indicate the concentration being detected as affinity binding is designed for association of analytes to their receptors and sensor surface regeneration is not feasible[147]. As shown in Figure 5.6C, the DDS change from 0ng/mL (baseline) to first 1ng/mL (low dose) was observed to be 6.55KΩ; the DDS change from last 1ng/mL dose (low dose) to the first 100ng/mL dose (high dose) was found to be from 5.8 KΩ to 9.7KΩ; the DDS change from the last 100ng/mL dose (high dose) to the first 10ng/mL dose (intermediate dose) was found to be from 3.6 KΩ to 5.1 KΩ. The porous structure of the membrane allows for nanoconfinement of biomolecules leading to a steep rise in impedance is observed for low to high concentration dosing while the change in impedance begins to taper with high to intermediate dose concentration. The cortisol biosensor's long-term temporal response to the ebb and flow of cortisol levels within 12 am to 12 pm sleep cycle of the day is mimicked on the sensor platform as a proof-of-concept for utility as a wearable sensor. The cortisol biomarker level cycling is carried in the 6-hour time period to mimic the cortisol rise and fall response with the onset of rise in cortisol at 12 PM, peaking of cortisol levels during 6 AM to 9 AM time period, and fall in cortisol levels towards the late afternoon. Herein, we have chosen the cortisol levels appearing in sweat during the 6AM- 12PM time period to capture the response of the sensor during the transition from rise to fall of cortisol levels. The accumulative cortisol dosing concentrations representing the rise and fall of cortisol in the 6 hours.

sleep window of the day is shown in Figure 5.6D wherein dose levels increasing from 20ng/mL – 80ng/mL represent the rise in cortisol, 100ng/mL represents the peak cortisol level followed by the fall in cortisol doses from 100ng/mL to 60ng/mL. The percentage change in impedance and the DDS change registered by the cortisol biosensor in response to the accumulative dosing input at a loading interval of 5 minutes are shown in Figures 5.6E and 5.6F. The percentage change in impedance for the 20ng/mL to 100ng/mL rise cycle increases from 23% to 64%; the percentage change in impedance for the fall cycle from 100ng/mL to 60ng/mL dose concentrations is found vary from 64% to 67%. The dynamic percentage signal change computed considering the previous dosing step as the baseline for the rise cycle decreases from 24% to 7.1%. For the fall cycle, the percentage signal change decreases from 7.1% to 2% for 100ng/mL to 80ng/mL cortisol doses. Beyond 80ng/mL cortisol dose, the sensor begins to show signs of saturation as the percentage signal change increases from 2% to 3.8% for 80ng/mL to 60ng/mL cortisol dose. The cortisol biosensor can detect the cortisol rise and fall dose levels presented to it over a 5.5-hr duration beyond which an inflection point is reached indicating slow saturation of the immobilized immunoassay. The developed biosensing platform demonstrated in this work is dynamically responsive to cortisol rise and falls levels over a period of 5.5 hours continuously thus enabling early detection of circadian dysregulation and understanding its connection with the etiology and pathophysiology of disorders.

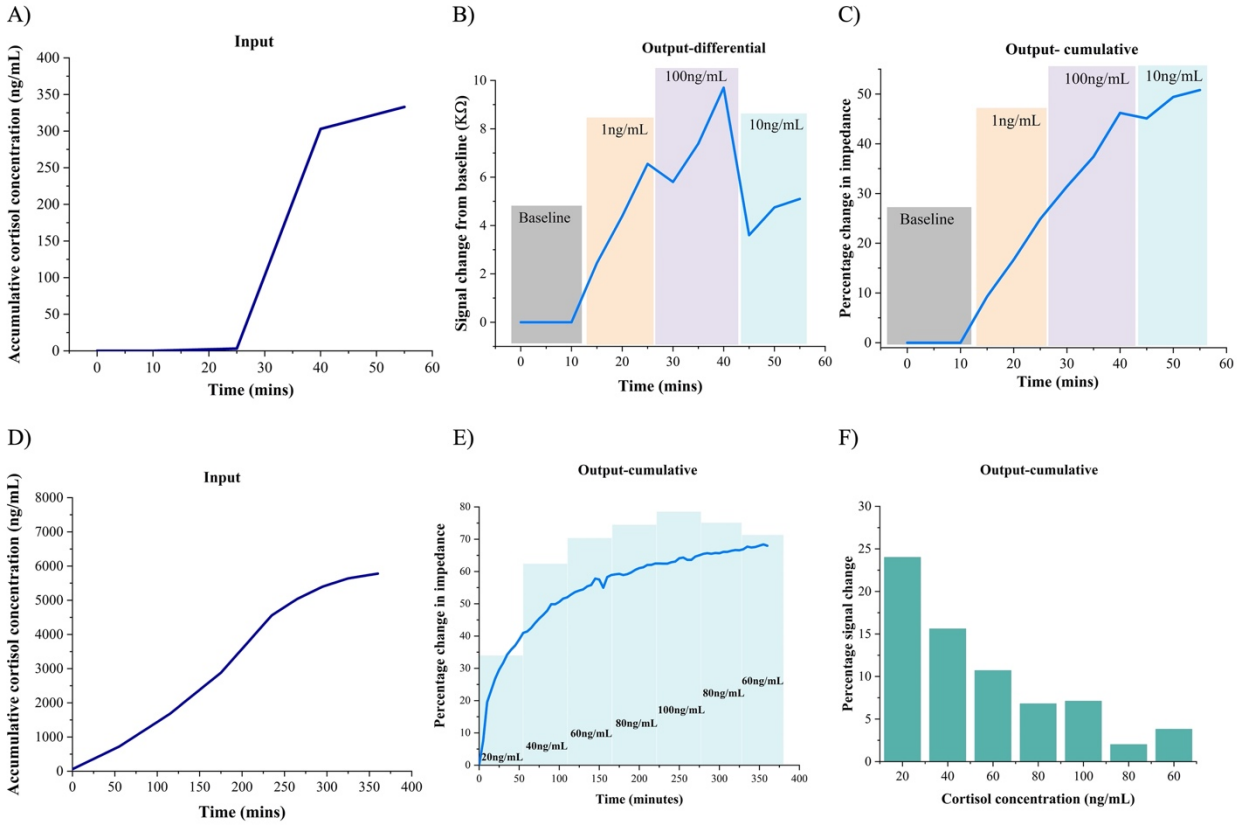

Figure 5.6.Long term stability study over a period of an hour (A) Input for long term stability experiment versus time (B) Cumulative output for low, mid, and high doses of cortisol (C) Differential output (change from baseline) highlighting rise and fall for cortisol levels. Long term stability over a period of 6 hours (D) Input for 6-hour stability study (E) Cumulative output for rise and fall for cortisol levels (F) Differential output highlighting percentage change from baseline for cortisol concentrations over 6 hours

5.3.7 Cross-reactivity of sensing platform

As discussed earlier, an antibody system is functionalized on the sensor surface which binds to the target molecule creating a response signal. However, there are certain instances when the antibody system might show some cross-reactivity between the signaling molecules due to inaccurate

binding between the antigen epitope and antibody paratope. Sweat has a plethora of interferent molecules like hormones, proteins, urea, lactic acid, creatinine, and lactic acid for example, that may be capable of generating such a false-positive response. Previous studies performed to characterize the selectivity of the system for similarly structured compounds has confirmed that the capture probes are specific for the specific molecule e.g., cortisol. In this section, as this is a multi-biomarker detection platform, the cross-reactivity signal between the two molecules of interest was evaluated. This study was performed in pooled human sweat, so that the biological fluid driven variance can also be accounted for while evaluating the cross-reactivity of the sensing platform. The two graphs illustrated in Figure 5.7 represent testing on two separate biosensors, one which is immobilized with cortisol antibody as depicted in Figure, 5.7A, and the second graph is immobilized with TNF-α antibody as shown in Figure 5.7B. For the sensor demonstrated in Figure 5.7A, three high doses (300pg/mL*3) of TNF-α were consecutively introduced onto the functionalized sensor surface and the signal impedance response was recorded. This non-specific signal was compared to the specific signal response of low (1ng/mL), medium (10ng/mL) and high dose of cortisol (200ng/mL). The impedance response from non-specific TNF-α doses is below the noise threshold and it is significantly lower than that of the medium and high doses of cortisol. Physiologically we would see a spike in TNF-α levels with the occurrence of inflammation, however, under normal conditions, we would not expect to see a high biomarker spike. Since the system is an irreversible binding model, the final response is a cumulative signal. From the results, it can be observed that after three subsequent high doses of TNF-α, the final cumulative signal is significantly lower than the cortisol doses with a p value < 0.05. This indicates that the system can sensitively differentiate between the two molecules and recognize the target molecule. Similarly,

the reverse analysis was carried out to evaluate the sensitivity and selectivity of TNF-α capture probe functionalized membrane surface. The cross-reactivity for TNF-α antibody immobilized surface has been illustrated in Figure 5.7B. This is especially important because out of the two molecules, the physiological levels are a magnitude lower for TNF-α than cortisol. Thus, it is imperative that the signal for cortisol, which will physiologically be present in sweat in higher concentration, does not cross react with the TNF-α response. We can observe that for high concentrations of both cortisol and TNF-α, the signal response is significantly higher for TNF-α (specific) molecule as compared to cortisol (non-specific molecule). The change for TNF-α is approximately 23% from baseline (unspiked pooled human sweat) and the change for high dose of cortisol is approx. 7% from the baseline. The significance tests were carried out by performing a t-test analysis with confidence condition of $\alpha = 0.05$. Thus, the sensing platform has specificity for the target biomarker of interest and can differentiate it from the non-specific target.

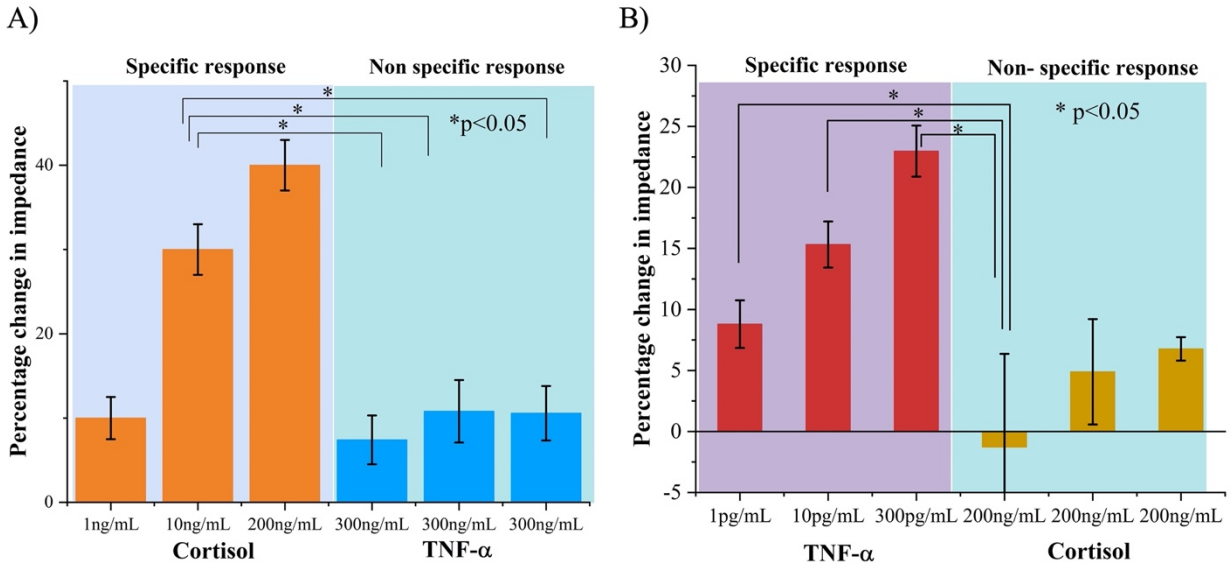

Figure 5.7.(A) Cross-reactivity on cortisol antibody immobilized platform using TNF-α (non-specific) (B) Cross-reactivity on TNF-α antibody immobilized platform using cortisol (non-specific) molecule. Significance *p<0.05, **p<0.01.

5.4 Materials and Methods

5.4.1 Reagents and materials

Cortisol antibodies and cortisol molecules were procured from Abcam (Cambridge, MA, USA). The TNF-α antibody and antigen, thiol linker used DSP (Dithiobis (succinimidyl propionate)) and DMSO (Dimethyl Sufloxide) were purchased from Thermofisher Scientific Inc. (Waltham, MA, USA). Milipore DI water (conductivity – 18 MΩ cm) was used to prepare the solutions. Nanoporous polyamide membranes were obtained from GE Healthcare Life sciences (Piscataway, NJ, USA). Pooled human sweat was procured from Lee Biosolutions (St Louis, MO, USA). No animal or human subjects were tested in this work.

5.4.2 Sensor Fabrication

The gold sensors were fabricated in-house utilizing the facilities provided by the cleanroom at University of Texas at Dallas (TX, USA). Cryo e-beam evaporator was used to deposit a thin gold film (150 nm) on the nanoporous polyamide membrane. Shadow masks were placed on the electrode surface during deposition to create the interdigitated gold electrode pattern on the sensors. This was then used for functionalization followed by testing. The sensor is designed to operate with ultra-low volumes of sweat to enable passive sample collection. The volume of sample needed is 3 µl, which aligns with the passive eccrine sweat rate and sweat production amount at rest [45].

5.4.3 COMSOL Multiphysics® software simulations

Finite element analysis was carried out utilizing licensed software version of COMSOL Multiphysics v5.4. The module used for performing simulations are transport of diluted species in porous media, electrostatics, and primary current distribution. 3D multislice plots for electrolyte potential, 1D plot group for current density and wicking simulations were exported through the software.

5.4.4 FTIR Experimental details

Infrared spectra of functionalized electrode were recorded with a Thermo Scientific Nicole iS50 FTIR using an Attenuated Total Reflectance (ATR) stage. The tool was equipped with a deuterated triglycine sulfate (DTGS) detector and KBr window. A Harrick VariGATR sampling stage with a 65° Germanium ATR crystal was used in this study. ATR-FTIR specimens were prepared by

deposition solutions on polyamide membrane as substrate. The contact area was about 1 cm^2. All spectra were recorded between 4000 and 700 cm^{-1} with a resolution of 0.5 cm^{-1} and 256 scans.

5.4.5 Experimental details for electrochemical analysis

Fabricated gold electrodes were tested for baseline stability and then employed for functionalization. This was performed by incubation with DSP/DMSO for 1.5 hours followed by incubation of 10µg/mL of antibody solution for 30 minutes. Incubation times were optimized using wicking simulation and baseline studies. Functionalized electrodes were utilized for testing by building an immunoassay using increments of target dose concentrations. During measurements of EIS, a 10mV AC potential bias was applied to the working electrode against the reference electrode and the response was recorded. These electrochemical measurements were carried out using Gamry Reference 600 potentiostat (Gamry Instruments, PA, USA). Dose concentrations of target biomarkers were tested within the physiologically relevant concentrations. These dose concentrations were prepared by artificially spiking the human sweat and analyzing the data as change from the baseline. Human sweat already has proteins, steroids, and other molecules present in the solution. The process in which the biofluid was spiked was by adding a known concentration of target biomarker ranging from 1ng/mL to 200 ng/mL for cortisol, and 1pg/mL to 1000 pg/mL for TNF-α. These spiked biofluid doses were then introduced on the functionalized sensor surface and the change in response from the blank human sweat was recorded as sensor response. The optimal frequency was 100Hz, where maximum capacitive behavior was observed.

5.4.6 Experimental detail for long-term studies

For the long-term studies, single frequency EIS was performed over the study time period (60 minutes and 6 hours) and the sensor was loaded at 5-minute intervals. The frequency of operation was set at 100Hz. For the short study of 60-minute duration, increments of cortisol dose concentrations ranging from1ng/mL to 100 ng/mL were loaded on the sensor surface. To capture the rise, concentrations of 1ng/mL and 100 ng/mL were loaded consecutively on the sensor surface. And to capture the fall, concentrations of 100ng/mL and 10ng/mL were loaded on the surface consecutively. The cumulative impedance response was then recorded using single frequency EIS. Similarly, for the long term 6-hour continuous study, concentrations were ramped up from 20 ng/mL to 100 ng/mL in increments of 20 ng and fall was captured by loading concentrations of 80 ng/mL followed by 60 ng/mL.

5.4.7 Statistical analysis

Data is represented as mean±SEM with an N=3, where n is the number of biosensor replicates tested. The inter-assay and intra-assay variations are less than 10 % which is compliant with CLSI guidelines. Statistical analysis for dose dependent response was performed using ANOVA followed by Tukey test to establish significance. Unpaired *T*-test was employed when the test for significance was between two groups. The confidence interval was fixed at 95% and α was 0.05. The analyses were performed using GraphPad Prism version 8.01 (Graph Pad Software Inc., La Jolla, CA, USA)

5.5 Conclusions

This work demonstrates the feasibility of using a sweat-based platform for tracking the intricate relationship between the endocrine and inflammatory pathway using sweat based biomarkers-cortisol and TNF-α. A detailed analysis for the optimal electrode design and platform wicking is provided using COMSOL Multiphysics® simulations. Binding characterization studies performed using FTIR validated the immunochemistry used for performing affinity-based detection. Sensor showed enhanced sensitivity to biomarker concentrations in sweat with a limit of detection of 1ng/mL for cortisol and 1pg/mL for TNF-α. Dynamic range of the sensor encompassed the physiologically relevant ranges with low noise. Additionally, long term stability of the sensing platform was demonstrated with continuous measurements to understand the temporal response of the sensor to rise and fall cortisol concentrations in accordance with the cortisol diurnal cycle over a diagnostically relevant time period. Finally, cross-reactivity studies confirm the specificity and selectivity of the sensor for the target biomarker. In conclusion, this work uses a novel, electrochemical wearable platform to offer enhanced sensitivity and improved sensor stability to map the endocrine -inflammatory relationship towards advancement of chronic disease diagnosis and management.

5.6 Future Perspective

The focus of healthcare tools has shifted from bulky, expensive diagnostic equipment to rapid, economical, and miniaturized diagnostic tools. There is a rise in patient-centric treatment approach which leads to increase in the demand of point-of-use devices. These point-of-use devices assist with performing healthcare related tasks on a miniaturized platform like a chip. In the next few

years, there will be a significant change in the appearance of healthcare technologies, where lab-on-a chip devices will be taken into consideration as a predominant healthcare choice. Also, with the growing awareness in people for monitoring their health e.g., smart watches etc., self-monitoring devices will simplify the arduous task of pricking for blood to obtain biomarker levels, by employing non-invasive biofluids instead. However, there are several challenges that need to be tackled towards creating highly sensitive wearable sensing/ detection platforms. These include optimizing for on-body device use, system integration using hardware, improving analytical reliability of results, and improving accuracy and stability.

5.7 Prior Publication

Shalini Prasad conceived the work. Sayali Upasham, Ashlesha Bhide, and Kai-Chun Lin performed the experiments. Sayali Upasham, Ashlesha Bhide, and Kai-Chun Lin wrote the paper, and all authors reviewed the work. This article was published in Future Science open access in 2020. This article has been reproduced by permission from Future Science publishing group and the link to this article is: https://doi.org/10.2144/fsoa-2020-0097

CHAPTER 6

EBC-SURE (EXHALED BREATH CONDENSATE- SCANNING USING RAPID ELECTRO ANALYTICS): A NON-FARADAIC AND NON-INVASIVE ELECTROCHEMICAL ASSAY TO SCREEN FOR PRO-INFLAMMATORY BIOMARKERS IN HUMAN BREATH CONDENSATE

6.1 Abstract

The innovation of this work lies in the trace detection of inflammatory biomarkers (IL-6, hs-CRP) in human exhaled breath condensate on the developed EBC-SURE platform as a point-of-care aid for respiratory disorder diagnosis. The unique design of the EBC-SURE leverages non-faradaic electrochemical impedance spectroscopy to capture target-specific biomolecular interactions for highly sensitive biomarker detection. For sensor calibration, EBC-SURE's performance is assessed to measure the response of the sensor to a known concentration by spike and recovery analysis with a recovery error of <20% and an extended dynamic range over 3-log orders. The lowest detection limits for IL-6 and hs-CRP detection in EBC were found to be 3.2 pg/mL and 4 pg/mL respectively. The efficacy of EBC-SURE for its usage as a diagnostic device was tested rigorously through reproducibility and repeatability studies. The percentage variation (< 20%) met the CLSI standards indicating a highly stable performance for robust biomarker detection. EBC-SURE generated highly selective IL-6 and hs-CRP responses in the presence of other non-specific cytokines. Statistical validation methods- Correlation and Bland Altman analysis established the one-to-one agreement between EBC-SURE and the reference method. Correlation analysis generated a Pearson's R value of 0.99 for IL-6 and hs-CRP. Bland-Altman analysis indicated a

good agreement between both the methods with all data points confined within the ±2SD limits. We have demonstrated EBC-SURE's ability in detecting inflammatory biomarkers in human breath condensate towards developing a non-invasive technology that can quantify biomarker levels associated with healthy and acute inflammatory conditions.

6.2 Introduction

Identification of inflammatory biomarkers related to airway diseases has been of emergent research interest in recent times. These biomarkers should be representative of the degree of lung inflammation and disease severity; provide reproducible results in clinical settings; allow non-invasive determination of the disease; and be repeatable during patient follow-ups[148], [149]. Inflammation plays a critical role in lung diseases like asthma and chronic obstructive pulmonary disease (COPD). Hence, the initial detection of lung disease biomarkers is relevant in disease management for early clinical intervention and further guided drug therapy. Understanding the body's inflammatory response has been a subject of immense interest amongst researchers over the decades. The human pulmonary system is constantly exposed to pathogens and toxic molecules present in the environment thus requiring resilient pulmonary defense mechanisms for survival. Innate and adaptive immunity systems fight together against pathogens to induce an inflammatory response. The epithelium of the airway tract is the first site of the microbial attack and secretes cytokines in response to infection which further stimulates inflammation [150]. Macrophages present in the airway lining orchestrate the acute and chronic inflammatory responses through the release of proteases and cytokines that attract neutrophils into the airways [151]. The neutrophils release pro-inflammatory cytokines such as tumor necrosis factor (TNF)-α, interleukin (IL)-1β,

IL-6, IL-8, and interferon (IFN)-γ that activate the immune system and generate an inflammatory response. Evidence from the literature indicates a physiological link between IL-6 and C- reactive protein (CRP), an acute phase protein induced by IL-6 [152]–[154]. IL-6 and CRP are present in higher concentrations in serum and can be easily detected during low-grade inflammation. During inflammation, IL-6 is released into the circulation by macrophages, neutrophils by initiation from TNF-α and IL-1β. IL-6 stimulates the production of CRP in the liver and its release into the blood circulation; IL-6 also stimulates the production of neutrophils in the bone marrow and is attracted to the infection site. Further, as IL-6 crosses the blood-brain barrier inducing an increased body temperature and causing a fever. IL-6 supports the differentiation of T-cells and B-cells leading them to target the infected cells and foreign antigens. IL-6 plays three important roles- instigating tissue damaging inflammatory responses, reducing inflammation, initiating tissue repair. During an inflammatory episode, as IL-6 rises there is a dramatic rise in CRP which begins to rise 4-6 hours and peaks after 1-2 days. CRP also binds to the damaged cells and activates phagocytosis by neutrophils and macrophages[155].

At present, lung inflammation is quantified by invasive methods such as sampling of bronchoalveolar lavage (BAL) fluid, tissue biopsies; less invasive methods such as sputum induction, plasma, and urine sampling. These methods indicate systemic inflammation rather than pulmonary inflammation. Direct sampling from the lungs such as BAL suffers from dilution and metabolism of inflammatory biomarkers within the lungs; sputum induction suffers from the expectorated fluid altering the collected sample[156]. Other practical concerns such as the invasiveness and patient discomfort of sample collection have made EBC a promising diagnostic fluid for non-invasive biomarker analysis in personalized and clinical settings[157]. EBC is

derived from the oral cavity, respiratory tract, and alveoli but the source of biomarkers in it is uncertain. There is a general understanding in the research space that EBC is a representation of the airway lining fluid (ALF) that aerosolizes during turbulent airflow containing primarily consisting of non-volatile substances. EBC has been explored for non-invasive measurement of lung cytokines related to pulmonary disorders associated with a triad of symptoms- airway inflammation, bronchial hyperresponsiveness, and airway obstruction[19]. Stiegel et.al. investigated pair-wise correlation within an across of 10 different cytokines across human blood and exhaled breath condensate[158]. Within the same medium, pro-inflammatory cytokines showed positive correlations amongst themselves and negative correlations with anti-inflammatory cytokines. However, no specific pattern was observed for blood and EBC cytokines correlations indicating differences in cytokine expressions between individual subjects. The majority of the blood pro-inflammatory cytokines showed statistically significant correlations with those in EBC showing a promise that EBC can be a potential, non-invasive medium to investigate respiratory inflammation. Standard techniques utilized for the detection of biomarkers in EBC include enzyme-based assay, fluorometric assays, and chemiluminescence; highly sensitive detection of biomarkers necessitates the use of liquid chromatography and tandem mass spectroscopy techniques. Although these techniques provide detection limits in lower pg/mL ranges, EBC samples require pre-treatment to stimulate reactions and removal of interferents, use of expensive equipment, slow response time, and the need of skilled technicians[84]. Electrochemical analysis techniques offer high sensitivity, rapid sensor response, ease of use, cost-effectiveness, minimal sample pretreatment, use of low fluid volumes, miniaturized sensor, and

readout interface enabling its incorporation into point-of-care diagnostic platforms for biomarker detection[159].

Cytokines play an important role in inflammation leading to the release and regulation of other cytokines. Literature on EBC has reported the presence of interleukins (IL-1β, IL-2, IL-4, IL-6, IL-8, IL-10), IFN-γ, and TNF-α in low pg/mL concentrations in human EBC[160][161]. IL-6 concentration in EBC ranges from 4pg/mL in normal healthy volunteers to 200pg/mL in acute exacerbated conditions[162]. hs-CRP is a sensitive biomarker for the identification of systemic inflammation and tissue damage. It is not disease-specific but can help in guiding clinical decisions in patients with lower respiratory tract infections; hs-CRP levels are found to significantly elevated in acute exacerbation conditions[163]. In airway inflammation, hs-CRP levels in EBC are reported to be in varying ranges from lower pg/mL to higher ng/mL[164]–[166]. IL-6 and hs-CRP can be utilized as early diagnostic biomarkers to track lung inflammation, identify the onset of pulmonary disease flare-ups, and to provide effective treatment. Our work is a first-time demonstration of early inflammatory biomarker detection in human EBC to show its usability in rapid, single-measurement platforms for point-of-care diagnostics. The proposed sensor platform is highly sensitive and captures the lower regime of biomarker concentration with the ability to distinguish between healthy and acute inflammation conditions. Figure 6.1 illustrates the end-to-end process flow from the origin of inflammatory biomarkers in EBC to the envisioned practical implementation of EBC-SURE in personalized and clinical settings for tracking inflammation.

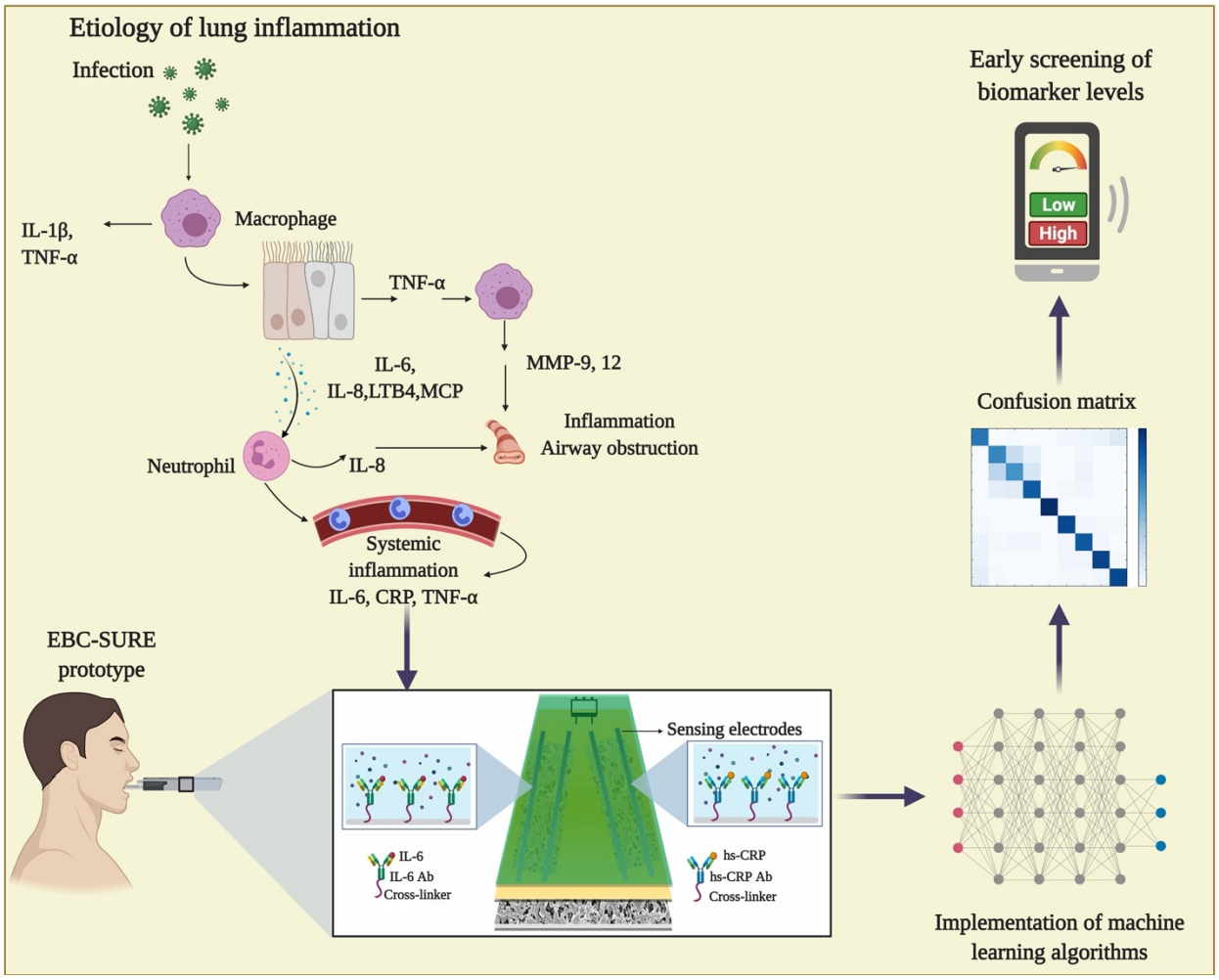

Figure 6.1.Process flow from the origin of inflammatory biomarkers in breath condensate to the envisioned practical implementation of the EBC-SURE platform for tracking inflammation. Created using BioRender.com

6.3 Materials and Methods

6.3.1 Reagents and Instrumentation

The capture antibodies for IL-6 and hs-CRP were procured from Abcam (Cambridge, MA, USA). The IL-6 ELISA kit was purchased from Abcam, and the hs-CRP ELISA kit was purchased from Invitrogen

(Waltham, MA, USA). The cross-linker 3,3'-dithiobis (sulfosuccinimidyl propionate) and phosphate buffered saline (PBS) were purchased from Thermo Fisher (Waltham, MA, USA). Simulated exhaled breath condensate (SEBC) was prepared by diluting simulated airway lining fluid with PBS (Boisa et al., 2014). The sensor substrates were purchased from PharmChek (Fort Worth, TX, USA). All reagents were used without any purification and were stored under appropriate conditions as mentioned by the vendor.

6.3.2 EBC-SURE device

The EBC-SURE device comprises an electronic reader enclosed in the prototype casing onto which a replaceable sensor strip functionalized with antibodies for specific target biomarker detection is mounted. The electronic reader transduces the impedance signal produced from the target probe-biomarker binding that is required to build the calibration curves of SEBC biomarkers. The signal transduction is enabled by a 2-electrode design fabricated on the substrate by screen printing technique which allows a relevant electrochemical signal to be measured in response to the affinity binding. The sensor fabrication process has been described in detail by our group previously[80]. Figure 6.2 shows the sensor device and the envisioned prototype for the rapid detection of inflammatory biomarkers in real-time. Non-faradaic EIS was employed to measure the sensor response wherein a low-voltage sinusoidal input was applied, and the impedance obtained from the affinity binding was recorded over a 100Hz to 1000Hz frequency range[79]. A calibration curve was constructed from the impedance produced by the increasing biomarker concentrations in SEBC and pooled human EBC.

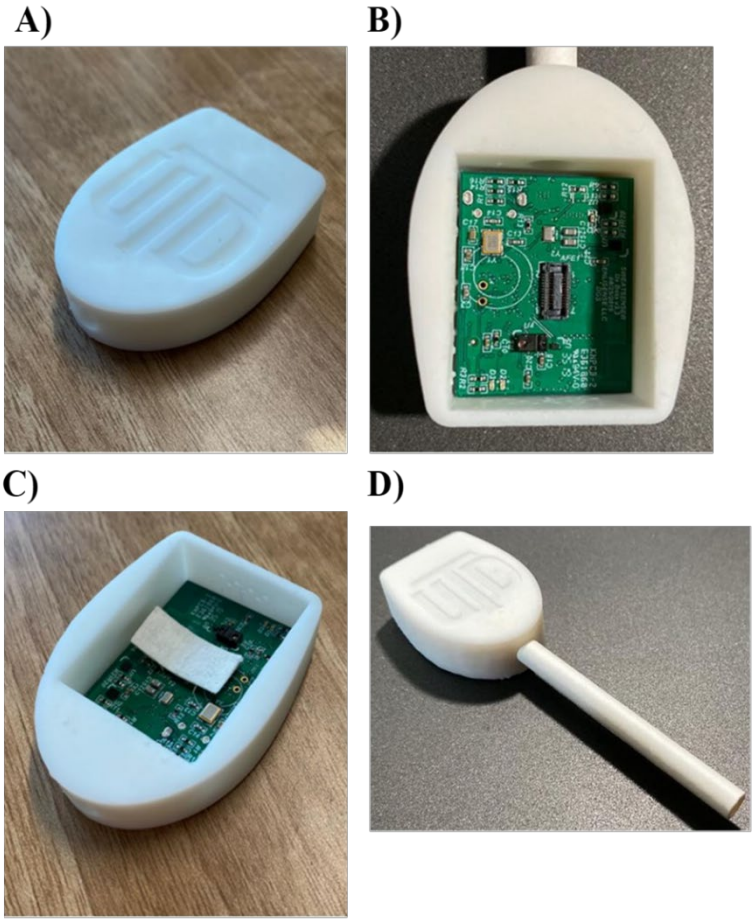

Figure 6.2.(A) Electronic reader top view (B) Electronic reader bottom view (C) Sensor mounted on the reader (D) Envisioned EBC-SURE prototype.

6.3.3 Sensor immunoassay development

The sensing platform was fabricated with a 2-electrode interdigitated system sputtered with zinc oxide in the overlap region as described in our previous work. The electrodes were incubated with a thiol crosslinker of 10mM concentration on one end while the other end was functionalized with 10µg/mL of monoclonal IL-6 or hs-CRP antibody. Monoclonal antibodies were chosen to achieve specificity during binding interactions. 10mM thiol cross-linker was dissolved in PBS and

functionalized on the sensing electrodes for 3 hours in dark. Further, IL-6/hs-CRP antibodies were immobilized on the electrodes to attach to the NHS ester group of the cross-linker through aminolysis. IL-6/hs-CRP antibodies were spiked in SEBC (pH ~7.0) and pooled human EBC to prepare doses of varying concentrations for constructing the calibration response curve. A sample volume of 3μL was utilized throughout the study.

6.3.4 Evaluation of EBC-SURE performance

The calibration curve for the detection of IL-6 and hs-CRP in SEBC and pooled human EBC was built from the impedance data gathered through conducting benchtop experiments with EBC-SURE for a sample size of N=6 for each concentration. SEBC was used to mimic the true breath condensate samples for characterization of biomarker detection on the developed platform, and protocol standardization for biomarker detection. The biomarker concentrations were increased from low to high and the impedance response generated in response to the dosing was recorded. The data was represented as a percentage change in impedance with respect to the baseline (devoid of any biomarker of interest). A 4-parameter logistic curve was fit to the obtained impedance response for each of the biomarkers; the calibration equation obtained from the curve fit was used for the spike and recovery experiments to evaluate the performance of the EBC-SURE.

6.3.5 Evaluation of EBC-SURE selectivity in SEBC and pooled human EBC

For the specificity studies in SEBC, a cocktail solution of IL-8 and IL-10 spiked in SEBC with concentrations in the range 3.2-819.2pg/mL was prepared without any IL-6 and was tested on the IL-6 sensor to record the impedance. Albumin was spiked in SEBC with concentrations in the range 4-1024pg/mL in the absence of hs-CRP for gauging EBC-SURE's specificity to hs-CRP.

For specificity studies in pooled human EBC, two cocktail solutions of low concentration and high concentration interferents (IL-8, IL-10, IL-1β, TNF-α) were made in pooled EBC. The two cocktail solutions were spiked with low and high IL-6 and hs-CRP concentrations and their impedances were recorded (See supplementary section S2 for more details).

6.3.6 ELISA Analysis

ELISA was used as the reference method for performance comparison with the EBC-SURE device. SEBC samples were spiked with varying IL-6 and hs-CRP concentrations and tested on the ELISA kits in accordance with the protocols described by the manufacturers. The SEBC and pooled human EBC samples were spiked with varying concentrations of IL-6 and hs-CRP and were tested on the EBC-SURE and ELISA platforms simultaneously. N=3 and N=2 samples for each concentration were tested on the ELISA platform after dilution with diluent buffer in SEBC and pooled human EBC respectively.

6.3.7 Collection of human exhaled breath condensate and sample pooling

The EBC samples were collected from three healthy volunteers with an informed consent for participation as per the approved IRB from UT Dallas (IRB # 20-38). The EBC samples were collected using a commercially available FDA approved device, RTube™.The subjects were asked to breathe normally into the mouthpiece of the device at tidal volume for 10-15 mins which yielded a sample volume between 0.5- 2mL. The samples were aliquoted and stored in -80°C. The samples from three subjects were pooled in equal volumes to create the pooled samples for further analysis.

6.3.8 Statistical Analysis

All statistical tests were performed using Origin Pro. ANOVA was carried out with 95% confidence intervals for spike and recovery experiments to show that the concentrations recovered are statistically different from each other. The degree of agreement between the EBC-SURE and the reference method were determined by using Pearson correlation and Bland-Altman analysis.

6.4 Results

6.4.1 Demonstration of EBC-SURE for IL-6 and hs-CRP detection and evaluation of its specificity in simulated exhaled breath condensate

In these trying times of COVID-19, elevated levels of IL-6 and hs-CRP have been established to be predictive biomarkers of forthcoming respiratory failure[153]. Thus, the approach towards detection of IL-6 and hs-CRP on a non-invasive, all electronic sensor integrated on a portable FDA-approved breath condensate collection device would be feasible for guiding clinicians on hyperinflammatory treatments. The sensor was calibrated individually to detect IL-6 and hs-CRP in SEBC covering a dynamic range including physiological and elevated levels of the chosen biomarkers. Spike and recovery analysis was used as a figure of merit to determine the analytical performance of the sensing platform in detecting IL-6 and hs-CRP. The efficiency of the platform was validated by spiking known concentrations of biomarkers and determining the recovered concentration from a calibration curve. Recovery reports the proportion of the biomarker that can be extracted after being spiked in the test sample[167]. The spike and recovery analysis for IL-6 and hs-CRP in SEBC for the concentration ranges spanning over three log concentration ranges are shown in Figures 6.3A and 6.3B. The error between the spiked and recovered concentrations

is computed to be 0.2-20%. The non-overlapping error bars quantify the reliability in distinguishing between individual target concentrations. Statistical ANOVA performed with $p<0.05$ and 95% confidence intervals reveals that the means of the groups are significantly different from each other. The smallest detectable IL-6 concentration this sensor can reliably distinguish from blank is found to be 3.2pg/mL with a dynamic detection range of 3.2pg/mL to 819.2pg/mL. hs-CRP showed a dynamic detection range from 4pg/mL to 1024pg/mL with a lower limit of detection of 4pg/mL.

Specificity is a key requirement that influences the biosensing performance in preferentially detecting the target biomarkers of interest in the biological samples consisting of non-specific molecules that can be lower in concentration[168]. Ideally, it is expected that the signals produced by the non-specifics in proportion to the concentration of the target biomarkers should be negligible. The % reactivity was calculated as the ratio of measured concentration to the actual concentration of the biomarkers loaded on the sensor. As shown in Figure 6.3C, the EBC-SURE demonstrates a 99%-106% selectivity for IL-6 specific interactions in the 3.2pg/mL to 819.2pg/mL range and negative non-specific response for the interactions with IL-8+IL-10 mix. The selectivity of hs-CRP detection antibody was tested against albumin diluted in SEBC for the concentration range 4pg/mL to 1024pg/mL[169]. The non-specific interactions demonstrate a reactivity of -25% indicating minimal crosstalk between the hs-CRP antibody and albumin as shown in Figure 6.3D. A high average reactivity of 105% was seen for hs-CRP specific interactions in the range 4pg/mL to 1024pg/mL.

We attribute the increased sensitivity, extended dynamic range, and selectivity of biomarker detection to a unique electrode design with a specialized surface coating functionalized

with target-specific capture probes on a porous substrate. The scaffolds of the porous membrane provide enhanced surface area for target-analyte interaction while accelerating the target probe-analyte binding kinetics[170]. Herein, a label- free, impedimetric approach is employed to measure the target probe-analyte interactions by sensing variations in the electric double layer. The impedance changes occurring in response to the target probe-analyte interactions occurring at the electrode- electrolyte interface is reflective of the target analyte's concentration. The use of impedimetric sensing in the detection of inflammatory biomarkers in sweat and serum has been previously demonstrated by our group[171], [172].

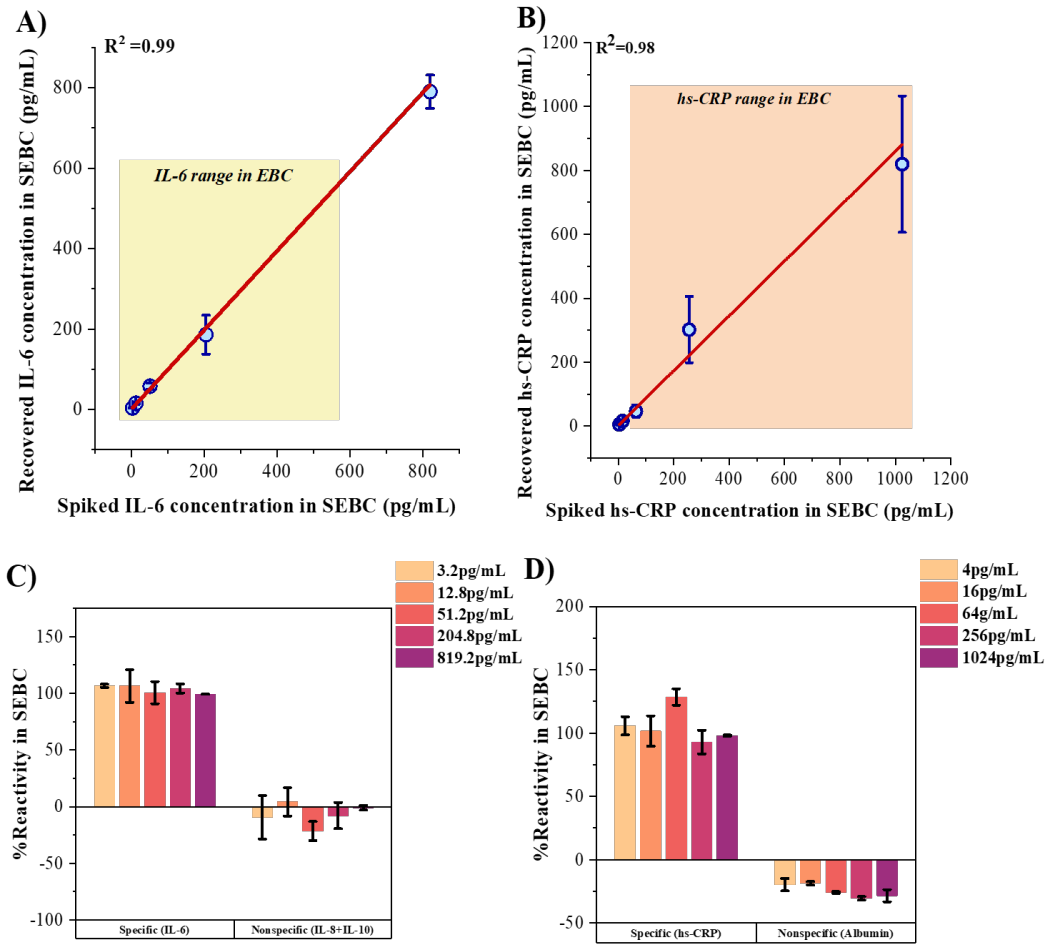

Figure 6.3.Spike and recovery analysis curves for the detection and quantification of inflammatory biomarkers in SEBC (A) IL-6 (B) hs-CRP. Linear regression analysis performed between spiked and recovered concentrations reported an R2 ≈ 0.99. Assessment of EBC-SURE's selectivity for (C) IL-6 detection in the presence of IL-8 and IL-10 in SEBC (D) hs-CRP detection in the presence of albumin in SEBC. The EBC-SURE demonstrates a minimal to negative reactivity of <30% to non-specific molecules and a highly specific response >95% to target molecules.

6.4.2 Evaluation of EBC-SURE's repeatability and reproducibility performance for IL-6 and CRP detection in simulated exhaled breath condensate

Clinical investigations require the measurement of quantities multiple times for diagnosis and outcome prediction. Measurements are prone to errors, and it is necessary to understand the origin of variations; a small error degree may not affect the clinical measurement while large errors skew the investigation and make the measurements unusable[173]. Repeatability measures the variations in measurements performed on multiple trials using the same procedure, operating conditions, and location[174]. To evaluate the repeatability, two sensors each were functionalized with IL-6 and hs-CRP detection antibodies, and five replicate measurements were performed in the same session at room temperature. Normal and elevated concentrations within the physiological range of presence in EBC were chosen for IL-6 and hs-CRP – 5pg/mL and 50pg/mL for IL-6; 100pg/mL and 1000pg/mL for CRP. The mean recovered IL-6 concentrations in response to repeatedly dosed normal and elevated IL-6 concentrations for the two test sensors, as shown in Figure 6.4A, are 6.9± 0.5pg/mL and 51.4± 4.2pg/mL respectively. Acceptable sensor performance is associated with allowable standard deviation in measurement (% CV), as set by CLSI, taken repeatedly for the same dose concentrations on the two sensors. Figure 6.4B shows the percent coefficient variation that the sensor reports for normal and elevated IL-6 dose concentrations on repeated sensor dosing. The %CV reported by the sensor lies below <10% well within the 20% threshold of acceptable variation confirming the repeatability metric of the IL-6 sensor. The spike and recovery hs-CRP concentrations obtained on dosing the same sensor repeatedly, as shown in Figure 6.4E, report mean normal and elevated hs-CRP concentrations of 172 ± 16pg/mL and 833 ± 61.5pg/mL respectively. The %CV computed for normal and elevated CRP concentrations when

the sensor is subjected to repeated dosing protocol is found to be 9.2% and 7.3% respectively as shown in Figure 6.4F. Statistical analysis reports $p < 0.05$ confirming that the normal and elevated concentrations of IL-6 and hs-CRP can be reliably distinguished individually.

Reproducibility is the degree of variations in measurements performed under varying conditions to understand the stability of sensor performance for point-of-care use. Storage stability was assessed to understand the decline in the sensor sensitivity on storage at particular conditions over a period of time. The sensors were functionalized with IL-6 and hs-CRP antibodies and stored in 4°C for performance investigation over 48 hours. The functionality of new sensor in response to varying IL-6 and hs-CRP concentrations was examined every 24 hours over a 48-hour duration. Figure 3C shows the reproducibility response of IL-6 functionalized sensors over 48 hours with a low average IL-6 concentration reported to be 3.3± 0.06pg/mL and high IL-6 concentration reported at 155± 33.5pg/mL. The functionalized sensors report a %CV of 2- 21% over 48 hours, as shown in Figure 6.4D, indicating the reproducible nature of the sensor platform for utilization in practical scenarios. The reproducibility response and %CV for hs-CRP functionalized sensors over a 48-hour duration are shown in Figures 6.4G and 6.4H respectively. The low and high hs-CRP concentrations reported by the hs-CRP functionalized sensor after 48 hours was found to be

17.7± 0.7pg/mL and 841± 85.7pg/mL respectively with %CV found to be <10% indicating time-based stability in sensor response.

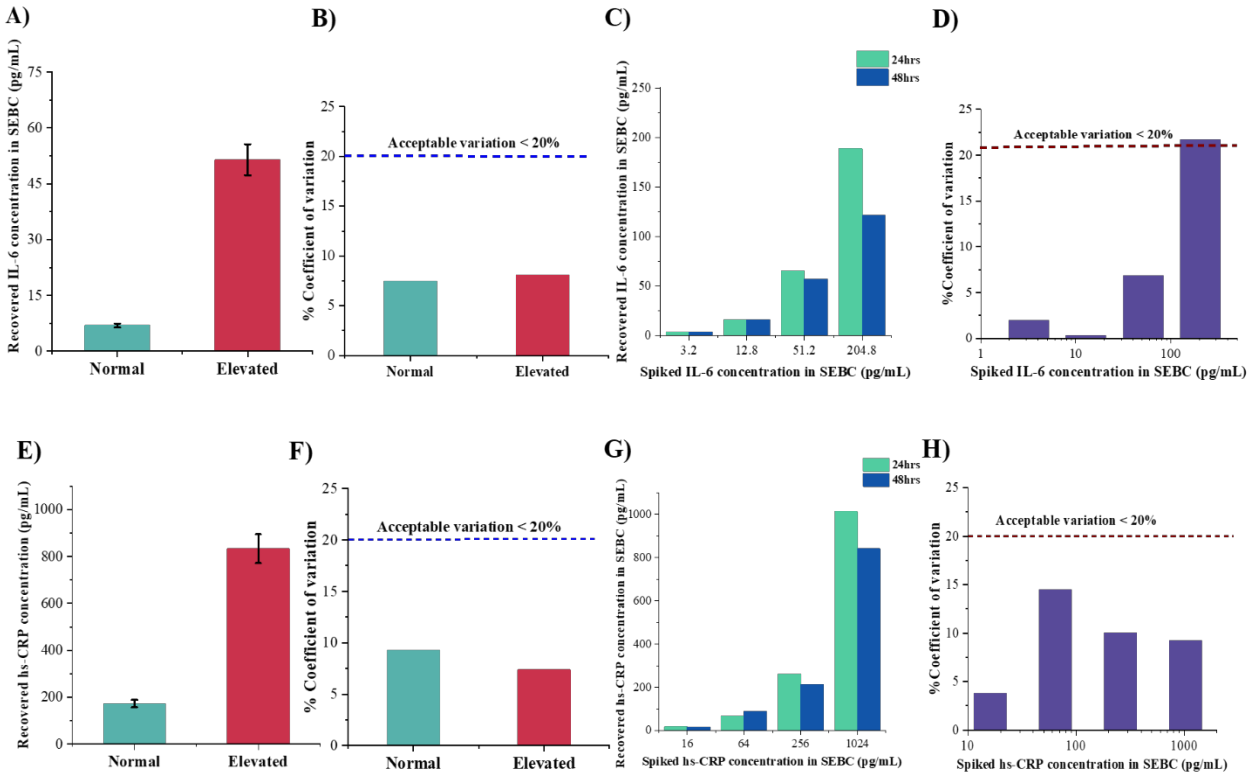

Figure 6.4.Assessment of sensor performance metrics. Repeatability performance of EBC- SURE for (A-B) IL-6 detection (E-F) hs-CRP detection. Reproducibility performance of EBC-SURE for (C-D) IL-6 detection and (G-H) hs-CRP detection over 48 hours to confirm sensor stability. The dotted line 20% indicates the acceptable limit of variation according to CLSI standards. EBC-SURE demonstrates a %CV < 20% confirming the repeatable and reproducible sensor response to target molecules.

6.4.3 Performance comparison of EBC-SURE with standard reference method for IL-6 and hs-CRP quantification

The developed EBC-SURE must be compared with a gold reference standard to validate the efficiency of the platform in reporting accurate biomarker levels. The measurements obtained from EBC-SURE are correlated with those obtained from a standard ELISA platform. The degree of agreement between the EBC-SURE and the reference ELISA technique was established by Pearson's correlation analysis and Bland-Altman (BA) analysis (Bunce, 2009). A higher correlation closer to 1.0 indicates a strong dependence between the sensor and the reference method. The EBC-SURE exhibits a Pearson's r= 0.99 and 0.98 for IL-6 and hs-CRP, as shown in Figures 6.5A and 6.5C, representing a significant linear relationship between the recovered IL-6 and hs-CRP concentrations obtained from the sensor and the reference method. BA analysis gives a quantification of the agreement levels between the sensor and the reference method by emphasizing on any biases and differences between the two measurement methods. The BA plots for IL-6 and hs-CRP, as shown in Figures 6.5B and 6.5D, show a good agreement of the EBC-SURE with the reference method. In the BA scatter plot, x- axis represents the average biomarker concentration reported by both the methods, and the y-axis represents the difference in biomarker concentrations reported by the two methods. The mean bias is the differences in the mean biomarker concentrations reported by the two methods and the data points are restricted to ±2 SD. The BA analysis for IL-6 and hs-CRP sensor with the reference, mean biases of -11.62pg/mL and 16.5pg/mL were obtained indicating no significant difference between the two measurement methods. At lower IL-6 and hs-CRP concentrations, the scatter points were packed closer to zero;

however, at higher IL-6 and hs-CRP concentrations, most of the scatter points were spread above and below the mean bias within ±2 SD limits in a random order suggesting no treatment bias.

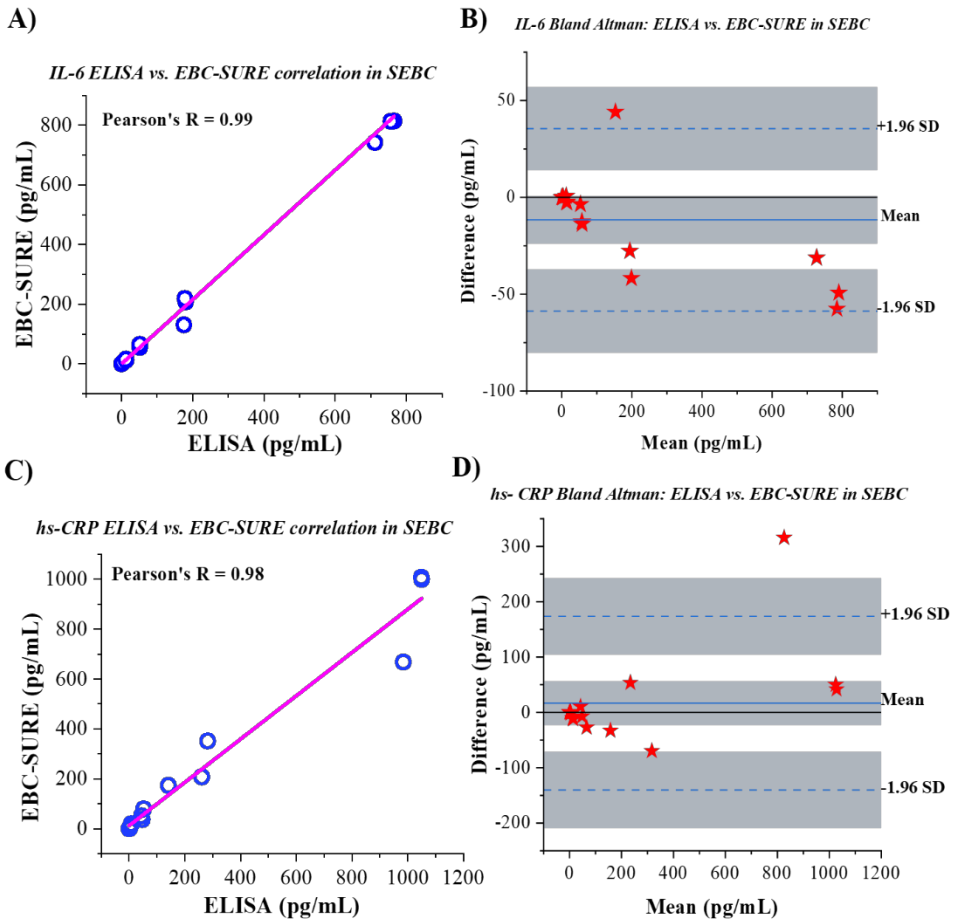

Figure 6.5.Evaluation of EBC-SURE's in comparison with reference ELISA method using linear correlation for (A) IL-6 and (C) hs-CRP in SEBC. A Pearson's correlation coefficient of R≈ 0.99 is observed between EBC-SURE and the reference method. Bland-Altman analysis performed between EBC-SURE and reference method (B) IL-6 (D) hs-CRP in SEBC demonstrate a mean bias of (B) -11.62pg/mL for IL-6 (D) 16.5pg/mL for hs-CRP

6.4.4 Demonstration of EBC-SURE for IL-6 and hs-CRP detection and its analytical validation with standard reference method in pooled human exhaled breath condensate

We report for the first time the possibility of using an electrochemical platform to detect inflammatory biomarkers in human EBC for tracking inflammation in healthy and diseased individuals. The efficacy of EBC-SURE in detecting IL-6 and hs-CRP in pooled human exhaled breath condensate by spiking biomarkers of varying concentrations on the platform and the determination of recovered concentrations from the individually constructed calibration dose response curves are shown in Figures 6.6A and 6.6D. A series of ten concentrations spiked in pooled human EBC encompassing the physiologically reported ranges for healthy and acute inflammatory conditions were tested on the EBC-SURE. A linear response was observed over a dynamic range of 3pg/mL to 820pg/mL for IL-6 and 10pg/mL to 1000pg/mL for hs-CRP with an R^2 of 0.99. The tight range of recovered biomarker concentrations and the non-overlapping error bars allow the ability to distinguish between each biomarker with assurance. The %CV is computed to be <17%, which is well below the accepted CLSI standards of < 20% indicates the precision of EBC-SURE in detecting the biomarker concentrations. Seifi et.al. reported an IL-6 detection range of 0.05pg/mL to 1.17pg/mL using ELISA in their investigation on the relationship between the concentration of respiratory air particulate matter and inflammatory biomarkers in EBC[175]. In another study performed by Zee et.al. to detect cytokines and chemokines in the EBC of mechanically ventilated patients, an IL-6 detection range of 0pg/mL to 131.8 pg/mL was demonstrated by a multiplexed assay[176]. hs-CRP detection ranges of 0ng/mL to 0.1ng/mL and 0.08mg/L to 0.17mg/L in EBC have been reported in studies based on the assessment of biomarkers related to airway inflammation in asthma using ELISA as the detection method[164],

[177]. The performance of EBC-SURE was further evaluated to assess the selectivity and specificity while detecting each biomarker as shown in Figure S2. A statistical significance of $p<0.05$ was achieved between the non-specific and specific responses.

The commercial viability of a platform for use in clinical studies can be assessed by comparing the performance of EBC-SURE with a widely accepted reference standard such as ELISA. The pooled EBC samples collected from healthy subjects were spiked with varying IL-6 and hs-CRP biomarker concentrations and tested concurrently on EBC-SURE and ELISA. The degree of agreement between the two methods under test was determined by Pearson's correlation and Bland-Altman analysis. The two methods showed a linear response with a Pearson's R of 0.98 for IL-6 and 0.99 for hs-CRP detection indicating a good agreement between the two methods as shown in Figures 6.6B and 6.6E. Furthermore, the BA analysis yields a low mean bias of -1.5pg/mL for IL-6 and 0.85pg/mL for hs-CRP in pooled human EBC as shown in Figures 6.6C and 6.6F. Most of the scatter points lie closer to 0 indicating neither method overestimate nor underestimate the biomarker concentrations. Although at higher IL-6 and hs-CRP concentrations the scatter points lie close to the 95% CI bands (±1.96SD) or beyond the CI band, a clear distinction between normal and elevated biomarkers can be made. The one-to-one agreement between the EBC-SURE and ELISA performances ensures the robustness of the developed platform in quantifying human EBC biomarker concentrations precisely.

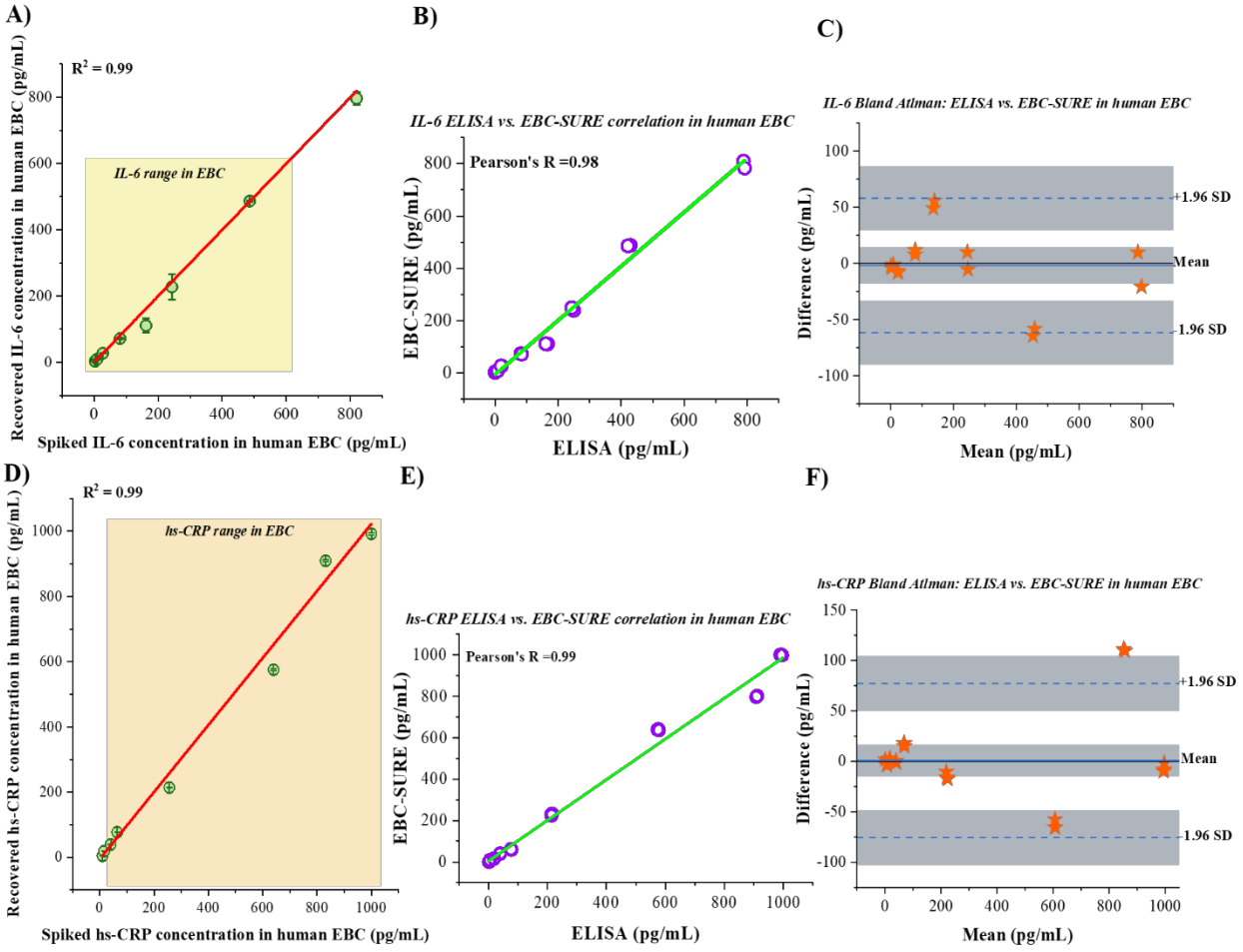

Figure 6.6.Spike and recovery analysis curves for the detection and quantification of inflammatory biomarkers in pooled human EBC (A) IL-6 (D) hs-CRP. Linear regression analysis performed between spiked and recovered concentrations reported an $R^2 \approx 0.99$. Evaluation of EBC-SURE's in comparison with reference ELISA method using linear correlation for (B) IL-6 and (E) hs-CRP in pooled human EBC. A Pearson's correlation coefficient of $R \approx 0.99$ is observed between EBC-SURE and the reference method. Bland-Altman analysis performed between EBC-SURE and

reference method (C) IL-6 (F) hs-CRP in pooled human EBC demonstrate a mean bias of (C) -1.5pg/mL for IL-6 (F) 0.85pg/mL for hs-CRP.

6.5 Summary and Conclusions

In summary, this work demonstrates a rapid, non-invasive, electrochemical EBC-SURE platform for the rapid screening of inflammatory biomarkers in exhaled breath condensate for pulmonary disorder management such that clinicians can initiate treatment at an earlier stage. This research can be extended towards developing a multiplexed sensor for the detection of an inflammatory biomarker panel in human EBC. The developed sensing platform facilities reliable and robust detection through affinity based monoclonal antibody-target biomarker interaction mechanism captured by a highly sensitive electrochemical impedance based-technique (EIS). The advantages of using the EBC-SURE for diagnostic purposes are the sensor portability; rapid response time (~5mins); multiplexing capability to detect a biomarker panel to distinguish between healthy and acute conditions; sensitive, selective, stable sensor response; requirement of low sample volumes (>3uL). The strategic design of the EBC-SURE provides a promise of non-invasive technology for the detection of biomarkers associated with pulmonary inflammation further paving a way for the developed platform to be integrated on a handheld prototype device to detect a host of inflammatory biomarkers in human EBC for pulmonary disease diagnostics. The limitation of this platform is the inherent nature of EBC rather the technology wherein biomarkers are present in low concentrations due to dilution by water vapor, low reproducibility, high variability in EBC samples, no accepted dilution markers, the requirement of expensive cross-validation techniques, lack of standardization and, data validation with known biofluids. In the future, studies will be conducted to understand the temporal variations in EBC cytokines in healthy and sick cohorts.

6.6 Acknowledgments

We acknowledge Vikram Narayanan Dhamu for the development and implementation of the machine learning algorithm. We acknowledge Paul Rice for his assistance is designing and 3D printing the prototype sensor.

6.7 Author Contributions

Ashlesha Bhide - Conceptualization, Resources, Methodology, Validation, Data curation, Investigation, Writing - original draft, Visualization. Sriram Muthukumar - Conceptualization, Resources, Writing- review & editing. Madhavi Pali - Methodology, Data collection, Shalini Prasad- Conceptualization, Resources, Writing - review & editing

CHAPTER 7

CONCLUSION AND FUTURE WORK

The key contribution of this research is the feasibility of CLASP and EBC-SURE platforms for the detection of biomarkers, that serve as physiological cues, non-invasively in health and disease management. These platforms can be characterized further to enable on-body, continuous, real-time monitoring of biomarkers to get a deep understanding of temporal and spatial fluctuations in health conditions. This research explores the nano dimensionality of the substrate and the hybrid electrode stack to enhance the detection sensitivity and extend the dynamic range of detection without the use of external redox reagents. The stability of the platforms is evaluated by metrics such as accuracy, specificity, reproducibility, repeatability, analytical validation with gold standards. The affinity binding events occurring at the electrode-body fluid interface is captured by non-faradaic electrochemical impedance spectroscopy. A charged electrode in contact with an electrolyte result in the formation of an electrical double layer that is equivalent to a capacitance system. The output signal produced is the reflection of interfacial charge modulation that is recorded as the biosensing response.

This work demonstrates the combinatorial detection of alcohol and glucose in human sweat aimed at monitoring the effects of alcohol intake on the glucose levels of pre-diabetic and diabetic populations. The effects of varying pH environments, buffer ionicity, and cross-reactive molecules were tested on the platform from which we drew an inference that the sensing response is stable and does not degrade under these variations. CLASP demonstrated a feasible low-volume detection of alcohol and glucose within the physiologically relevant ranges (0.1mg/dL to 100mg/dL) found in human sweat.

Agreement analysis methods approved by CLSI such as regression and Bland-Altman analysis were used to correlate the biosensor performance with a commercial breathalyzer and a glucometer. The dynamic interplay between alcohol and glucose in human sweat was monitored continuously over a 1.5-hour window through the incremental rate of change in impedance signifying the increased biomolecule-receptor interaction. This research demonstrated that CLASP has the potential to function as a wearable lifestyle monitor for alcohol and glucose management.

The next progression of this work was the demonstration of on-demand monitoring of elevated sweat lactate levels in sedentary populations. The skin conformable interface of the lactate biosensor when placed in close proximity to the human epidermis captured the sweat lactate variations in individuals in a sedentary and less active phase. Firstly, the on-body lactate levels extracted after a 60min period showed sweat lactate levels in the range 5mM to 20mM which can be mapped to the physiologically relevant ranges (4mM to 80mM) of lactate found in sweat. Secondly, the stability of the functionalized bioreceptor was evaluated to understand the duration of its stability for long-term usage. The biosensor signal degraded by ~30% over 4-days with a percent variation of less than 20% which is an acceptable CLSI standard. Spectroscopic and zeta analysis techniques confirmed the successful bioreceptor binding to the electrode surface and the bioreceptor- analyte interactions. Further, the utility of CLASP to quantify healthy and elevated cortisol and TNF-α levels were demonstrated to track endocrine-inflammatory relationship. The dynamic range of operation encompassed the diagnostic ranges of 8ng/mL to 141ng/mL for cortisol and 9pg/mL to 362pg/mL for TNF-α expressed in human sweat. Simulations were performed to demonstrate the optimal electrode design and the wicking capabilities of the nanoporous substrate. Long-term stability studies indicated the ability of the sensing platform to

capture the diurnal or inflammation related cycling of biomarkers over long time periods without compromised sensitivity.

Lastly, we explored the potential of human exhaled breath condensate as a non-invasive source of biomarker detection in tracking respiratory inflammation. Interleukin-6 and high sensitivity C-reactive protein are established as biomarkers to detect the flare of respiratory inflammation. The detection efficiency of the developed EBC-SURE platform was validated by spike and recovery analysis, and specificity studies performed in simulated and human EBC. The non-overlapping recovered concentration ranges and negative reactivity to cross-reactive molecules indicated the accuracy of EBC-SURE in determining the biomarker concentration reliably. Repeatability studies performed by repeatedly subjecting EBC-SURE to normal and elevated biomarker concentrations in EBC produced distinguishable signals confirmed by statistical tests. Reproducibility studies generated similar responses over a 48-hour duration with a decline in sensor performance after 72hrs of bioreceptor immobilization. The performance of EBC-SURE was compared against a standard reference method -ELISA to validate its use for further clinical studies. A correlation coefficient of ~0.99 obtained from regression analysis, and a mean bias close to zero obtained from Bland-Altman analysis indicated the platform's robustness in detecting EBC biomarkers.

Future work for recruiting EBC-SURE as a point-of-aid screening platform is directed towards enhancing its multiplexing capabilities to detect other inflammatory biomarkers; studying a larger set of human EBC samples to understand subject to subject variability for clinical studies; correlation of EBC biomarker levels with salivary biomarker levels; continuous monitoring of

biomarkers; and the development of a hand-held device prototype that houses the EBC-SURE and condenser to enable real-time biomarker monitoring.

REFERENCES

[1] "Biomarkers & Diagnostics: Essential elements of precision medicine." https://www.acobiom.com/en/biomarkers-diagnostics/ (accessed Nov. 04, 2020).

[2] C. Dincer, R. Bruch, A. Kling, P. S. Dittrich, and G. A. Urban, "Multiplexed Point-of-Care Testing – xPOCT," Trends in Biotechnology, vol. 35, no. 8. Elsevier Ltd, pp. 728–742, Aug. 01, 2017. doi: 10.1016/j.tibtech.2017.03.013.

[3] K. Guk et al., "Evolution of wearable devices with real-time disease monitoring for personalized healthcare," Nanomaterials, vol. 9, no. 6, Jun. 2019, doi: 10.3390/nano9060813.

[4] L. M. McShane, "In Pursuit of Greater Reproducibility and Credibility of Early Clinical Biomarker Research," Clinical and Translational Science, vol. 10, no. 2, pp. 58–60, Mar. 2017, doi: 10.1111/cts.12449.

[5] M. J. Selleck, M. Senthil, and N. R. Wall, "Making Meaningful Clinical Use of Biomarkers," Biomarker Insights, vol. 12, Jun. 2017, doi: 10.1177/1177271917715236.

[6] J. Li, J. Y. Liang, S. J. Laken, R. Langer, and G. Traverso, "Clinical Opportunities for Continuous Biosensing and Closed-Loop Therapies," Trends in Chemistry, vol. 2, no. 4, pp. 319–340, Apr. 2020, doi: 10.1016/j.trechm.2020.02.009.

[7] J. Kim, A. S. Campbell, B. E. F. de Ávila, and J. Wang, "Wearable biosensors for healthcare monitoring," Nature Biotechnology, vol. 37, no. 4, pp. 389–406, Apr. 2019, doi: 10.1038/s41587-019-0045-y.

[8] B. Heidt et al., "Point of care diagnostics in resource-limited settings: A review of the present and future of PoC in its most needed environment," Biosensors, vol. 10, no. 10, Sep. 2020, doi: 10.3390/BIOS10100133.

[9] A. J. Bandodkar and J. Wang, "Non-invasive wearable electrochemical sensors: A review," Trends in Biotechnology, vol. 32, no. 7, pp. 363–371, Jul. 2014, doi: 10.1016/j.tibtech.2014.04.005.

[10] K. Strimbu and J. A. Tavel, "What are biomarkers," Current Opinion in HIV and AIDS, vol. 5, no. 6, pp. 463–466, Nov. 2010, doi: 10.1097/COH.0b013e32833ed177.

[11] "The Emerging Influence of Digital Biomarkers on Healthcare | Rock Health | We're powering the future of healthcare. Rock Health is a seed and early-stage venture fund that supports startups building the next generation of technologies transforming healthcare.", [Online]. Available: https://rockhealth.com/reports/the-emerging-influence-of-digital-biomarkers-on-healthcare/

[12] K. Mahato and J. Wang, “Electrochemical sensors: From the bench to the skin,” Sensors and Actuators B: Chemical, vol. 344, p. 130178, Oct. 2021, doi: 10.1016/j.snb.2021.130178.

[13] R. Ghaffari, J. A. Rogers, and T. R. Ray, “Recent progress, challenges, and opportunities for wearable biochemical sensors for sweat analysis,” Sensors and Actuators B: Chemical, p. 129447, Jan. 2021, doi: 10.1016/j.snb.2021.129447.

[14] M. Chung, G. Fortunato, and N. Radacsi, “Wearable flexible sweat sensors for healthcare monitoring: a review,” Journal of The Royal Society Interface, vol. 16, no. 159, p. 20190217, Oct. 2019, doi: 10.1098/rsif.2019.0217.

[15] J. Xu, Y. Fang, and J. Chen, “Wearable Biosensors for Non-Invasive Sweat Diagnostics,” Biosensors, vol. 11, no. 8, Art. no. 8, Aug. 2021, doi: 10.3390/bios11080245.

[16] “Temporal profiling of cytokines in passively expressed sweat for detection of infection using wearable device - Jagannath - 2021 - Bioengineering & Translational Medicine - Wiley Online Library.” https://aiche.onlinelibrary.wiley.com/doi/full/10.1002/btm2.10220 (accessed Oct. 09, 2021).

[17] S. Jadoon, S. Karim, … M. A.-I., and undefined 2015, “Recent developments in sweat analysis and its applications,” hindawi.com, [Online]. Available: https://www.hindawi.com/journals/ijac/2015/164974/abs/

[18] J. Daniels et al., “A mask-based diagnostic platform for point-of-care screening of Covid-19,” Biosensors and Bioelectronics, vol. 192, p. 113486, Nov. 2021, doi: 10.1016/j.bios.2021.113486.

[19] N. M. Grob, M. Aytekin, and R. A. Dweik, “Biomarkers in exhaled breath condensate: A review of collection, processing and analysis,” Journal of Breath Research, vol. 2, no. 3, Sep. 2008, doi: 10.1088/1752-7155/2/3/037004.

[20] Z. L. Borrill, K. Roy, and D. Singh, “Exhaled breath condensate biomarkers in COPD,” European Respiratory Journal, vol. 32, no. 2, pp. 472–486, Aug. 2008, doi: 10.1183/09031936.00116107.

[21] A. Vasilescu, B. Hrinczenko, G. M. Swain, and S. F. Peteu, “Exhaled breath biomarker sensing,” Biosensors and Bioelectronics, vol. 182, p. 113193, Jun. 2021, doi: 10.1016/j.bios.2021.113193.

[22] L. L. J. Koppes, J. M. Dekker, H. F. J. Hendriks, L. M. Bouter, and R. J. Heine, “Moderate Alcohol Consumption Lowers the Risk of Type 2 Diabetes,” Diabetes care, vol. 28, no. 3, p. 719, 2005.

[23] N. V. Emanuele, T. F. Swade, and M. A. Emanuele, “Consequences of alcohol use in diabetics,” Alcohol Health and Research World, vol. 22, no. 3, pp. 211–219, 1998.

[24] D. Alromaihi, J. Zielke, and A. Bhan, “Challenges of Type 2 Diabetes in Patients with Alcohol Dependence,” Clinical Diabetes, vol. 30, no. 3, pp. 120–122, 2012, doi: 10.2337/diaclin.30.3.120.

[25] V. Lambert, “Empowering patients to track their health through wearable tech,” https://www.raconteur.net/healthcare/empowering-patients-to-track-their-health-through-wearable-tech, Aug. 2016.

[26] W. Gao et al., “Fully integrated wearable sensor arrays for multiplexed in situ perspiration analysis,” Nature, vol. 529, no. 7587, pp. 509–514, 2016.

[27] M. Gandhi and T. Wang, “The Future of Biosensing Wearables,” https://rockhealth.com/reports/the-future-of-biosensing-wearables/, 2014.

[28] A. Bhide, S. Muthukumar, A. Saini, and S. Prasad, “Simultaneous lancet-free monitoring of alcohol and glucose from low-volumes of perspired human sweat,” Scientific Reports, vol. 8, no. 1, 2018, doi: 10.1038/s41598-018-24543-4.

[29] A. Avogaro and A. Tiengo, “Alcohol, glucose metabolism and diabetes,” Diabetes/metabolism reviews, vol. 9, no. 2, pp. 129–146, 1993, doi: 10.1002/dmr.5610090205.

[30] R. Swift, “Direct measurement of alcohol and its metabolites,” Addiction, vol. 98, pp. 73–80, 2003, doi: 10.1046/j.1359-6357.2003.00605. x.

[31] J. S. Hawthorne and M. H. Wojcik, “Transdermal Alcohol Measurement: A Review of the Literature,” Canadian Society of Forensic Science Journal, vol. 39, no. 2, pp. 65–71, 2006, doi: 10.1080/00085030.2006.10757138.

[32] M. Gamella et al., “A novel non-invasive electrochemical biosensing device for in situ determination of the alcohol content in blood by monitoring ethanol in sweat,” Analytica Chimica Acta, vol. 806, pp. 1–7, 2014, doi: //doi.org/10.1016/j.aca.2013.09.020.

[33] O. Olarte, J. Chilo, J. Pelegri-Sebastia, K. Barb, and W. V. Moer, “Glucose detection in human sweat using an electronic nose,” in 2013 35th Annual International Conference of the IEEE Engineering in Medicine and Biology Society (EMBC), 2013, pp. 1462–1465. doi: 10.1109/EMBC.2013.6609787.

[34] B. C. Turner, E. Jenkins, D. Kerr, R. S. Sherwin, and D. A. Cavan, “The Effect of Evening Alcohol Consumption on Next-Morning Glucose Control in Type 1 Diabetes,” Diabetes care, vol. 24, no. 11, pp. 1888–1893, 2001, doi: 10.2337/diacare.24.11.1888.

[35] Z. Sonner et al., “The microfluidics of the eccrine sweat gland, including biomarker partitioning, transport, and biosensing implications,” Biomicrofluidics, vol. 9, no. 3, p. 31301, 2015, doi: 10.1063/1.4921039.

[36] R. D. Munje, S. Muthukumar, A. P. Selvam, and S. Prasad, “Flexible nanoporous tunable electrical double layer biosensors for sweat diagnostics,” Scientific Reports, vol. 5, p. 14586, 2015.

[37] S. Park, H. C. Kim, and T. D. Chung, “Electrochemical analysis based on nanoporous structures,” Analyst, vol. 137, no. 17, pp. 3891–3903, Sep. 2012, doi: 10.1039/c2an35294j.

[38] A. P. Minton, “Models for Excluded Volume Interaction between an Unfolded Protein and Rigid Macromolecular Cosolutes: Macromolecular Crowding and Protein Stability Revisited,” Biophysical journal, vol. 88, no. 2, pp. 971–985, doi: 10.1529/biophysj.104.050351.

[39] H.-X. Zhou, G. Rivas, and A. P. Minton, “Macromolecular Crowding and Confinement: Biochemical, Biophysical, and Potential Physiological Consequences,” Annual Review of Biophysics, vol. 37, no. 1, pp. 375–397, 2008, doi: 10.1146/annurev.biophys.37.032807.125817.

[40] D. C. Grahame, “The Electrical Double Layer and the Theory of Electrocapillarity,” Chemical reviews, vol. 41, no. 3, pp. 441–501, 1947, doi: 10.1021/cr60130a002.

[41] Z. Stojek, “The Electrical Double Layer and Its Structure,” in Electroanalytical Methods: Guide to Experiments and Applications, F. Scholz, Ed. Berlin, Heidelberg: Springer, 2002, pp. 3–8. doi: 10.1007/978-3-662-04757-6_1.

[42] D. A. Armbruster and T. Pry, “Limit of Blank, Limit of Detection and Limit of Quantitation,” The Clinical Biochemist Reviews, vol. 29, pp. S4–S52, 2008.

[43] O. Pänke, T. Balkenhohl, J. Kafka, D. Schäfer, and F. Lisdat, “Impedance spectroscopy and biosensing,” Advances in Biochemical Engineering/Biotechnology, vol. 109, pp. 195–237, Nov. 2007, doi: 10.1007/10_2007_081.

[44] S. Heinonen, J.-P. Nikkanen, E. Huttunen-Saarivirta, and E. Levänen, “Investigation of long-term chemical stability of structured ZnO films in aqueous solutions of varying conditions,” Thin Solid Films, vol. 638, pp. 410–419, 2017, doi: https://doi.org/10.1016/j.tsf.2017.07.055.

[45] S. Maleknia, H. Ahmadi, and D. Norouzian, “Immobilization of Pichia pastoris cells containing alcohol oxidase activity,” Iranian journal of microbiology, vol. 3, no. 4, pp. 210–215, Dec. 2011.

[46] A. Fulati, S. M. Usman Ali, M. Riaz, G. Amin, O. Nur, and M. Willander, “Miniaturized pH Sensors Based on Zinc Oxide Nanotubes/Nanorods,” Sensors, vol. 9, no. 11, Art. no. 11, Nov. 2009, doi: 10.3390/s91108911.

[47] J. Kim et al., “Noninvasive Alcohol Monitoring Using a Wearable Tattoo-Based Iontophoretic-Biosensing System,” ACS Sensors, vol. 1, no. 8, pp. 1011–1019, 2016, doi: 10.1021/acssensors.6b00356.

[48] D. Zhao, D. Miller, X. Xian, F. Tsow, and E. S. Forzani, “A novel real-time carbon dioxide analyzer for health and environmental applications,” Sensors and Actuators B: Chemical, vol. 195, pp. 171–176, May 2014, doi: 10.1016/j.snb.2013.12.110.

[49] J. Moyer, D. Wilson, I. Finkelshtein, B. Wong, and R. Potts, “Correlation between sweat glucose and blood glucose in subjects with diabetes,” Diabetes technology & therapeutics, vol. 14, no. 5, pp. 398–402, May 2012, doi: 10.1089/dia.2011.0262 [doi].

[50] H. Lee et al., “A graphene-based electrochemical device with thermoresponsive microneedles for diabetes monitoring and therapy,” Nature Nanotechnology, vol. 11, p. 566, 2016.

[51] R. D. Munje, S. Muthukumar, and S. Prasad, “Lancet-free and label-free diagnostics of glucose in sweat using Zinc Oxide based flexible bioelectronics,” Sensors and Actuators B: Chemical, vol. 238, pp. 482–490, Jan. 2017, doi: 10.1016/j.snb.2016.07.088.

[52] A. Rebel, M. A. Rice, and B. G. Fahy, “The Accuracy of Point-of-Care Glucose Measurements,” Journal of Diabetes Science and Technology, vol. 6, no. 2, pp. 396–411, 2012.

[53] M. Dumett et al., “Deconvolving an Estimate of Breath Measured Blood Alcohol Concentration from Biosensor Collected Transdermal Ethanol Data,” Applied mathematics and computation, vol. 196, no. 2, pp. 724–743, 2008, doi: 10.1016/j.amc.2007.07.026.

[54] R. J. McEnroe and Clinical and Laboratory Standards Institute, Interference testing in clinical chemistry: approved guideline. Wayne, PA: Clinical and Laboratory Standards Institute, 2005.

[55] N. R. Shanmugam, A. P. Selvam, T. W. Barrett, S. C. Kazmierczak, M. N. Rana, and S. Prasad, “Portable nanoporous electrical biosensor for ultrasensitive detection of Troponin-T,” Future Science OA, vol. 1, no. 3, 2015, doi: 10.4155/fso.15.22.

[56] M. T. Mathew, E. Ariza, L. A. Rocha, A. C. Fernandes, and F. Vaz, “TiCxOy thin films for decorative applications: Tribocorrosion mechanisms and synergism,” Tribology International, vol. 41, no. 7, pp. 603–615, Jul. 2008, doi: 10.1016/j.triboint.2007.11.011.

[57] X. Du, J. Anzai, T. Osa, and R. Motohashi, “Amperometric alcohol sensors based on protein multilayers composed of avidin and biotin-labeled alcohol oxidase,” Electroanalysis, vol. 8, no. 8–9, pp. 813–816, 1996, doi: 10.1002/elan.1140080820.

[58] C. J. Harvey, R. F. LeBouf, and A. B. Stefaniak, “Formulation and stability of a novel artificial human sweat under conditions of storage and use,” Toxicology in vitro: an international journal published in association with BIBRA, vol. 24, no. 6, pp. 1790–1796, Sep. 2010, doi: 10.1016/j.tiv.2010.06.016 [doi].

[59] M. Haghi, K. Thurow, and R. Stoll, “Wearable Devices in Medical Internet of Things: Scientific Research and Commercially Available Devices,” Healthcare informatics research, vol. 23, no. 1, pp. 4–15, Jan. 2017, doi: 10.4258/hir.2017.23.1.4 [doi].

[60] S. Hiremath, G. Yang, and K. Mankodiya, “Wearable Internet of Things: Concept, architectural components and promises for person-centered healthcare,” in 2014 4th International Conference on Wireless Mobile Communication and Healthcare - Transforming Healthcare Through Innovations in Mobile and Wireless Technologies (MOBIHEALTH), 2014, pp. 304–307. doi: 10.1109/MOBIHEALTH.2014.7015971.

[61] M. Swan, “Sensor Mania! The Internet of Things, Wearable Computing, Objective Metrics, and the Quantified Self 2.0,” Journal of Sensor and Actuator Networks, vol. 1, no. 3, Art. no. 3, Dec. 2012, doi: 10.3390/jsan1030217.

[62] P. US, “Wearable Technology Future is Ripe for Growth - Most Notably among Millennials, Says PwC US.” https://www.prnewswire.com/news-releases/wearable-technology-future-is-ripe-for-growth--most-notably-among-millennials-says-pwc-us-515861911.html (accessed Oct. 05, 2021).

[63] D. Evans, The Internet of Things: How the Next Evolution of the Internet is Changing Everything, vol. 1. 2011.

[64] S. C. Mukhopadhyay, “Wearable Sensors for Human Activity Monitoring: A Review,” IEEE Sensors Journal, vol. 15, no. 3, pp. 1321–1330, 2015, doi: 10.1109/JSEN.2014.2370945.

[65] S. Seneviratne et al., “A Survey of Wearable Devices and Challenges,” IEEE Communications Surveys & Tutorials, vol. 19, no. 4, pp. 2573–2620, 2017, doi: 10.1109/COMST.2017.2731979.

[66] H. Jason, “Non-invasive Analyte Access and Sensing through Eccrine Sweat: Challenges and Outlook circa 2016,” Electroanalysis, vol. 28, no. 6, pp. 1242–1249, 2016, doi: 10.1002/elan.201600018.

[67] J. Heikenfeld, “Technological leap for sweat sensing,” Nature, vol. 529, p. 475, 2016.

[68] A. M. Azevedo, D. M. F. Prazeres, J. M. S. Cabral, and L. P. Fonseca, “Ethanol biosensors based on alcohol oxidase,” Biosensors and Bioelectronics, vol. 21, no. 2, pp. 235–247, Aug. 2005, doi: 10.1016/j.bios.2004.09.030.

[69] S. Anastasova et al., “A wearable multisensing patch for continuous sweat monitoring,” Biosensors and Bioelectronics, vol. 93, pp. 139–145, Jul. 2017, doi: 10.1016/j.bios.2016.09.038.

[70] “Statistics About Diabetes | ADA.” https://www.diabetes.org/resources/statistics/statistics-about-diabetes (accessed Oct. 05, 2021).

[71] “National Institute on Alcohol Abuse and Alcoholism (NIAAA) | National Institute on Alcohol Abuse and Alcoholism (NIAAA).” https://www.niaaa.nih.gov/ (accessed Oct. 05, 2021).

[72] T. Babor, J. Rehm, D. Jernigan, P. Vaeth, M. Monteiro, and H. Lehman, “Alcohol, diabetes, and public health in the Americas,” Revista panamericana de salud pública = Pan American journal of public health, vol. 32, no. 2, pp. 151–151, Aug. 2012.

[73] F. Scholz, “Voltammetric techniques of analysis: the essentials,” ChemTexts, vol. 1, no. 4, pp. 1–24, Dec. 2015, doi: 10.1007/s40828-015-0016-y.

[74] A. J. Bard and L. R. Faulkner, Electrochemical Methods: Fundamentals and Applications. Wiley, 2000. [Online]. Available: https://books.google.com/books?id=kv56QgAACAAJ

[75] Z. Zhao, W. Lei, X. Zhang, B. Wang, and H. Jiang, “ZnO-based amperometric enzyme biosensors,” Sensors, vol. 10, no. 2, pp. 1216–1231, Feb. 2010, doi: 10.3390/s100201216.

[76] N. R. Shanmugam, S. Muthukumar, and S. Prasad, “A review on ZnO-based electrical biosensors for cardiac biomarker detection,” Future Science OA, vol. 3, no. 4, p. FSO196, 2017, doi: 10.4155/fsoa-2017-0006.

[77] J. S. Daniels and N. Pourmand, “Label-free impedance biosensors: Opportunities and challenges,” Electroanalysis, vol. 19, no. 12, pp. 1239–1257, Jun. 2007, doi: 10.1002/elan.200603855.

[78] E. P. Randviir and C. E. Banks, “Electrochemical impedance spectroscopy: an overview of bioanalytical applications,” Analytical Methods, vol. 5, no. 5, pp. 1098–1115, 2013, doi: 10.1039/C3AY26476A.

[79] F. Lisdat and D. Schäfer, “The use of electrochemical impedance spectroscopy for biosensing,” Analytical and Bioanalytical Chemistry, vol. 391, no. 5, p. 1555, 2008, doi: 10.1007/s00216-008-1970-7.

[80] A. Bhide, S. Muthukumar, and S. Prasad, “CLASP (Continuous lifestyle awareness through sweat platform): A novel sensor for simultaneous detection of alcohol and glucose from passive perspired sweat,” Biosensors and Bioelectronics, vol. 117, pp. 537–545, Oct. 2018, doi: 10.1016/j.bios.2018.06.065.

[81] F. M. Omar, H. A. Aziz, and S. Stoll, “Aggregation and disaggregation of ZnO nanoparticles: Influence of pH and adsorption of Suwannee River humic acid,” The Science of the total environment, vol. 468–469, pp. 195–201, Jan. 2014, doi: //doi.org/10.1016/j.scitotenv.2013.08.044.

[82] M. Moretti, D. Sisti, M. B. Rocchi, and E. Delprete, “CLSI EP17-A protocol: A useful tool for better understanding the low-end performance of total prostate-specific antigen assays,” Clinica Chimica Acta, vol. 412, no. 11, pp. 1143–1145, 2011, doi: 10.1016/j.cca.2011.03.002.

[83] D. Hashoul and H. Haick, “Sensors for detecting pulmonary diseases from exhaled breath,” European Respiratory Review, vol. 28, no. 152, Jun. 2019, doi: 10.1183/16000617.0011-2019.

[84] A. Gholizadeh et al., “Toward point-of-care management of chronic respiratory conditions: Electrochemical sensing of nitrite content in exhaled breath condensate using reduced graphene oxide,” Microsystems and Nanoengineering, vol. 3, no. 1, pp. 1–8, May 2017, doi: 10.1038/micronano.2017.22.

[85] A. Shalaby, O. Khalafallah, M. Galal, H. H. Assal, and N. Ahmed, “Correlation between serum lactate and other oxygenation indices as a predictor of outcome in respiratory ICU patients,” Egyptian Journal of Chest Diseases and Tuberculosis, vol. 65, no. 3, pp. 695–700, Jul. 2016, doi: 10.1016/j.ejcdt.2016.04.010.

[86] B. A. Katchman, M. Zhu, J. Blain Christen, and K. S. Anderson, “Eccrine Sweat as a Biofluid for Profiling Immune Biomarkers,” Proteomics - Clinical Applications, vol. 12, no. 6, Nov. 2018, doi: 10.1002/prca.201800010.

[87] J. N. Hussain, N. Mantri, M. M. Cohen, and J. Hussain, “Working Up a Good Sweat-The Challenges of Standardising Sweat Collection for Metabolomics Analysis.” [Online]. Available: http://www.hmdb.

[88] K. Mitsubayashi, M. Suzuki, E. Tamiya, and I. Karube, “Analysis of metabolites in sweat as a measure of physical condition,” Analytica Chimica Acta, vol. 289, no. 1, pp. 27–34, Apr. 1994, doi: 10.1016/0003-2670(94)80004-9.

[89] M. J. Buono, N. V. L. Lee, and P. W. Miller, “The relationship between exercise intensity and the sweat lactate excretion rate,” Journal of Physiological Sciences, vol. 60, no. 2, pp. 103–107, Mar. 2010, doi: 10.1007/s12576-009-0073-3.

[90] J. M. Green, R. C. Pritchett, T. R. Crews, J. R. McLester, and D. C. Tucker, "Sweat lactate response between males with high and low aerobic fitness," European Journal of Applied Physiology, vol. 91, no. 1, pp. 1–6, Jan. 2004, doi: 10.1007/s00421-003-0968-2.

[91] X. Cai, J. Yan, H. Chu, M. Wu, and Y. Tu, "An exercise degree monitoring biosensor based on electrochemiluminescent detection of lactate in sweat," Sensors and Actuators, B: Chemical, vol. 143, no. 2, pp. 655–659, Jan. 2010, doi: 10.1016/j.snb.2009.10.002.

[92] W. Jia et al., "Electrochemical tattoo biosensors for real-time noninvasive lactate monitoring in human perspiration," Analytical Chemistry, vol. 85, no. 14, pp. 6553–6560, Jul. 2013, doi: 10.1021/ac401573r.

[93] P. J. Derbyshire, H. Barr, F. Davis, and S. P. J. Higson, "Lactate in human sweat: A critical review of research to the present day," Journal of Physiological Sciences, vol. 62, no. 6, pp. 429–440, Nov. 2012, doi: 10.1007/s12576-012-0213-z.

[94] K. C. Lin, S. Muthukumar, and S. Prasad, "Flex-GO (Flexible graphene oxide) sensor for electrochemical monitoring lactate in low-volume passive perspired human sweat," Talanta, vol. 214, pp. 120810–120810, Jul. 2020, doi: 10.1016/j.talanta.2020.120810.

[95] A. Bhide, K.-C. Lin, S. Muthukumar, and S. Prasad, "On-demand lactate monitoring towards assessing physiological responses in sedentary populations," Analyst, vol. 146, no. 11, pp. 3482–3492, 2021.

[96] T. Terse-Thakoor et al., "Thread-based multiplexed sensor patch for real-time sweat monitoring," npj Flexible Electronics, vol. 4, no. 1, pp. 1–10, Dec. 2020, doi: 10.1038/s41528-020-00081-w.

[97] R. Wang, Q. Zhai, T. An S. Gong, and W. Cheng, "Stretchable Gold Fiber-based Wearable Textile Electrochemical Biosensor for Lactate Monitoring in Sweat," Talanta, pp. 121484–121484, Aug. 2020, doi: 10.1016/j.talanta.2020.121484.

[98] Q. Zhang et al., "Wearable electrochemical biosensor based on molecularly imprinted Ag nanowires for noninvasive monitoring lactate in human sweat," Sensors and Actuators, B: Chemical, vol. 320, p. 128325, Oct. 2020, doi: 10.1016/j.snb.2020.128325.

[99] L. Zhang, J. Liu, Z. Fu, and L. Qi, "A Wearable Biosensor Based on Bienzyme Gel-Membrane for Sweat Lactate Monitoring by Mounting on Eyeglasses," Journal of Nanoscience and Nanotechnology, vol. 20, no. 3, pp. 1495–1503, Sep. 2019, doi: 10.1166/jnn.2020.16952.

[100] M. E. Payne, A. Zamarayeva, V. I. Pister, N. A. D. Yamamoto, and A. C. Arias, "Printed, Flexible Lactate Sensors: Design Considerations Before Performing On-Body Measurements," Scientific Reports, vol. 9, no. 1, pp. 1–10, Dec. 2019, doi: 10.1038/s41598-019-49689-7.

[101] J. H. Bae, J. H. Han, and T. D. Chung, “Electrochemistry at nanoporous interfaces: New opportunity for electrocatalysis,” Physical Chemistry Chemical Physics, vol. 14, no. 2, pp. 448–463, Jan. 2012, doi: 10.1039/c1cp22927c.

[102] S. Prasad, A. P. Selvam, R. K. Reddy, and A. Love, “Silicon nanosensor for diagnosis of Cardiovascular proteomic markers,” Journal of Laboratory Automation, vol. 18, no. 2, pp. 143–151, Apr. 2013, doi: 10.1177/2211068212460038.

[103] I. M. Kuznetsova, K. K. Turoverov, and V. N. Uversky, “What macromolecular crowding can do to a protein,” International Journal of Molecular Sciences, vol. 15, no. 12, pp. 23090–23140, Dec. 2014, doi: 10.3390/ijms151223090.

[104] S. Upasham, K. Thai, R. Muthyala, and S. Prasad, “Flexible, low volume detection of chronobiology biomarkers from human sweat,” Analyst, vol. 145, no. 3, pp. 784–796, 2020, doi: 10.1039/C9AN01968E.

[105] N. Tripathy and D. H. Kim, “Metal oxide modified ZnO nanomaterials for biosensor applications,” Nano Convergence, vol. 5, no. 1, pp. 1–10, Dec. 2018, doi: 10.1186/s40580-018-0159-9.

[106] S. K. Arya, S. Saha, J. E. Ramirez-Vick, V. Gupta, S. Bhansali, and S. P. Singh, “Recent advances in ZnO nanostructures and thin films for biosensor applications: Review,” Analytica Chimica Acta, vol. 737, pp. 1–21, Aug. 2012, doi: 10.1016/j.aca.2012.05.048.

[107] R. D. Munje, M. Jacobs, S. Muthukumar, B. Quadri, N. R. Shanmugam, and S. Prasad, “A novel approach for electrical tuning of nano-textured zinc oxide surfaces for ultra-sensitive troponin-T detection,” Analytical Methods, vol. 7, no. 24, pp. 10136–10144, Dec. 2015, doi: 10.1039/c5ay02052b.

[108] N. Wiesmann, W. Tremel, and J. Brieger, “Zinc oxide nanoparticles for therapeutic purposes in cancer medicine,” Journal of Materials Chemistry B, vol. 8, no. 23, pp. 4973–4989, Jun. 2020, doi: 10.1039/d0tb00739k.

[109] A. Bogomolova et al., “Challenges of electrochemical impedance spectroscopy in protein biosensing,” Analytical Chemistry, vol. 81, no. 10, pp. 3944–3949, May 2009, doi: 10.1021/ac9002358.

[110] B. L. Garrote, A. Santos, and P. R. Bueno, “Perspectives on and Precautions for the Uses of Electric Spectroscopic Methods in Label-free Biosensing Applications,” ACS Sensors, vol. 4, no. 9, pp. 2216–2227, Sep. 2019, doi: 10.1021/acssensors.9b01177.

[111] D. A. Sakharov, M. U. Shkurnikov, M. Y. Vagin, E. I. Yashina, A. A. Karyakin, and A. G. Tonevitsky, “Relationship between lactate concentrations in active muscle sweat and whole blood,” Bulletin of experimental biology and medicine, vol. 150, no. 1, pp. 83–85, Dec. 2010, doi: 10.1007/s10517-010-1075-0.

[112] J. I. Njagi and S. M. Kagwanja, “The interface in biosensing: Improving selectivity and sensitivity,” 2011, vol. 1062, pp. 225–247. doi: 10.1021/bk-2011-1062.ch011.

[113] T. D. Gibson, “Biosensors: the stabilité problem,” Analusis, vol. 27, no. 7, pp. 630–638, Sep. 1999, doi: 10.1051/analusis:1999270630.

[114] M. Harker, “Psychological Sweating: A Systematic Review Focused on Aetiology and Cutaneous Response,” Skin Pharmacology and Physiology, vol. 26, no. 2, pp. 92–100, Apr. 2013, doi: 10.1159/000346930.

[115] L. B. Baker, “Physiology of sweat gland function: The roles of sweating and sweat composition in human health,” Temperature, vol. 6, no. 3, pp. 211–259, Jul. 2019, doi: 10.1080/23328940.2019.1632145.

[116] O. N. Kokiko-Cochran, J. P. Godbout, and Z. M. Tapp, “A tilted axis: maladaptive inflammation and HPA axis dysfunction contribute to consequences of TBI,” Frontiers in neurology, vol. 10, pp. 345–345, 2019.

[117] R. S. Hardy et al., “Differential expression, function and response to inflammatory stimuli of 11β-hydroxysteroid dehydrogenase type 1 in human fibroblasts: a mechanism for tissue-specific regulation of inflammation,” Arthritis research & therapy, vol. 8, no. 4, pp. R108–R108, 2006.

[118] S. Sekula, “Inhibition of c-Jun/ATF2 phosphorylation, transrepression of c-Jun/c-Fos: two modes of regulation of the transcription factor AP-1 activity by glucocorticoid receptor,” 2007.

[119] R. H. Straub and M. Cutolo, “Glucocorticoids and chronic inflammation,” Rheumatology, vol. 55, no. suppl_2, pp. ii6–ii14, Nov. 2016, doi: 10.1093/rheumatology/kew348.

[120] S. Pellissier et al., “Relationship between vagal tone, cortisol, TNF-alpha, epinephrine and negative effects in Crohn’s disease and irritable bowel syndrome,” PloS one, vol. 9, no. 9, 2014.

[121] K. D. Sudheimer et al., “Cortisol, cytokines, and hippocampal volume interactions in the elderly,” Frontiers in Aging Neuroscience, vol. 6, pp. 153–153, 2014.

[122] E. Russell, G. Koren, M. Rieder, and S. H. M. Van Uum, “The Detection of Cortisol in Human Sweat: Implications for Measurement of Cortisol in Hair,” Therapeutic Drug Monitoring, vol. 36, no. 1, pp. 30–34, 2014.

[123] A. Marques-Deak et al., “Measurement of cytokines in sweat patches and plasma in healthy women: Validation in a controlled study,” Journal of Immunological Methods, vol. 315, no. 1, pp. 99–109, 2006, doi: 10.1016/j.jim.2006.07.011.

[124] A. J. Steckl and P. Ray, “Stress Biomarkers in Biological Fluids and Their Point-of-Use Detection,” ACS Sens., vol. 3, no. 10, pp. 2025–2044, Oct. 2018, doi: 10.1021/acssensors.8b00726.

[125] X. Zhu, W. Liu, S. Shuang, M. Nair, and C.-Z. Li, “6 - Intelligent tattoos, patches, and other wearable biosensors,” in Medical Biosensors for Point of Care (POC) Applications, R. J. Narayan, Ed. Woodhead Publishing, 2017, pp. 133–150. doi: 10.1016/B978-0-08-100072-4.00006-X.

[126] E. C. S. Wilder, “Human Subjects Testing of Sweat Stimulation Technologies,” University of Cincinnati, 2016. Accessed: Oct. 07, 2021. [Online]. Available: https://etd.ohiolink.edu/apexprod/rws_olink/r/1501/10?clear=10&p10_accession_num=ucin1468512004

[127] D. Purvis, O. Leonardova, D. Farmakovsky, and V. Cherkasov, “An ultrasensitive and stable potentiometric immunosensor,” Biosensors and Bioelectronics, vol. 18, no. 11, pp. 1385–1390, Oct. 2003, doi: 10.1016/S0956-5663(03)00066-6.

[128] H. J. Qureshi et al., “Toward Automation of the Supine Pressor Test for Preeclampsia,” Journal of Engineering and Science in Medical Diagnostics and Therapy, 2019, doi: 10.1115/1.4045203.

[129] “Sensors | Free Full-Text | Ultrasensitive Immunosensor Array for TNF-α Detection in Artificial Saliva using Polymer-Coated Magnetic Microparticles onto Screen-Printed Gold Electrode.” https://www.mdpi.com/1424-8220/19/3/692 (accessed Oct. 07, 2021).

[130] B.-Y. Kim, H.-B. Lee, and N.-E. Lee, “A durable, stretchable, and disposable electrochemical biosensor on three-dimensional micro-patterned stretchable substrate,” Sensors and Actuators B: Chemical, vol. 283, pp. 312–320, Mar. 2019, doi: 10.1016/j.snb.2018.12.045.

[131] D. Kinnamon, R. Ghanta, K. C. Lin, S. Muthukumar, and S. Prasad, “Portable biosensor for monitoring cortisol in low-volume perspired human sweat,” Scientific Reports, vol. 7, no. 1, pp. 1–13, Dec. 2017, doi: 10.1038/s41598-017-13684-7.

[132] F. Wei et al., “Electrochemical sensor for multiplex biomarkers detection,” Clinical Cancer Research, vol. 15, no. 13, pp. 4446–4452, Jul. 2009, doi: 10.1158/1078-0432.CCR-09-0050.

[133] L. Huang, S. Tian, W. Zhao, K. Liu, X. Ma, and J. Guo, “Multiplexed detection of biomarkers in lateral-flow immunoassays,” Analyst, vol. 145, no. 8, pp. 2828–2840, Apr. 2020, doi: 10.1039/c9an02485a.

[134] R. Vaidyanathan, L. M. Van Leeuwen, S. Rauf, M. J. A. Shiddiky, and M. Trau, “A multiplexed device based on tunable Nanoshearing for specific detection of multiple protein

biomarkers in serum," Scientific Reports, vol. 5, no. 1, pp. 1–7, May 2015, doi: 10.1038/srep09756.

[135] C. Dincer, R. Bruch, A. Kling, P. S. Dittrich, and G. A. Urban, "Multiplexed Point-of-Care Testing – xPOCT," Trends in Biotechnology, vol. 35, no. 8, pp. 728–742, Aug. 2017, doi: 10.1016/j.tibtech.2017.03.013.

[136] S. Jung, C. C. L. McCrory, I. M. Ferrer, J. C. Peters, and T. F. Jaramillo, "Benchmarking nanoparticulate metal oxide electrocatalysts for the alkaline water oxidation reaction," Journal of Materials Chemistry A, vol. 4, no. 8, pp. 3068–3076, Feb. 2016, doi: 10.1039/c5ta07586f.

[137] I. Jeerapan, S. P.-J. of T. Electrochemical, and undefined 2020, "Flexible and Stretchable Electrochemical Sensing Systems: Materials, Energy Sources, and Integrations," iopscience.iop.org, [Online]. Available: https://iopscience.iop.org/article/10.1149/1945-7111/ab7117/meta

[138] S. Upasham, A. Bhide, K.-C. Lin, and S. Prasad, "Point-of-use sweat biosensor to track the endocrine–inflammation relationship for chronic disease monitoring," Future science OA, vol. 7, no. 1, pp. FSO628–FSO628, 2020.

[139] S. P. Adiga et al., "Nanoporous materials for biomedical devices," JOM, vol. 60, no. 3, pp. 26–32, 2008, doi: 10.1007/s11837-008-0028-9.

[140] R. D. Munje, S. Muthukumar, B. Jagannath, and S. Prasad, "A new paradigm in sweat based wearable diagnostics biosensors using Room Temperature Ionic Liquids (RTILs)," Sci Rep, vol. 7, no. 1, p. 1950, May 2017, doi: 10.1038/s41598-017-02133-0.

[141] J.-M. Yuan et al., "The effects of macromolecular crowding on the mechanical stability of protein molecules," Protein Science, vol. 17, no. 12, pp. 2156–2166, Dec. 2008, doi: 10.1110/ps.037325.108.

[142] A. Bhide, B. Jagannath, A. Tanak, R. Willis, and S. Prasad, "CLIP: Carbon Dioxide testing suitable for Low power microelectronics and IOT interfaces using Room temperature Ionic Liquid Platform," Scientific Reports, vol. 10, no. 1, pp. 2557–2557, 2020, doi: 10.1038/s41598-020-59525-y.

[143] R. Masoodi and K. M. Pillai, "Darcy's law-based model for wicking in paper-like swelling porous media," AIChE Journal, vol. 56, no. 9, pp. 2257–2267, Sep. 2010, doi: 10.1002/aic.12163.

[144] C. K. Camplisson, K. M. Schilling, W. L. Pedrotti, H. A. Stone, and A. W. Martinez, "Two-ply channels for faster wicking in paper-based microfluidic devices," Lab on a Chip, vol. 15, no. 23, pp. 4461–4466, 2015, doi: 10.1039/C5LC01115A.

[145] J. Vatamanu, Z. Hu, D. Bedrov, C. Perez, and Y. Gogotsi, “Increasing energy storage in electrochemical capacitors with ionic liquid electrolytes and nanostructured carbon electrodes,” Journal of Physical Chemistry Letters, vol. 4, no. 17, pp. 2829–2837, Sep. 2013, doi: 10.1021/jz401472c.

[146] M. I. Prodromidis, “Impedimetric immunosensors—A review,” Electrochimica Acta, vol. 55, no. 14, pp. 4227–4233, 2010, doi: https://doi.org/10.1016/j.electacta.2009.01.081.

[147] Y. Liu, Z. Matharu, M. C. Howland, A. Revzin, and A. L. Simonian, “Affinity and enzyme-based biosensors: recent advances and emerging applications in cell analysis and point-of-care testing”, doi: 10.1007/s00216-012-6149-6.

[148] P. Montuschi, “Indirect monitoring of lung inflammation,” Nature Reviews Drug Discovery, vol. 1, no. 3, pp. 238–242, 2002, doi: 10.1038/nrd751.

[149] M. Khoubnasabjafari, K. Ansarin, and A. Jouyban, “Critical Review of Malondialdehyde Analysis in Biological Samples”.

[150] J. Yu, “Inflammatory mechanisms in the lung,” Journal of Inflammation Research, vol. 2, pp. 1–1, Dec. 2008, doi: 10.2147/jir. s4385.

[151] M. Cazzola, M. G. Matera, P. Rogliani, and C. Page, “Treating systemic effects of COPD,” Trends in Pharmacological Sciences, vol. 28, no. 10, pp. 544–550, Oct. 2007, doi: 10.1016/j.tips.2007.09.006.

[152] M. D. Giudice and S. W. Gangestad, “Rethinking IL-6 and CRP: Why they are more than inflammatory biomarkers, and why it matters,” Brain, Behavior, and Immunity, vol. 70, pp. 61–75, May 2018, doi: 10.1016/j.bbi.2018.02.013.

[153] T. Herold et al., “Elevated levels of IL-6 and CRP predict the need for mechanical ventilation in COVID-19,” Journal of Allergy and Clinical Immunology, vol. 146, no. 1, pp. 128-136.e4, Jul. 2020, doi: 10.1016/j.jaci.2020.05.008.

[154] S. S. Chang, C. A. V. Fragoso, P. H. V. Ness, L. P. Fried, and M. E. Tinetti, “Association between combined interleukin-6 and c-reactive protein levels and pulmonary function in older women: Results from the women’s health and aging studies i and II,” Journal of the American Geriatrics Society, vol. 59, no. 1, pp. 113–119, Jan. 2011, doi: 10.1111/j.1532-5415.2010.03203. x.

[155] M. Del Giudice and S. W. Gangestad, “Rethinking IL-6 and CRP: Why they are more than inflammatory biomarkers, and why it matters,” Brain, Behavior, and Immunity, vol. 70, pp. 61–75, May 2018, doi: 10.1016/j.bbi.2018.02.013.

[156] O. Holz, “New Perspectives in Monitoring Lung Inflammation: Analysis of Exhaled Breath Condensate,” European Respiratory Journal, vol. 26, no. 1, 2005.

[157] J. Hunt, “Exhaled Breath Condensate: An Overview,” Immunology and Allergy Clinics of North America, vol. 27, no. 4, pp. 587–596, Nov. 2007, doi: 10.1016/j.iac.2007.09.001.

[158] M. A. Stiegel, J. D. Pleil, J. R. Sobus, M. K. Morgan, and M. C. Madden, “Analysis of inflammatory cytokines in human blood, breath condensate, and urine using a multiplex immunoassay platform,” Biomarkers, vol. 20, no. 1, pp. 35–46, Feb. 2015, doi: 10.3109/1354750X.2014.988646.

[159] H. Filik and A. A. Avan, “Electrochemical immunosensors for the detection of cytokine tumor necrosis factor alpha: A review,” Talanta, vol. 211, pp. 120758–120758, May 2020, doi: 10.1016/j.talanta.2020.120758.

[160] E. Rahimpour, M. Khoubnasabjafari, V. Jouyban-Gharamaleki, and A. Jouyban, “Non-volatile compounds in exhaled breath condensate: review of methodological aspects,” Anal Bioanal Chem, vol. 410, no. 25, pp. 6411–6440, Oct. 2018, doi: 10.1007/s00216-018-1259-4.

[161] M. Khoubnasabjafari, M. R. A. Mogaddam, E. Rahimpour, J. Soleymani, A. A. Saei, and A. Jouyban, “Breathomics: Review of Sample Collection and Analysis, Data Modeling and Clinical Applications,” Critical Reviews in Analytical Chemistry, 2021, doi: 10.1080/10408347.2021.1889961.

[162] C. Gessner et al., “Exhaled breath condensate cytokine patterns in chronic obstructive pulmonary disease,” Respiratory Medicine, vol. 99, no. 10, pp. 1229–1240, Oct. 2005, doi: 10.1016/j.rmed.2005.02.041.

[163] H. J. Prins et al., “CRP-guided antibiotic treatment in acute exacerbations of COPD in hospital admissions,” The European respiratory journal, vol. 53, no. 5, May 2019, doi: 10.1183/13993003.02014-2018.

[164] Z. Zietkowski, M. M. Tomasiak-Lozowska, R. Skiepko, B. Mroczko, M. Szmitkowski, and A. Bodzenta-Lukaszyk, “High-sensitivity C-reactive protein in the exhaled breath condensate and serum in stable and unstable asthma,” Respiratory Medicine, vol. 103, no. 3, pp. 379–385, Mar. 2009, doi: 10.1016/J.RMED.2008.10.003.

[165] Z. Zietkowski, R. Skiepko, M. M. Tomasiak-Lozowska, B. Mroczko, M. Szmitkowski, and A. Bodzenta-Lukaszyk, “Changes in high-sensitivity C-reactive protein in serum and exhaled breath condensate after intensive exercise in patients with allergic asthma,” International Archives of Allergy and Immunology, vol. 153, no. 1, pp. 75–85, Aug. 2010, doi: 10.1159/000301582.

[166] E. F. Klein et al., “Ultrafine particles in airways: A novel marker of COPD exacerbation risk and inflammatory status,” International Journal of COPD, vol. 14, pp. 557–564, 2019, doi: 10.2147/COPD.S187560.

[167] E. Desimoni and B. Brunetti, “Data Treatment of Electrochemical Sensors and Biosensors,” Springer, New York, NY, 2015, pp. 1137–1151. doi: 10.1007/978-1-4939-1301-5_18.

[168] W. J. Peveler, M. Yazdani, and V. M. Rotello, “Selectivity and Specificity: Pros and Cons in Sensing,” ACS Sensors, vol. 1, no. 11, pp. 1282–1285, Nov. 2016, doi: 10.1021/acssensors.6b00564.

[169] P. Larsson et al., “Surfactant protein A and albumin in particles in exhaled air,” Respiratory Medicine, vol. 106, no. 2, pp. 197–204, Feb. 2012, doi: 10.1016/j.rmed.2011.10.008.

[170] S. Brandigampala, P. Feikert, K. Vattipalli, and S. Prasad, “Designing better nano biosensors: Role of pore confinement of biomolecules,” 2011, pp. 176–180. doi: 10.1109/NANO.2011.6144552.

[171] B. Jagannath, K. C. Lin, M. Pali, D. Sankhala, S. Muthukumar, and S. Prasad, “A Sweat-based Wearable Enabling Technology for Real-time Monitoring of IL-1β and CRP as Potential Markers for Inflammatory Bowel Disease,” Inflammatory bowel diseases, vol. 26, no. 10, pp. 1533–1542, Oct. 2020, doi: 10.1093/ibd/izaa191.

[172] A. S. Tanak, S. Muthukumar, S. Krishnan, K. L. Schully, D. V. Clark, and S. Prasad, “Multiplexed cytokine detection using electrochemical point-of-care sensing device towards rapid sepsis endotyping,” Biosensors and Bioelectronics, vol. 171, pp. 112726–112726, Jan. 2021, doi: 10.1016/j.bios.2020.112726.

[173] J. W. Bartlett and C. Frost, “Reliability, repeatability and reproducibility: Analysis of measurement errors in continuous variables,” Ultrasound in Obstetrics and Gynecology, vol. 31, no. 4, pp. 466–475, Apr. 2008, doi: 10.1002/uog.5256.

[174] H. E. Plesser, “Reproducibility vs. Replicability: A brief history of a confused terminology,” Frontiers in Neuroinformatics, vol. 11, pp. 76–76, Jan. 2018, doi: 10.3389/fninf.2017.00076.

[175] M. Seifi et al., “Investigating the relationship between particulate matter and inflammatory biomarkers of exhaled breath condensate and blood in healthy young adults,” Scientific Reports 2021 11:1, vol. 11, no. 1, pp. 1–11, Jun. 2021, doi: 10.1038/s41598-021-92333-6.

[176] P. Van Der Zee et al., “Cytokines and chemokines are detectable in swivel-derived exhaled breath condensate (SEBC): A pilot study in mechanically ventilated patients,” Disease Markers, vol. 2020, 2020, doi: 10.1155/2020/2696317.

[177] T. UENO et al., “Inflammatory markers in exhaled breath condensate from patients with asthma,” Respirology, vol. 13, no. 5, pp. 654–663, Jul. 2008, doi: 10.1111/J.1440-1843.2008.01315. X.

BIOGRAPHICAL SKETCH

Ashlesha pursued her Bachelors in Instrumentation Technology from Visvesvaraya Technological University (VTU) in Bengaluru, India, and further obtained her Master of Science degree in Electrical and Computer Engineering from the University of Manitoba in Winnipeg, Canada in 2014. Subsequently, she worked as a research engineer at the Centre for Nano Science and Engineering (CeNSE), Indian Institute of Science in Bengaluru, India. At IISc, her research was focused towards developing SERS based microfluidic devices for single molecule detection. Ashlesha began her doctoral journey in Bioengineering at The University of Texas at Dallas in 2016. Her research interests are focused on developing wearable platforms for lifestyle management. Her current research is based on developing wearable and point-of-care platforms sensors for biomarker monitoring in non-invasive body fluids. She currently has 12 peer-reviewed publications and has received multiple fellowships and awards for her PhD research. Recently, her latest research was featured on the two covers: RSC Analyst and ACS Omega, which gained recognition in the sweat wearables space.

CURRICULUM VITAE

ASHLESHA BHIDE, PhD

Ashlesha.Bhide@utdallas.edu

PROFILE

- Highly motivated, experienced individual setting out to seek a career as a biomedical scientist with the eagerness to learn and adapt to cutting-edge technologies
- Extensive R&D background in wearable electrochemical and optical biosensor platforms
- Hands-on experience in micro/nano fabrication processing in a clean-room environment.
- Diverse background in interdisciplinary problem-solving skills and engineering design

EXPERIENCE

Doctoral Candidate, University of Texas at Dallas — 2016- Present

- Developed a rapid screening platform for detection of inflammatory biomarkers in exhaled breath condensate for monitoring respiratory disorders
- Developed a non-invasive biosensor for sweat- based diagnostic wearable platforms towards continuous, on-body detection of metabolites for health tracking
- Investigated the attributes of proprietary membranes for usability in sweat biosensing as a part of sponsored research for W.L Gore and associates.
- Design and development of a CO_2 and humidity sensor suitable for low power microelectronics and IoT interfaces using Room-temperature ionic liquids as a part of sponsored research for Texas Instruments

Research Engineer, Centre for Nano Science and Engineering — 2014- 2016

- Design and fabrication of an optical biosensor based on Raman spectroscopy for molecular fingerprinting of biomolecules

Graduate Research Assistant, University of Manitoba — 2011- 2014

- Deployment of a neural network-based signal classifier system for identification of electronic signals generated in real-time by a cytometer for monitoring apoptosis in biological cells

EDUCATION

- University of Texas at Dallas — Doctorate in Biomedical Engineering, 2016- 2021
- University of Manitoba — Master's in Electrical & Computer Engineering, 2011- 2014
- Visvesvaraya Technological University — Bachelor's in Instrumentation Technology, 2006-2010

SKILLS- Photolithography, Etching, Sputter deposition, thin film deposition, SEM, EDAX, FTIR, SPR, Zetasizer (DLS), Electrochemistry, Skin-worn sensors, Point of care diagnostics, Assay development, Data Analysis, Statistical methods

AWARDS

- Jonsson School Industry Advisory Council Fellowship- 2020
- Louis Beechrel, Jr. Graduate Fellowship- 2019
- Department of Bioengineering graduate award- 2018
- Semiconductor Research Corporation and Texas Analog Centre of Excellence Best poster award- 2017 & 2018
- Society of Laboratory Automation Tony B. Academic Travel award- 2018
- Jonsson Family Bioengineering Fellowship- 2017

PUBLICATIONS

1) Bhide, K.-C. Lin, S. Muthukumar, and S. Prasad, "On-demand lactate monitoring towards assessing physiological responses in sedentary populations," Analyst, vol. 146, no. 11, pp. 3482–3492, 2021.
2) Bhide, A. Ganguly, T. Parupudi, M. Ramasamy, S. Muthukumar, and S. Prasad, "Next-Generation Continuous Metabolite Sensing toward Emerging Sensor Needs," ACS omega, vol. 6, no. 9, pp. 6031–6040, 2021.
3) S. Upasham, A. Bhide, K.-C. Lin, and S. Prasad, "Point-of-use sweat biosensor to track the endocrine–inflammation relationship for chronic disease monitoring," Future science OA, vol. 7, no. 1, p. FSO628, 2020.
4) Bhide, B. Jagannath, A. Tanak, R. Willis, and S. Prasad, "CLIP: Carbon Dioxide testing suitable for Low power microelectronics and IOT interfaces using Room temperature Ionic Liquid Platform," Scientific reports, vol. 10, no. 1, pp. 1–12, 2020.

5) H. S. Stevenson, S. S. Shetty, N. J. Thomas, V. N. Dhamu, A. Bhide, and S. Prasad, "Ultrasensitive and rapid-response sensor for the electrochemical detection of antibiotic residues within meat samples," ACS omega, vol. 4, no. 4, pp. 6324–6330, 2019.
6) H. Stevenson et al., "A rapid response electrochemical biosensor for detecting THC in saliva," Scientific reports, vol. 9, no. 1, pp. 1–11, 2019.
7) Bhide, S. Cheeran, S. Muthukumar, and S. Prasad, "Enzymatic low volume passive sweat based assays for multi-biomarker detection," Biosensors, vol. 9, no. 1, p. 13, 2019.
8) Bhide, S. Muthukumar, A. Saini, and S. Prasad, "Simultaneous lancet-free monitoring of alcohol and glucose from low-volumes of perspired human sweat," Scientific reports, vol. 8, no. 1, pp. 1–11, 2018.
9) Bhide, S. Muthukumar, and S. Prasad, "CLASP (Continuous lifestyle awareness through sweat platform): A novel sensor for simultaneous detection of alcohol and glucose from passive perspired sweat," Biosensors and Bioelectronics, vol. 117, pp. 537–545, 2018.
10) Bhide, B. Jagannath, E. Graef, R. Willis, and S. Prasad, "Versatile duplex electrochemical sensor for the detection of CO2 and relative humidity using room temperature ionic liquid," ECS Transactions, vol. 85, no. 13, p. 751, 2018.
11) Bhide, B. Jagannath, E. Graef, and S. Prasad, "A robust electrochemical humidity sensor for the detection of relative humidity using room temperature ionic liquid (RTIL) for integration in semiconductor IC's," ECS Journal of Solid-State Science and Technology, vol. 7, no. 7, p. Q3043, 2018.
12) S. Rizi et al., "Semi-automated detection of single cell signatures from a dielectrophoretic cytometer," 2013, pp. 1083–1087.
13) M. Nikolic-Jaric et al., "Differential electronic detector to monitor apoptosis using dielectrophoresis-induced translation of flowing cells (dielectrophoresis cytometry)," Biomicrofluidics, vol. 7, no. 2, p. 024101, 2013.